TECHNICAL REPORT HSM-R114

METHODS
OF
DETERMINING THE SATURN I BUFFETING RESPONSE FROM RIGID MODEL WIND TUNNEL TESTS

VOLUME I

JUNE 1965

SPACE DIVISION CHRYSLER CORPORATION

HUNTSVILLE OPERATIONS

ABSTRACT

The experimental determination of the buffeting on a launch vehicle is analyzed. The statistical prediction of the gross vehicle loadings and displacements from wind tunnel data obtained from rigid models is considered. The dynamic response of the vehicle in bending and in sloshing is described. Design of a wind tunnel test that will determine the required data is outlined, and instrumentation requirements are discussed. Data reduction techniques are described that generate the power spectral densities of the aerodynamic forcing. The scaling rules are included. Saturn I test data are reduced and the results are compared with the results of an aeroelastic test and a flight test. The main part of the report is presented in Volume I. The classified portion is contained in Volume II.

FOREWORD

This report was prepared by the Aero-Space Mechanics Branch, Structures & Mechanics Engineering Department, Huntsville Space Operations, Chrysler Corporation. The work was authorized by task assignment R-AERO-SAT-I/IB-1-65, work assignment AU-4, Contract NAS8-4016, issued by the Unsteady Aerodynamics Branch, Aerodynamics Division, Aero-Astrodynamics Laboratory, Marshall Space Flight Center. The purpose of this study is to establish the data reduction procedures for wind tunnel buffeting tests conducted with rigid models. Saturn I data are reduced and compared with the results of an aeroelastic test and with flight test data. Suggestions are made concerning the design of rigid model tests.

TABLE OF CONTENTS

LIST OF ILLUSTRATIONS

LIST OF ILLUSTRATIONS (Cont.)

LIST OF TABLES

APPENDICES

NOMENCLATURE

b	Damping coefficient of a bending mode, $\frac{\text{lbs sec}}{\text{ft slug}}$
c	Damping coefficient of sloshing liquid, $\frac{\text{ft lbs sec}}{\text{radian}}$
f	A typical function
g	Constant in Eq. 59, usually set equal to $\pi/2$
h	Static pitching moment derivative, $\frac{\text{ft lbs}}{\text{radian}}$
k	Spring constant in representation of sloshing mass, $\frac{\text{ft lbs}}{\text{radian}}$
m	Linear density of vehicle, $\frac{\text{slugs}}{\text{ft}}$
p	X-coordinate
q	Dynamic pressure, $\frac{\text{lbs}}{\text{ft}^2}$
r	Radius of vehicle or model divided by its length
s	X-coordinate
t	Real time during flight, sec
u	X-coordinate
x	Longitudinal coordinate of the vehicle or model divided by its length
y	Radial coordinate of the vehicle or model divided by its length
z	X-coordinate
A	Real component of a complex function
B	Imaginary component of a complex function
$C_{M\alpha}$	Static pitching moment coefficient, positive clockwise
C_N	Local normal force coefficient based on local radius
C_{PL}	Local pressure coefficient
C_μ	Aerodynamic buffeting moment coefficient, positive clockwise

E	Elastic modulus of vehicle, $\frac{lbs}{ft^2}$
I	Area moment of inertia of vehicle, ft^4
$I_{\ell n}(\omega)$	Integrated power spectral density of the local normal force coefficients, sec ft^2
I_{sn}	Moment of inertia of the vehicle about the center of gravity excluding the mass of the sloshing liquid of the n^{th} mode (Eq. 94), slug ft^2
I_{vn}	Moment of inertia of the n^{th} mode about the vehicle center of gravity (Eq. 93), slug ft^2
IA_n, IB_n, IC_n, ID_n	Integrals defined in Appendix M
L	Length of vehicle, ft
M	Vehicle moment caused by bending, ft lbs
N_x	Local normal force, $\frac{lbs}{ft}$
T	Time, sec
V	Velocity, $\frac{ft}{sec}$
Y_n	Impedance of n^{th} mode (Eq. 26)
α	Bending mode of vehicle (Eq. 5)
β	Angular pitching deflection of the vehicle caused by buffeting, positive clockwise
γ	Time dependent coefficient in series that expresses bending displacements in terms of the bending modes
δ_n	Angular deflection of liquid with respect to vehicle center of gravity caused by sloshing, radians
ρ	Damping ratio
θ	Coefficient in the series expressing the local normal force coefficients in terms of the bending modes
μ	Buffeting moment about the vehicle center of gravity, ft lbs
$\phi_y(x,x',\omega)$	Power spectral density of y, sec
$\phi_{C\mu}(\omega)$	Power spectral density of C_μ, sec
$\phi_M(x,x',\omega)$	Power spectral density of M, ft^2 lbs^2 sec

$\phi_N(x,x',\omega)$	Power spectral density of C_N, sec
$\phi_{\beta n}(\omega)$	Power spectral density of β_n, radian^2 sec
$\phi_{\gamma \ell n}(x,x',\omega)$	Power spectral density of γ, sec
$\phi_{\delta n}(\omega)$	Power spectral density of δn, radian^2 sec
$\phi_{\delta n-\beta n}(\omega)$	Power spectral density of $(\delta n-\beta n)$, radian^2 sec
$\phi_{\delta n-\beta}(\omega)$	Power spectral density of $(\delta n-\beta)$, radian^2 sec
$\phi_{\mu}(\omega)$	Power spectral density of μ, ft^2 lbs^2 sec
ω	Real frequency during vehicle flight, $\frac{\text{radians}}{\text{sec}}$
$\Delta\omega$	Interval of frequency, $\frac{\text{radians}}{\text{sec}}$

Superscripts

$\cdot$	Derivative of parameter with respect to time
$\cdot\cdot$	Second derivative of parameter with respect to time
$'$	Derivative of parameter with respect to x
$'$	Denotes another variable
$-$	Denotes Fourier transform
$\sim$	Denotes reduced time base
*	Denotes real time during wind tunnel test

Subscripts

h	Homogeneous solution
i	Denotes particular mode
j	Denotes particular mode
ℓ	Denotes particular mode
n	Denotes particular mode
u	Denotes particular mode

w Denotes particular mode

$\langle\ \rangle$ Mean value

SECTION I. INTRODUCTION

This report is a study of the methods using wind tunnel data from rigid models to predict the gross vehicle loads caused by buffeting. Buffeting occurs on launch vehicles which have configurations that are not aerodynamically clean. The buffeting can be caused by oscillating shock waves, unstable flow separation, or vortices generated by these bodies. The problems caused by buffeting can be divided into two categories. One consists of local problems, which include local structural damage to the vehicle and discomfort or injury to passengers. The other category consists of the gross vehicle problems, which include the structural damage and control interference caused by the structural bending of the entire vehicle and the rigid body and sloshing dynamics of the vehicle.

The analysis presented in this study is confined to gross vehicle considerations. The magnitude of the gross unsteady aerodynamic forces acting on the vehicle is usually small compared to other vehicle loadings. However, the vehicle has various resonant characteristics, and the periodic nature of the buffeting can cause large bending and sloshing deflections if the buffeting acts near the resonant frequencies. The control system can be excited by these structural oscillations.

The methods used in analyzing wind tunnel buffeting data which will allow the effects of buffeting on the vehicle to be calculated are reviewed and extended here. These methods will allow statistical calculations to be made of the vehicle stresses and control deflections that are generated by the response of the vehicle to the buffeting loads. The techniques are restricted to the analysis of data taken with rigid models and no attempt is made to compensate for the effects that the vehicle deflections have on the flow field. The response of the control system to the buffeting is not included in the analysis, but it can be integrated into this work at a later date.

In analyzing the bending dynamics, the vehicle is considered to be a nonuniform slosh free beam. (The multitank configuration of the first stage of the Saturn I is assumed to behave as a single tank.) The power spectral densities of the transverse displacements and bending moments are determined in terms of the dynamic characteristics of the vehicle and in terms of the integrated power spectral densities of the local normal force coefficients. This allows the mean square of the transverse displacements and the mean square of the bending moments at any vehicle station to be evaluated. By extending the analysis, the effects of bending on the control system may also be determined.

In analyzing the rigid body and sloshing dynamics of the vehicle, it is assumed that the vehicle consists of a series of springs, dashpots, and masses attached to a rigid beam. The power spectral densities of the moment coefficient about the center of gravity will allow the mean square of the

displacement of the vehicle and the sloshing liquids to be determined. The stresses caused by the sloshing can also be determined.

There are several restrictions on the methods outlined in this report. It is necessary to follow the derivation of these methods closely to understand the implications of some of these restrictions. For the sake of completeness all of the restrictions are listed.

1. In determining the bending dynamics, the vehicle must be lightly damped and its behavior must be described by Eq. (1).

2. The dynamic modes (both bending and sloshing) must not interact with one another.

3. The control system is not considered in the analysis.

4. It is assumed that the bending deflections of the vehicle have no effect on the flow field about the vehicle. It is also assumed that small angles of attack have no effect on the buffeting.

5. The bending modes must be determined before the wind tunnel data can be reduced.

6. Buffeting must be stochastic.

7. The noise level of the tunnel must be low enough so that signals fed into the measuring system will be negligible.

8. The rigid model should have no dynamic characteristics that will cause erroneous measurements. If the model does possess some resonant characteristics that may be excited by the flow, signals in the resonant frequency ranges should be filtered.

9. All measurements must be referenced to the same time base.

10. The instrumentation generating cross power spectral densities must determine real and imaginary components.

II. GENERAL ANALYSIS OF BENDING DYNAMICS

The equation describing the bending dynamics of a slosh-free vehicle is the same as the one describing the dynamics of a non-uniform beam (Ref. 1).

$$m\ddot{y} + b\dot{m}\dot{y} + \left(\frac{EI}{L^4}\, y''\right)'' = \frac{N_x}{L} \tag{1}$$

The coordinate system is shown in figure 1. The local normal force is given by

$$N_x = qL\ r(x)\ C_N(x,t) \tag{2}$$

and the local normal force coefficient $C_N(x,t)$, based on the local radius, is given by

$$C_N(x,t) = \int_0^{2\pi} C_{PL} \cos\theta\ d\theta \tag{3}$$

The local normal force coefficient is a function of Mach number and Reynolds number.

For a lightly damped system, the homogeneous representation of Eq. (1) can be approximated by

$$m\ddot{y} + \left(\frac{EI}{L^4}\, y''\right)'' = 0 \tag{4}$$

whose solution is then

$$Y_h = \sum_n \alpha_n(x)\ \gamma_{hn}(t) \tag{5}$$

where

$$\gamma_{hn}(t) = e^{i\omega_n t} \tag{6}$$

and

$$\int_0^1 m\ \alpha_n{}^2(x)\ dx = 1 \tag{7}$$

Substituting Eq. (5) and (6) into Eq. (4) yields

$$(-m)\sum_n \alpha_n(x)\ \omega_n{}^2\ e^{i\omega_n t} + \sum_n \left(\frac{EI}{L^4}\, \alpha_n''(x)\right)'' e^{i\omega_n t} = 0 \tag{8}$$

Thus

$$\alpha_n(x) = \frac{1}{m\omega_n{}^2}\left(\frac{EI}{L^4}\, \alpha_n''(x)\right)'' \tag{9}$$

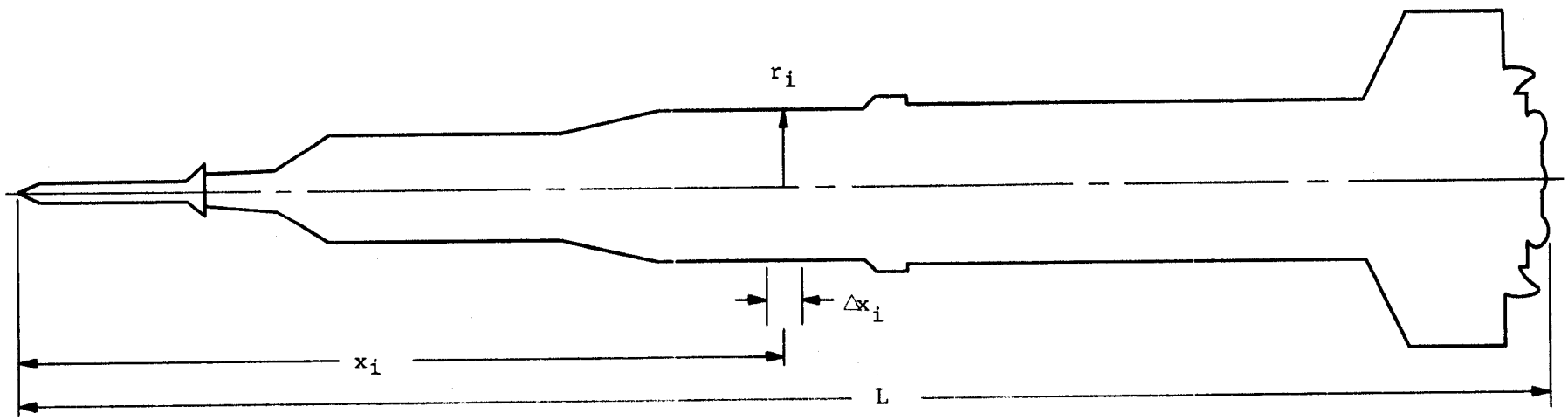

FIGURE 1. COORDINATE SYSTEM FOR THE ANALYSIS

Let the solution of Eq. (1) be written

$$y = \sum_n y_n \tag{10}$$

where

$$y_n = \alpha_n(x)\ \gamma_n(t) \tag{11}$$

This is permissible, since a lightly damped system has essentially the same mode shapes as if it were free of damping. Substituting Eq. (10) and (11) into Eq. (1) yields

$$m\sum_n \alpha_n(x)\ \ddot{\gamma}_n(t) + bm\sum_n \alpha_n(x)\ \dot{\gamma}_n(t) + \sum_n \left(\frac{EI}{L^4}\ \alpha_n''(x)\right)''\ \gamma_n(t)$$

$$= qr(x)\ C_N(x,t) \tag{12}$$

Substituting Eq. (9) into Eq. (12) and changing subscripts

$$m\sum_\ell \ddot{\gamma}(t)\ \alpha_\ell(x) + bm\sum_\ell \dot{\gamma}_\ell(t)\ \alpha_\ell(x) + m\sum_\ell \gamma_\ell(t)\ \omega_\ell^2\ \alpha_\ell(x)$$

$$= qr(x)\ C_N(x,t) \tag{13}$$

Multiplying both sides of Eq. (13) by $\alpha_n(x)$ and integrating with respect to x yields

$$\sum_\ell \ddot{\gamma}_\ell(t) \int_0^1 m\ \alpha_n(x)\ \alpha_\ell(x)\ dx + b\sum_\ell \dot{\gamma}_\ell(t) \int_0^1 m\ \alpha_n(x)\ \alpha_\ell(x)\ dx$$

$$+ \sum_\ell \omega_n^2\ \gamma_\ell(t) \int_0^1 m\ \alpha_n(x)\ \alpha_\ell(x)\ dx$$

$$= q\int_0^1 C_N(x,t)\ r(x)\ \alpha_n(x)\ dx \tag{14}$$

In Appendix A the following orthogonality condition is derived:

$$\int_0^1 m\ \alpha_\ell(x)\ \alpha_n(x)\ dx = 0 \qquad \text{when } \ell \neq n \tag{15}$$

From Eq. (7) and (15) Eq. (14) can be written

$$\ddot{\gamma}_n(t) + b\dot{\gamma}_n(t) + \omega_n^2\ \gamma_n(t) = q\int_0^1 C_N(x,t)\ r(x)\ \alpha_n(x)\ dx \tag{16}$$

Defining the damping ratio as

$$\rho_n = \frac{b}{2\omega_n} \tag{17}$$

Eq. (16) can be written

$$\ddot{\gamma}_n(t) + 2\rho_n\ \omega_n\ \dot{\gamma}_n(t) + \omega_n^2\ \gamma_n(t) = q\int_0^1 C_N(x,t)\ r(x)\ \alpha_n(x)\ dx \tag{18}$$

The Fourier transform of a function f(t) over time T is defined as

$$\overline{f(\omega)} = \lim_{T \to \infty} \frac{1}{2\pi} \int_{-T/2}^{T/2} f(t)\, e^{-i\omega t}\, dt \tag{19}$$

Where f(t) can be expressed as

$$f(t) = \int_{-\infty}^{\infty} \overline{f(\omega)}\, e^{i\omega t}\, d\omega \tag{20}$$

The power spectral density of a function f(t) is defined by

$$\phi_f(\omega) = \lim_{T \to \infty} \frac{4\pi}{T} \overline{f(\omega)}\ \overline{f(-\omega)} \tag{21}$$

Taking the Fourier transform of Eq. (18) yields

$$(-\omega^2 + 2i\,\rho_n\omega\,\omega_n + \omega_n^2)\ \overline{\gamma_n(\omega)} = q \int_0^1 \overline{C_N(x,\omega)}\ r(x)\ \alpha_n(x)\, dx \tag{22}$$

$$\overline{\gamma_n(\omega)} = \frac{q}{(-\omega^2 + 2i\rho_n\omega\,\omega_n + \omega_n^2)} \int_0^1 \overline{C_N(x,\omega)}\ r(x)\ \alpha_n(x)\, dx \tag{23}$$

The power spectral density of $\gamma_n(t)$ is

$$\phi\gamma_{\ell n}(\omega) = \lim_{T \to \infty} \frac{4\pi}{T} \overline{\gamma_\ell(\omega)}\ \overline{\gamma_n(-\omega)} \tag{24}$$

Substituting Eq. (23) into (24) yields

$$\phi\gamma_{\ell n}(\omega) = \lim_{T \to \infty} \frac{4\pi\, q^2 \int_0^1 \int_0^1 \overline{C_N(x,\omega)}\ \overline{C_N(x',-\omega)}\ r(x)\ r(x')\ \alpha_\ell(x)\ \alpha_n(x')\, dx dx'}{T\left[(\omega_\ell^2 - \omega^2) + 2i\rho_\ell\omega\,\omega_\ell\right]\left[(\omega_n^2 - \omega^2) - 2i\rho_n\omega\,\omega_n\right]} \tag{25}$$

Defining

$$Y_n(\omega) = (\omega_n^2 - \omega^2) + 2i\rho_n\omega\,\omega_n \tag{26}$$

$$\phi_n(x,x',\omega) = \lim_{T \to \infty} \frac{4\pi}{T} \overline{C_N(x,\omega)}\ \overline{C_N(x',-\omega)} \tag{27}$$

Thus Eq. (25) can be written

$$\phi\gamma_{\ell n}(\omega) = \frac{q^2 \int_0^1 \int_0^1 \phi_N(x,x',\omega)\ r(x)\ r(x')\ \alpha_\ell(x)\ \alpha_n(x')\, dx dx'}{Y_\ell(\omega)\ Y_n(-\omega)} \tag{28}$$

Defining the integrated power spectral density of the local normal force coefficients as

$$I_{\ell n}(\omega) = \int_0^1 \int_0^1 \phi_N(x,x',\omega)\ r(x)\ \alpha_\ell(x)\ r(x')\ \alpha_n(x')\ dxdx' \tag{29}$$

Equation (28) can be rewritten

$$\phi\gamma_{\ell n}(\omega) = \frac{q^2\ I_{\ell n}(\omega)}{Y_\ell(\omega)\ Y_n(-\omega)} \tag{30}$$

From Eq. (10) and (11)

$$y(x,t) = \sum_n \alpha_n(x)\ \gamma_n(t) \tag{31}$$

Taking Fourier transforms of Eq. (31) yields

$$\overline{y(x,\omega)} = \sum_n \alpha_n(x)\ \overline{\gamma_n(\omega)} \tag{32}$$

From Eq. (21)

$$\phi y(x,x',\omega) = \lim_{T \to \infty} \frac{4\pi}{T} \sum_\ell \sum_n \alpha_\ell(x)\ \alpha_n(x')\ \overline{\gamma_\ell(\omega)}\ \overline{\gamma_n(-\omega)} \tag{33}$$

From Eq. (24)

$$\phi_y(x,x',\omega) = \sum_\ell \sum_n \alpha_\ell(x)\ \alpha_n(x')\ \phi\gamma_{\ell n}(\omega) \tag{34}$$

From Eq. (30) this can be written

$$\phi_y(x,x',\omega) = \sum_\ell \sum_n \frac{\alpha_\ell(x)\ \alpha_n(x')\ q^2\ I_{\ell n}(\omega)}{Y_\ell(\omega)\ Y_n(-\omega)} \tag{35}$$

This is similar to the equation derived on page 192 of Ref. 2. From Appendix C (which is determined from Appendix B), the mean square of the deflection at a point is

$$\langle y^2(x)\rangle = \int_0^\infty \phi_y(x,x,\omega)\ d\omega \tag{36}$$

If the deflections are Gaussian, the 3-sigma values of the deflection are

$$3\sigma_y(x) = \pm[\overline{\langle y^2(x)\rangle}]^{1/2} \tag{37}$$

The deflection of a specific mode is given by Eq. (11)

$$y_n = \alpha_n(x)\ \gamma_n(t) \tag{11}$$

The power spectral density of the deflection of this mode is given by

$$\phi_{yn}(x,x',\omega) = \frac{\alpha_n(x)\ \alpha_n(x')\ q^2 I_{nn}(\omega)}{|Y_n^2\ (\omega)|} \tag{38}$$

The mean square of the deflection of the mode is

$$\langle y_n^2(x)\rangle = \int_0^1 \phi_{yn}(x,x,\omega)\ d\omega \tag{39}$$

The bending moment at a point is given by

$$M(x,t) = \frac{E(x)\ I(x)\ y''}{L} = \frac{E(x)\ I(x)}{L} \sum_n \alpha_n''(x)\ \gamma_n(t) \tag{40}$$

The power spectral density of the bending moment is given by

$$\phi_M(x,x',\omega) = \sum_\ell \sum_n \frac{E(x)\ I(x)\ E(x')\ I(x')\ \alpha_\ell''(x)\ \alpha_n''(x')\ q^2 I_{\ell_n}(\omega)}{Y_\ell(\omega)\ Y_n(-\omega)\ L^2} \tag{41}$$

and the mean square is given by

$$\langle M^2(x)\rangle = \int_0^\infty \phi_M(x,x,\omega)\ d\omega \tag{42}$$

If the moments are Gaussian, the 3-sigma values are

$$3\sigma_M(x) = \underset{+}{3}\ [\langle M^2(x)\rangle]^{1/2} \tag{43}$$

The power spectral density of the moment of a particular mode is

$$\phi_{Mn}(x,x',\omega) = \frac{E(x)\ I(x)\ E(x')\ I(x')\ \alpha_n''(x)\ \alpha_n''(x')\ q^2\ I_{nn}(\omega)}{|Y_n^2(\omega)|\ L^2} \tag{44}$$

The mean square of the moment generated by this mode is

$$\langle M_n^2(x)\rangle = \int_0^\infty \phi_{Mn}(x,x,\omega)\ d\omega \tag{45}$$

Each of these power spectral densities is a function of Mach number and Reynolds number.

Approximations can be made that will reduce the labor required in determining the bending dynamics of a vehicle.

A simplifying approximation can be made by considering Eq. (35) and (41):

$$\phi_y(x,x',\omega) = \sum_{\ell} \sum_{n} \frac{\alpha_\ell(x)\ \alpha_n(x')\ q^2\ I_{\ell n}(\omega)}{Y_\ell(\omega)\ Y_n(-\omega)} \tag{35}$$

$$\phi_M(x,x',\omega) = \sum_{\ell} \sum_{n} \frac{E(x)\ I(x)\ E(x')\ I(x')\ \alpha''_\ell(x)\ \alpha''_n(x')\ q^2\ I_\ell(\omega)}{Y_\ell(\omega)\ Y_n(-\omega)\ L^2} \tag{41}$$

If the variation in $I_{\ell n}(\omega)$ is relatively small over the frequency range, Eq. (35) and (41) show that the cross modal terms in the double series are negligible because $Y_\ell(\omega)\ Y_n(-\omega)$ (where $\ell \neq n$) is large for all frequencies. Thus Eq. (35) can be approximated by

$$\phi_y(x,x',\omega) = \sum_{n} \frac{\alpha_n(x)\ \alpha_n(x')\ q^2\ I_{nn}(\omega)}{|Y_n^2(\omega)|} \tag{46}$$

and Eq. (41) can be approximated by

$$\phi_M(x,x',\omega) = \sum_{n} \frac{E(x)\ I(x)\ E(x')\ I(x')\ \alpha''_n(x)\ \alpha''_n(x')\ q^2\ I_{nn}(\omega)}{|Y_n^2(\omega)|\ L^2} \tag{47}$$

From Eq. (38) and (44)

$$\phi_y(x,x',\omega) = \sum_{n} \phi_{yn}(x,x',\omega) \tag{48}$$

$$\phi_M(x,x',\omega) = \sum_{n} \phi_{Mn}(x,x',\omega) \tag{49}$$

From Eq. (36), (39), (42), and (45)

$$\langle y^2(x)\rangle = \sum_{n} \langle y_n^2(x)\rangle \tag{50}$$

$$\langle M^2(x)\rangle = \sum_{n} \langle M_n^2(x)\rangle \tag{51}$$

Thus, the approximation allows the cross modal terms in the integrated power spectral density of the local normal force coefficient to be omitted. This will greatly reduce the number of computations required in the data reduction. However, some calculations should be made which include these cross modal terms. The results of these calculations should be compared with those obtained from the approximate procedure to serve as a check on the accuracy of the approximation.

The approximation also shows that the mean square displacements and bending moments are the sum of the mean square displacements and bending moments of each mode. The mean square displacements and moments of each mode can be determined and then summed. If the displacements and moments of a given mode are excessive, the approximation will aid in identifying the mode in question.

A further simplification can be introduced by observing that the impedance, defined by Eq. (26), is large for all frequencies except those near the resonant frequency.

$$Y_n(\omega) = (\omega_n^2 - \omega^2) - 2i\rho_n\omega\,\omega_n \tag{26}$$

Thus, if $I_{\ell n}(\omega)$ does not vary greatly over the frequency range, Eq. (38) and (44) show that $\phi_{yn}(x,x',\omega)$ and $\phi_{Mn}(x,x',\omega)$ will be approximately zero except for frequencies near the natural frequency of each mode. Thus, Eq. (38) and (44) can be approximated by

$$\phi_{yn}(x,x',\omega) = \frac{\alpha_n(x)\,\alpha_n(x')\,q^2\,I_{nn}(\omega_n)}{|Y_n^2(\omega_n)|} \tag{52}$$

$$\phi_{Mn}(x,x',\omega) = \frac{E(x)\,I(x)\,E(x')\,I(x')\,\alpha''(x)\,\alpha''(x')\,q^2\,I_{nn}(\omega_n)}{|Y_n^2(\omega_n)|\,L^2} \tag{53}$$

for

$$\omega_n - \frac{\Delta\omega_n}{2} \le \omega \le \omega_n + \frac{\Delta\omega_n}{2}$$

and

$$\phi_{yn}(x,x',\omega) = 0 \tag{54}$$

$$\phi_{Mn}(x,x',\omega) = 0 \tag{55}$$

for

$$\omega < \omega_n - \frac{\Delta\omega_n}{2} \text{ and } \omega > \omega_n + \frac{\Delta\omega_n}{2}$$

From Eq. (26)

$$|Y_n^2(\omega_n)| = 4\rho_n^2\,\omega_n^4 \tag{56}$$

Equations (52) and (53) can be rewritten

$$\phi_{yn}(x,x',\omega) = \frac{\alpha_n(x)\,\alpha_n(x')\,q^2\,I_{nn}(\omega_n)}{4\rho_n^2\,\omega_n^4} \tag{57}$$

$$\phi_{Mn}(x,x',\omega) = \frac{E(x)\,I(x)\,E(x')\,I(x')\,\alpha_n''(x)\,\alpha_n''(x')\,q^2\,I_{nn}(\omega_n)}{4\rho_n^2\,\omega_n^4\,L^2} \tag{58}$$

for

$$\omega_n - \frac{\Delta\omega_n}{2} \le \omega \le \omega_n + \frac{\Delta\omega_n}{2}$$

The frequency range, or band width, for which Eq. (52), (53), (57), and (58) are applicable is given by

$$\Delta\omega_n = 2g\ \rho_n\ \omega_n \tag{59}$$

where g is usually set equal to $\pi/2$. Substituting Eq. (54), (55), (57), (58), and (59) into (39) and (45) yields

$$\langle y_n^2(x)\rangle = \frac{g\ \alpha_n^2(x)\ q^2\ I_{nn}(\omega_n)}{2\rho_n\ \omega_n^3} \tag{60}$$

$$\langle M_n^2(x)\rangle = \frac{g\ E^2(x)\ I^2(x)\ \alpha_n''^2(x)\ q^2\ I_{nn}(\omega_n)}{2\rho_n\ \omega_n^3\ L^2} \tag{61}$$

The sum of the mean squares of the displacements and bending moments of each mode will yield the mean squares of the displacements and bending moments of the vehicle by Eq. (50) and (51). Thus, the approximation allows the mean squares of the displacement and moments to be obtained without performing the integration of Eq. (36), (39), (42), or (45). Furthermore, it is only necessary to determine the integrated power spectral density at the natural frequencies of the bending modes. Thus, a considerable decrease in data reduction effort is effected. Before relying entirely on these approximate methods, sample calculations should be compared with those obtained from the exact method to establish the accuracy of the approximations.

The geometric scaling rules are implied in the equations that have been derived. The time t used in the equations is the real time of the vehicle in flight. This real time of the vehicle t is related to the reduced time $\tilde{t}$ of aerodynamic phenomena by

$$t = \frac{L}{V}\,\tilde{t} \tag{62}$$

and the reduced time $\tilde{t}$ is related to the real time t* during wind tunnel tests by

$$\tilde{t} = \frac{V^*}{L^*}\,t^* \tag{63}$$

The frequencies are related by

$$\omega = \frac{V}{L}\,\tilde{\omega} \tag{64}$$

and

$$\tilde{\omega} = \frac{L^*}{V^*}\,\omega^* \tag{65}$$

The scaling of the power spectral densities will now be determined.

From Eq. (19)

$$\overline{C_N(x,\omega)} = \lim_{T \to \infty} \frac{1}{2\pi} \int_{-T/2}^{T/2} C_N(x,t)\, e^{-i\omega t}\, dt \tag{66}$$

Changing $C_N(x,t)$ to the reduced time base $C_N(x,\tilde{t})$,

$$\overline{C_N(x,\omega)} = \lim_{T \to \infty} \frac{1}{2\pi} \frac{L}{V} \int_{-\tilde{T}/2}^{\tilde{T}/2} C_N(x,\tilde{t})\, e^{-i\tilde{\omega}\tilde{t}}\, d\tilde{t} \tag{67}$$

Thus

$$\overline{C_N(x,\omega)} = \frac{L}{V} \overline{C_N(x,\tilde{\omega})} \tag{68}$$

From Eq. (27)

$$\phi_N(x,x',\omega) = \lim_{T \to \infty} \frac{4\pi}{T} \overline{C_N(x,\omega)}\ \overline{C_N(x',-\omega)} \tag{27}$$

Substituting Eq. (62) and (68)

$$\phi_N(x,x',\omega) = \lim_{T \to \infty} \frac{4\pi}{\left(\frac{L}{V}\right)\tilde{T}} \left(\frac{L}{V}\right)^2 \overline{C_N(x,\tilde{\omega})}\ \overline{C_N(x',-\omega)} \tag{69}$$

$$\phi_N(x,x',\omega) = \frac{L}{V} \phi_N(x,x',\tilde{\omega}) \tag{70}$$

likewise

$$\phi_N(x,x',\tilde{\omega}) = \frac{V^*}{L^*} \phi_N(x,x',\omega^*) \tag{71}$$

The integrated power spectral density of the local normal force coefficient scales by the same rule. In Ref. 3 tests were conducted with a 1.6% model and an 8% model. The data taken with these models were scaled by essentially the above relations to the full scale vehicle. Virtually the same results were obtained from both sets of test data for the full scale vehicle. These results give experimental verification to the scaling rules.

SECTION III. TEST METHODS FOR BENDING DYNAMICS

In evaluating Eq. (35), (38), (41), (44), (52), and (53), the integrated power spectral density of the local normal force coefficients $I_{\ell n}(\omega)$ must be generated from the experimental data. In the approximate methods it is only necessary that $I_{nn}(\omega)$ or $I_{nn}(\omega_n)$ be determined from the data. In determining the integrated power spectral density of the local normal force coefficients, two methods are available. The first one is termed the series method. The second one is called the cross spectrum method.

The series method will evaluate Eq. (29).

$$I_{\ell n}(\omega) = \int_0^1 \int_0^1 \phi_N(x,x',\omega)\ r(x)\ \alpha_\ell(x)\ r(x')\ \alpha_n(x')\ dxdx' \tag{29}$$

From Eq. (27)

$$\phi_N(x,x',\omega) = \lim_{T \to \infty} \frac{4\pi}{T} \overline{C_N(x,\omega)}\ \overline{C_N(x',-\omega)} \tag{27}$$

Expressing the local normal force coefficients as a series in terms of the vehicle bending modes

$$C_N(x,t) = \sum_w \theta_w(t)\ \frac{m(x)}{r(x)}\ \alpha_w(x) \tag{72}$$

Taking Fourier transforms yields

$$\overline{C_N(x,\omega)} = \sum_w \overline{\theta_w(\omega)}\ \frac{m(x)}{r(x)}\ \alpha_w(x) \tag{73}$$

Substituting Eq. (73) into Eq. (27) yields

$$\phi_N(x,x',\omega) = \lim_{T \to \infty} \frac{4\pi}{T} \sum_u \sum_w \overline{\theta_u(\omega)}\ \overline{\theta_w(-\omega)}\ \frac{m(x)}{r(x)}\ \alpha_u(x)\ \frac{m(x')}{r(x')}\ \alpha_w(x') \tag{74}$$

Substituting Eq. (74) into Eq. (29) yields

$$I_{\ell n}(\omega) = \lim_{T \to \infty} \frac{4\pi}{T} \sum_u \sum_w \overline{\theta_u(\omega)}\ \overline{\theta_w(-\omega)} \int_0^1 \int_0^1 m(x)\ \alpha_\ell(x)\ \alpha_u(x)\ m(x')\ \alpha_n(x')\ \alpha_w(x')\ dxdx' \tag{75}$$

From Eq. (7) and (15) this can be written:

$$I_{\ell n}(\omega) = \lim_{T \to \infty} \frac{4\pi}{T} \overline{\theta_\ell(\omega)}\ \overline{\theta_n(-\omega)} \tag{76}$$

This is the cross modal power spectrum of the time dependent coefficients in Eq. (72) that express the local normal force coefficients as series of the bending modes. In order to determine these coefficients, multiply both sides of Eq. (72) by $r(x)\alpha_n(x)$ and integrate with respect to x.

$$\int_0^1 C_N(x,t)\ r(x)\ \alpha_n(x)\ dx = \sum_\ell \theta_\ell(t) \int_0^1 m(x)\ \alpha_\ell(x)\ \alpha_n(x)\ dx \tag{77}$$

From the orthogonality conditions given by Eq. (7) and (15)

$$\theta_n(t) = \int_0^1 C_N(x,t)\ r(x)\ \alpha_n(x)\ dx \tag{78}$$

Consider that the vehicle is divided into segments as shown in figure 1. The dimensionless distance to the center of the i^{th} segment is given by x_i. The dimensionless length of the i^{th} segment is given by Δx_i.

Assume that the local normal force coefficients $C_N(x,t)$ have unity spatial correlation over the length of each segment. Thus

$$C_N(x,t) = C_N(x_i,t) \tag{79}$$

from

$$x_i - \frac{\Delta x_i}{2} \le x \le x_i + \frac{\Delta x_i}{2}$$

Equation (78) can then be written

$$\theta_n(t) = \sum_i C_N(x_i,t) \int_{x_i - \frac{\Delta x_i}{2}}^{x_i + \frac{\Delta x_i}{2}} r(x)\ \alpha_n(x)\ dx \tag{80}$$

If the variation in the product $r(x)\ \alpha_n(x)$ is small over each segment, this can be written

$$\theta_n(t) = \sum_i C_N(x_i,t)\ r(x_i)\ \alpha_n(x_i)\ \Delta x_i \tag{81}$$

Assume that the local normal force coefficients do not necessarily have unity spatial correlation over the length of each segment, but that variations of the product $r(x)\ \alpha_n(x)$ are small over each segment. Then Eq. (78) can be written

$$\theta_n(t) = \sum_i r(x_i)\ \alpha_n(x_i) \left[\frac{\int_{x_i - \frac{\Delta x_i}{2}}^{\Delta x_i + \frac{\Delta x_i}{2}} C_N(x,t)\ dx}{\Delta x_i} \right] \Delta x_i \tag{82}$$

The quantity in the bracket is the average value of the normal force coefficient over the length of the segment and will be designated $C_N(x_i,t)$. Thus Eq. (78) can be written

$$\theta_n(t) = \sum_i C_N(x_i,t)\ r(x_i)\ \alpha_n(x_i)\ \Delta x_i \tag{83}$$

The Fourier transform of Eq. (80), (81), or (83) will allow Eq. (76) to be evaluated.

In applying the cross spectrum method, Eq. (29) will be evaluated. Assume first that the model is divided into segments as shown in figure 1. Assume that the local normal force coefficients $C_N(x,t)$ have unity spatial correlation over the length of each segment. Thus

$$C_N(x,t) = C_N(x_i,t) \tag{79}$$

over the range

$$x_i - \frac{\Delta x_i}{2} \le x \le x_i + \frac{\Delta x_i}{2}$$

From Eq. (27)

$$\phi_n(x_i,x_j,\omega) = \lim_{T \to \infty} \frac{4\pi}{T}\ \overline{C_N(x_i,\omega)}\ \overline{C_N(x_j,-\omega)} \tag{84}$$

Thus Eq. (29) can be written

$$I_{\ell n}(\omega) = \sum_i \sum_j \phi_N(x_i,x_j,\omega) \int_{x_j - \frac{\Delta x_j}{2}}^{x_j + \frac{\Delta x_j}{2}} \int_{x_i - \frac{\Delta x_i}{2}}^{x_i + \frac{\Delta x_i}{2}} r(x)\ \alpha_\ell(x)\ r(x')\ \alpha_n(x')\ dx dx' \tag{85}$$

If the segments are such that the variations in the product $r(x)\ \alpha_n(x)$ are small over the segments, then Eq. (85) can be approximated by

$$I_{\ell n}(\omega) = \sum_i \sum_j \phi_N(x_i,x_j,\omega)\ r(x_i)\ \alpha_\ell(x_i)\ r(x_j)\ \alpha_n(x_j)\ \Delta x_i\ \Delta x_j \tag{86}$$

Now assume that the segments are such that the variations in the product $r(x)\ \alpha_n(x)$ are small over each segment but that the coefficients over each segment do not necessarily have unity spatial correlation. Then Eq. (29) can be written

$$I_{\ell n}(\omega) = \sum_i \sum_j r(x_i)\ \alpha_\ell(x_i)\ r(x_j)\ \alpha_n(x_j) \cdot$$

$$\left[\int_{x_j - \frac{\Delta x_j}{2}}^{x_j + \frac{\Delta x_j}{2}} \int_{x_i - \frac{\Delta x_i}{2}}^{x_i + \frac{\Delta x_i}{2}} \frac{\phi_N(x,x',\omega)\ dxdx'}{\Delta x_i\ \Delta x_j} \right] \Delta x_i\ \Delta x_j \tag{87}$$

Substituting Eq. (27) into the quantity in the brackets

$$\left[\int_{x_j - \frac{\Delta x_j}{2}}^{x_j + \frac{\Delta x_j}{2}} \int_{x_i - \frac{\Delta x_i}{2}}^{x_i + \frac{\Delta x_i}{2}} \frac{\phi_N(x,x',\omega)\ dxdx'}{\Delta x_i\ \Delta x_j} \right]$$

$$= \lim_{T \to \infty} \frac{4\pi}{T} \int_{x_j - \frac{\Delta x_j}{2}}^{x_j + \frac{\Delta x_j}{2}} \int_{x_i - \frac{\Delta x_i}{2}}^{x_i + \frac{\Delta x_i}{2}} \frac{\overline{C_N(x,\omega)}\ \overline{C_N(x',-\omega)}}{\Delta x_i\ \Delta x_j}\ dxdx' \tag{88}$$

$$= \lim_{T \to \infty} \frac{4\pi}{T} \int_{x_i - \frac{\Delta x_i}{2}}^{x_i + \frac{\Delta x_i}{2}} \frac{\overline{C_N(x,\omega)}}{\Delta x_i}\ dx \int_{x_j - \frac{\Delta x_j}{2}}^{x_j + \frac{\Delta x_j}{2}} \frac{\overline{C_N(x',-\omega)}}{\Delta x_j}\ dx' \tag{89}$$

The two integrals are the average values of the Fourier transform of the local normal force coefficients over the segments. Thus Eq. (87) can be written

$$I_{\ell n}(\omega) = \sum_i \sum_j \phi_N(x_i,x_j,\omega)\ r(x_i)\ \alpha_\ell(x_i)\ r(x_j)\ \alpha_n(x_j)\ \Delta x_i\ \Delta x_j \tag{90}$$

where

$$\phi_N(x_i,x_j,\omega) = \lim_{T \to \infty} \frac{4\pi}{T}\ \overline{C_N(x_i,\omega)}\ \overline{C_N(x_j,-\omega)} \tag{84}$$

and $\overline{C_N(x_i,\omega)}$ is the Fourier transform of the average local normal force coefficient acting over a segment.

If it can be determined that there is no correlation between stations along the body, then Eq. (90) can be written

$$I_{\ell n}(\omega) = \sum_i \phi_N(x_i,x_i,\omega)\ r(x_i)\ \alpha_\ell(x_i)\ r(x_i)\ \alpha_n(x_i)\ \Delta x_i\ \Delta x_i \tag{91}$$

If only the absolute value of the power spectral density of the local normal force coefficients is available, the maximum possible values of the integrated power spectral density of local normal force coefficients are given by

$$I_{\ell n}(\omega) = \sum_i \sum_j \left|\phi_N(x_i,x_j,\omega)\right| \cdot \left|\alpha_\ell(x_i)\ \alpha_n(x_j)\right| \cdot r(x_i)\ r(x_j)\ \Delta x_i\ \Delta x_j \quad (92)$$

where $\left|\phi_N(x_i,x_j,\omega)\right|$ is given as a function of $\phi_N(x_i,x_i,\omega)$ and $\phi_N(x_j,x_j,\omega)$ in Appendix D.

To determine the mean square of the vehicle bending deflections and bending moments, the power spectral densities of the bending deflections and bend-moments must be obtained as shown in Eq. (36) and (42). Equations (35) and (41) show that these can be obtained from the dynamic characteristics of the vehicle, the dynamic pressure, and the integrated power spectral density of the local normal force coefficients. This integrated power spectral density, given by Eq. (29), is determined from experimental force or pressure data. It must be scaled by the relations given in Eq. (70) and (71). The integrated power spectral density can be obtained by either of two different methods, the series method or the cross spectrum method. In both methods the body is divided into segments. These segments must be selected on the basis of criteria presented below. The calculation of the integrated power spectral density is based on the real time of the wind tunnel test. The calculation by the series method is outlined in Table I and by the cross spectrum method in Table II. These integrated power spectral densities of the local normal force coefficients must be scaled to the flight case by Eq. (70) and (71).

Table I Series Method of Determining $I_{\ell n}(\omega^*)$ and $I_{\ell n}(\omega_n^*)$

Factors to be Determined	Selection of Segments		
	Unity pressure correlation over segment	Small variation in $r(x)\ \alpha_n(x)$ over segment	Unity pressure correlation and small variation in $r(x)\ \alpha_n(x)$ over segment
$C_N(x_i,t^*)$	Measure local normal force over segments or pressure at points and integrate by Eq. (3)	Measure local normal force over segments	Measure local normal force over segments or pressure at points and integrate by Eq. (3)
$\theta_n(t^*)$	From $C_N(x_i,t^*)$ and Eq. (80)	From $C_N(x_i,t^*)$ and Eq. (83)	From $C_N(x_i,t^*)$ and Eq. (81)
$I_{\ell n}(\omega_n^*), I_{nn}(\omega_n^*)$	From $\theta_n(t^*)$ and Eq. (76)	From $\theta_n(t^*)$ and Eq. (76)	From $\theta_n(t^*)$ and Eq. (76)

Table II Cross Spectrum Method of Determining $I_{\ell n}(\omega^*)$ and $I_{\ell n}(\omega_n^*)$

Factors to be Determined	Selection of Segments		
	Unity pressure correlation over segment	Small variation in $r(x)\ \alpha_n(x)$ over segment	Unity pressure correlation and small variation in $r(x)\ \alpha_n(x)$ over segment
$C_N(x_i,t^*)$	Measure local normal force over segments or pressure at points and integrate by Eq. (3)	Measure local normal force over segments	Measure local normal force over segments or pressure at points and integrate by Eq. (3)
$\phi_N(x_i,x_j,\omega^*)$	From $C_N(x_i,t^*)$ and Eq. (84)	From $C_N(x_i,t^*)$ and Eq. (84)	From $C_N(x_i,t^*)$ and Eq. (84)
$I_{\ell n}(\omega^*), I_{nn}(\omega_n^*)$	From $\phi_N(x_i,x_j,\omega^*)$ and Eq. (85)	From $\phi_N(x_i,x_j,\omega^*)$ and Eq. (90)	From $\phi_N(x_i,x_j,\omega^*)$ and Eq. (86)

In both the series method and the cross spectrum method the body must be divided into segments so that either the local normal force coefficients have unity spatial correlation over each segment or be divided so that the variation in $r(x)\ \alpha_n(x)$ is small over each segment. It may be desirable to divide the body into segments such that the pressure has unity correlation over each segment and the variation in $r(x)\ \alpha_n(x)$ is small over each segment.

The local normal force coefficients over each segment can be determined directly by constructing the wind tunnel model as a sequence of segments that are independently suspended from a sting. The normal force acting on each segment will be measured with inertia-compensated balance systems. The normal force can also be determined by using standard pressure transducers and integrating the pressure readings by Eq. (3).

The local normal force coefficients can be used directly to compute the integrated power spectral density by Eq. (76) and (80), (81) or (83), or they can be used to determine the power spectral density of the local normal force coefficients, which in turn can be used to compute the integrated power spectral density by Eq. (85), (86), or (90).

The advantages of one criterion for selecting the segments are compared with the advantages of other criteria in Table III. The information is based on the assumption that the distance over which the pressure has unity correlation is small compared with the distance over which changes in $r(x)\ \alpha_n(x)$ are small.

Table III Comparison of Criteria for Selecting Segments

Advantages	Comparison		
	Unity pressure correlation over segment	Small variation in $r(x)\ \alpha_n(x)$ over segment	Unity pressure correlation and small variation in $r(x)\ \alpha_n(x)$ over segment
Unity pressure correlation over segment		If pressure transducers are used, fewer measuring instruments will be required at each segment.	Fewer measuring instruments required.
Small variation in $r(x)\ \alpha_n(x)$ over segment	If inertia-compensated balance systems are used, fewer measuring instruments required.		Fewer measuring instruments required.
Unity pressure correlation and small variation in $r(x)\ \alpha_n(x)$ over segment	$I_{\ell n}(\omega^*)$ can be determined by Eq. (81) instead of Eq. (80), or by Eq. (86) instead of (85)	If pressure transducers are used, fewer measuring instruments will be required at each segment.	

Table III shows that dividing the vehicle into segments so that the pressure has unity spatial correlation is advantageous because fewer measuring devices are required at each segment if conventional pressure transducers are used. Dividing the vehicle into segments, so that the variation in $r(x)\ \alpha_n(x)$ is small over the segment, is advantageous because fewer measuring devices are required if inertia-compensated balances are used to measure the local normal force coefficients. Generally there is not much to be gained by dividing the vehicle into segments so that over each segment both unity pressure correlations and small variations in $r(x)\ \alpha_n(x)$ exist. It may be advantageous to select some of the segments by one criterion and the others by another criterion.

The series method is preferred to the cross spectrum method because, if the cross terms in the integrated power spectral densities are not required, fewer power spectral densities must be computed. This is illustrated by the two following cases. In both illustrations, assume that only the first five bending modes are of interest and that only the terms $I_{nn}(\omega^*)$ or $I_{nn}(\omega_n^*)$ need be evaluated. These terms will have to be evaluated for several Mach numbers.

In the first case, assume that the vehicle is divided into twenty-five segments such that the variation in $r(x)\ \alpha_n(x)$ is small over each segment. Let the local normal force be measured with an inertia-compensated balance at each segment. Thus, twenty-five measuring devices will be required. Using the series method, only five power spectral densities will have to be computed.

In the second case, assume that the vehicle is divided into fifty segments such that the pressure has unity spatial correlation over each segment. Let the pressure be measured at eight points around each segment. Four hundred measuring devices will be required. Using the cross spectrum method, as many as 1,275 power spectral densities will have to be computed. Undoubtedly, many of these power spectral densities will be approximately zero. The relation derived in Appendix D will allow the absolute values of the cross term to be determined. This relation may greatly reduce the number of power spectral densities that will have to be computed by determining which terms are negligible.

The smaller quantity of instrumentation and need for calculating fewer power spectral densities indicate that the segments should be selected on the basis of small variation in $r(x)\ \alpha_n(x)$, inertia-compensated balances should be used, and the series method should be used. Further development is necessary in order to obtain a satisfactory inertia-compensated balance system of this type.

Various vehicle parameters can be calculated from the integrated power spectral density of the local normal force coefficients, as shown in Table IV.

Table IV Determination of Vehicle Bending Displacements and Strains

Factors to be Determined	From
$I_{\ell n}(\tilde{\omega})$	$I_{\ell n}(\omega^*)$ and Eq. (71)
$I_{\ell n}(\omega)$	$I_{\ell n}(\tilde{\omega})$ and Eq. (70)
$\phi_{yn}(x,x,\omega)$	$I_{\ell n}(\omega)$ and Eq. (38)
$\langle y_n^2(x)\rangle$	$\phi_{yn}(x,x,\omega)$ and Eq. (39), or $I_{nn}(\omega)$ and Eq. (60)
$\phi_y(x,x,\omega)$	$I_{\ell n}(\omega)$ and Eq. (35)
$\langle y^2(x)\rangle$	$\phi_y(x,x,\omega)$ and Eq. (36), or $\langle y_n^2(x)\rangle$ and Eq. (50)
$3\sigma_y(x)$	Gaussian distribution and $\langle y^2(x)\rangle$ and Eq. (37)
$\phi_{Mn}(x,x,\omega)$	$I_{\ell n}(\omega)$ and Eq. (44)
$\langle M_n^2(x)\rangle$	$\phi_{Mn}(x,x,\omega)$ and Eq. (45), or $I_{nn}(\omega)$ and Eq. (61)
$\phi_M(x,x,\omega)$	$I_{\ell n}(\omega)$ and Eq. (41)

Table IV Determination of Vehicle Bending Displacements and Strains (Cont.)

Factors to be Determined	From
$\langle M^2(x) \rangle$	$\phi_M(x,x,\omega)$ and Eq. (42), or $\langle M_n^2(x) \rangle$ and Eq. (51)
$3\sigma_M(x)$	Gaussian distribution and $\langle M^2(x) \rangle$ and Eq. (43)

SECTION IV. RIGID BODY AND SLOSHING DYNAMICS

In determining the dynamic response of a vehicle, the rigid body and sloshing dynamics must be considered, as well as the bending dynamics. The sloshing liquid of a given mode is represented by a spring, dashpot and mass, as shown in figure 2. The vehicle is assumed to be rigid and only one slosh mode at a time is considered. The rigid body and sloshing dynamics can generate large vehicle stresses when the sloshing mass is asymmetrically positioned on the vehicle. The control system can be disturbed because of the attitude variations of the center line of the vehicle.

The equations of motion of a vehicle with a single slosh mode n can be developed from Newtonian mechanics as

$$I_{vn}\ddot{\beta}_n = +h\beta_n + k_n(\delta_n - \beta_n) + c_n(\dot{\delta}_n - \dot{\beta}_n) + \mu(t) \tag{93}$$

$$I_{sn}\ddot{\delta}_n = -k_n(\delta_n - \beta_n) - c_n(\dot{\delta}_n - \dot{\beta}_n) \tag{94}$$

where

I_{vn} is the moment of inertia of the vehicle about its center of gravity, excluding the mass of the sloshing liquid of the n^{th} mode

I_{sn} is the moment of inertia of the sloshing liquid of the n^{th} mode about the vehicle center of gravity

β_n is the angular deflection of the vehicle attitude angle caused by the oscillations of the n^{th} mode

δ_n is the angular deflection of the liquid of the n^{th} mode

$\mu(t)$ is the buffeting moment about the vehicle center of gravity

h is given by

$$h = C_{M\alpha}\, q\pi r^2\, L^3 \tag{95}$$

Taking Fourier transforms of Eq. (93) and (94) yields

$$[\{(k_n - h) - \omega^2 I_{vn}\} + i\omega c_n]\,\bar{\beta}_n = [k_n + i\omega c_n]\,\bar{\delta}_n + \bar{\mu} \tag{96}$$

$$[\{k_n - \omega^2 I_{sn}\} + i\omega c_n]\,\bar{\delta}_n = [k_n + i\omega c_n]\,\bar{\beta}_n \tag{97}$$

$$\bar{\beta}_n = \frac{\bar{\mu}}{\left[\{(k_n - h) - \omega^2 I_{vn}\} + i\omega c_n - \dfrac{k_n^2 - \omega^2 c_n^2 + 2i\omega c_n k_n}{\{(k_n - \omega^2 I_{sn}) + 2\omega c_n\}}\right]} \tag{98}$$

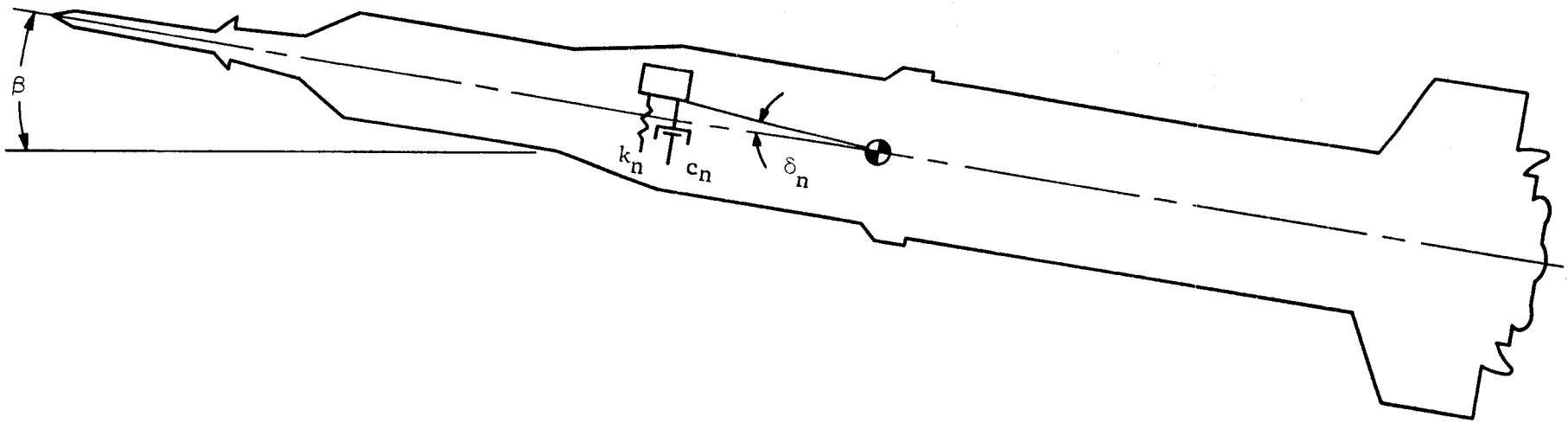

FIGURE 2. COORDINATE SYSTEM FOR THE RIGID BODY AND SLOSHING ANALYSIS

$$\bar{\beta}_n = [(k_n - \omega^2 I_{sn}) + i\omega c_n]\,\bar{\mu} \Big/ \{(k_n - h) - \omega^2 I_{vn}\}\{k_n - \omega^2 I_{sn}\} + i\omega c_n\{(k_n - \omega^2 I_{sn}) + (k_n - h - \omega^2 I_{vn})\} - k_n^2 - 2i\omega c_n k_n \tag{99}$$

$$\bar{\beta}_n = [(k_n - \omega^2 I_{sn}) + i\omega c_n]\,\bar{\mu} \Big/ [\{(k_n - h) - \omega^2 I_{vn}\}\{k_n - \omega^2 I_{sn}\} - k_n^2] - i\omega c_n[\omega^2 I_{sn} + \omega^2 I_{vn} + h] \tag{100}$$

$$\phi_{\beta n}(\omega) = [(k_n - \omega^2 I_{sn})^2 + \omega^2 c_n^2]\,\phi_\mu(\omega) \Big/ [\{(k_n - h) - \omega^2 I_{vn}\}\{k_n - \omega^2 I_{sn}\} - k_n^2]^2 + \omega^2 c_n^2\,[\omega^2 I_{sn} + \omega^2 I_{vn} + h]^2 \tag{101}$$

$$\bar{\beta}_n = \frac{[(k_n - \omega^2 I_{sn}) + i\omega c_n]\,\bar{\delta}_n}{k_n + i\omega c_n} \tag{102}$$

$$\phi_{\delta n}(\omega) = [k_n^2 + \omega^2 c_n^2]\,\phi_\mu(\omega) \Big/ [\{(k_n - h) - \omega^2 I_{vn}\}\{k_n - \omega^2 I_{sn}\} - k_n^2]^2 + \omega^2 c_n^2\,[\omega^2 I_{sn} + \omega^2 I_{vn} + h]^2 \tag{103}$$

$$\phi_{\delta n-\beta n}(\omega) = \omega^4 I_{sn}^2\,\phi_\mu(\omega) \Big/ [\{(k_n - h) - \omega^2 I_{vn}\}\{k_n - \omega^2 I_{sn}\} - k_n^2]^2 + \omega^2 c_n^2\,[\omega^2 I_{sn} + \omega^2 I_{vn} + h]^2 \tag{104}$$

From Appendix C

$$\langle \beta_n^2 \rangle = \int_0^\infty \phi_{\beta n}(\omega)\, d\omega \tag{105}$$

$$\langle \delta_n^2 \rangle = \int_0^\infty \phi_{\delta n}(\omega)\, d\omega \tag{106}$$

$$\langle (\delta_n - \beta_n)^2 \rangle = \int_0^\infty \phi_{\delta n-\beta n}(\omega)\, d\omega \tag{107}$$

It is assumed that the natural frequencies of the various sloshing modes are sufficiently far apart so that there is no coupling of the slosh modes or between the slosh and bending modes. Thus, by the same reasoning used in obtaining Eq. (48) through (51), the power spectral density of the center line deflection β can be written

$$\phi_{\beta}(\omega) = \sum_{n} \phi_{\beta n}(\omega) \tag{108}$$

and

$$\langle \beta^2 \rangle = \sum_{n} \langle \beta_n^2 \rangle \tag{109}$$

If $\langle \beta \rangle$ is small compared to $\langle \delta_n \rangle$, then

$$\langle (\delta_n - \beta)^2 \rangle \approx \langle (\delta_n - \beta_n)^2 \rangle \tag{110}$$

The buffeting moment $\mu(t)$ can be expressed as

$$\mu(t) = 2C_{\mu}(t)\ \pi R^3\ L^3 q \tag{111}$$

Thus

$$\phi_{\mu}(\omega) = 4\phi_{C\mu}(\omega)\ \pi^2 R^6 L^6 q^2 \tag{112}$$

As shown in Section II, the power spectral density of the buffeting moment coefficient in terms of the frequency of the vehicle is obtained from the power spectral density of the buffeting moment coefficient as a function of the reduced frequency by

$$\phi_{C\mu}(\omega) = \frac{L}{V}\ \phi_{C\mu}(\tilde{\omega}) \tag{113}$$

The power spectral density of the buffeting moment coefficient as a function of reduced frequency is obtained from the power spectral density of the moment coefficient in terms of the real frequency during a test by

$$\phi_{C\mu}(\tilde{\omega}) = \frac{V^*}{L^*}\ \phi_{C\mu}(\omega^*) \tag{114}$$

To calculate the sloshing dynamics of the vehicle, the power spectral density of the buffeting moment coefficient about the vehicle center of gravity must be determined. The buffeting moment can be obtained with virtually any choice of segments and measuring devices that is suitable for determining the bending dynamics of the vehicle. A procedure for calculating the sloshing displacements, which will allow the computation of the sloshing stresses, is given in Table V.

Table V Determination of Vehicle Sloshing Displacements

Factors to be Determined	From
$\mu(t^*)$	Pressure data or local normal force data
$\overline{\mu(\omega^*)}$	$\mu(t^*)$ and Eq. (19)
$\phi_\mu(\omega^*)$	$\lim_{T \to \infty} \frac{4\pi}{T} \overline{\mu(\omega^*)}\ \overline{\mu(-\omega^*)}$
$\phi_{C\mu}(\omega^*)$	$\phi_\mu(\omega^*)/(4\pi^2 R^6 L^6 q^2)$, Eq. (112)
$\phi_{C\mu}(\tilde{\omega})$	$\phi_{C\mu}(\omega^*)$ and Eq. (114)
$\phi_{C\mu}(\omega)$	$\phi_{C\mu}(\tilde{\omega})$ and Eq. (113)
$\phi_{\beta n}(\omega)$	$\phi_{C\mu}(\omega)$ and Eq. (101)
$\phi_{\delta n}(\omega)$	$\phi_{C\mu}(\omega)$ and Eq. (103)
$\phi_{\delta n-\beta n}(\omega)$	$\phi_{C\mu}(\omega)$ and Eq. (104)
$\langle \beta_n^2 \rangle$	$\phi_{\beta n}(\omega)$ and Eq. (105)
$\langle \delta_n^2 \rangle$	$\phi_{\delta n}(\omega)$ and Eq. (106)
$\langle (\delta_n-\beta_n)^2 \rangle$	$\phi_{\delta n-\beta n}(\omega)$ and Eq. (107)

SECTION V. BUFFETING CALCULATION METHODS

The primary results of a wind tunnel buffeting test on a rigid model will be time traces of the normal forces or pressures acting on the vehicle. These can be determined by direct measurement with a segmented model or by use of pressure transducers. As previously indicated there are two methods by which the data can be analyzed: the series and cross spectrum methods. If the series method is used, the average local normal force coefficients will be electrically summed by Eq. (82) to yield the coefficients of the series in Eq. (72) as functions of time. These coefficients will then be passed through a power spectral density analyzer to determine the integrated power spectral density, as shown in Eq. (76). If the cross spectrum method is used, the local normal force coefficients will be input to a power spectral density analyzer, which will yield the power spectral densities and the cross power spectral densities of the local normal force coefficients, as shown in Eq. (84). Then, using a digital computer, the integrated power spectral density can be determined by Eq. (90). The integrated power spectral density, determined by either method, must be scaled by Eq. (70) and (71).

From this point, the bending moments and deflections of a vehicle caused by buffeting can be calculated by the equations of Section II. The aerodynamic pitching moment due to buffeting can also be determined from the local normal force coefficients.

Programs have been written for the GE 225 computer that will reduce experimental data. These programs were written so that the PSTL-1 test results could be used as inputs. Modifications necessary to utilize these programs with the test procedure given in this report are presented in the final paragraph of this section. The program that determines the elastic body buffeting is presented in Appendix E. Two auxiliary programs must be used to generate the proper input bending modes. The program given in Appendix F normalizes the bending mode so that Eq. (7) is valid. To do this Appendix F must utilize Appendix G, an interpolation subroutine, which is used in several programs presented in this report. Appendix H describes the computer program that determines the unsteady aerodynamic moment that acts about the vehicle center of gravity.

Appendix E contains the program that calculates the bending moments (figures 1 through 8, Vol. II) and the bending deflections (figures 9 through 12, Vol. II) at each vehicle station. This program requires input of the power spectral densities of the normal force coefficients (figure 3), the bending stiffness (figure 4), the bending modes (figures 5, 6, and 7), and their second derivatives (figures 8, 9, and 10), the dimensionless local radii, the dimensionless vehicle station, and the incremental length of each segment. The program computes the root mean square bending moment and deflection of each missile segment for each mode and for the sum of the modes. The program can also output the power spectral densities of the bending moments and deflections

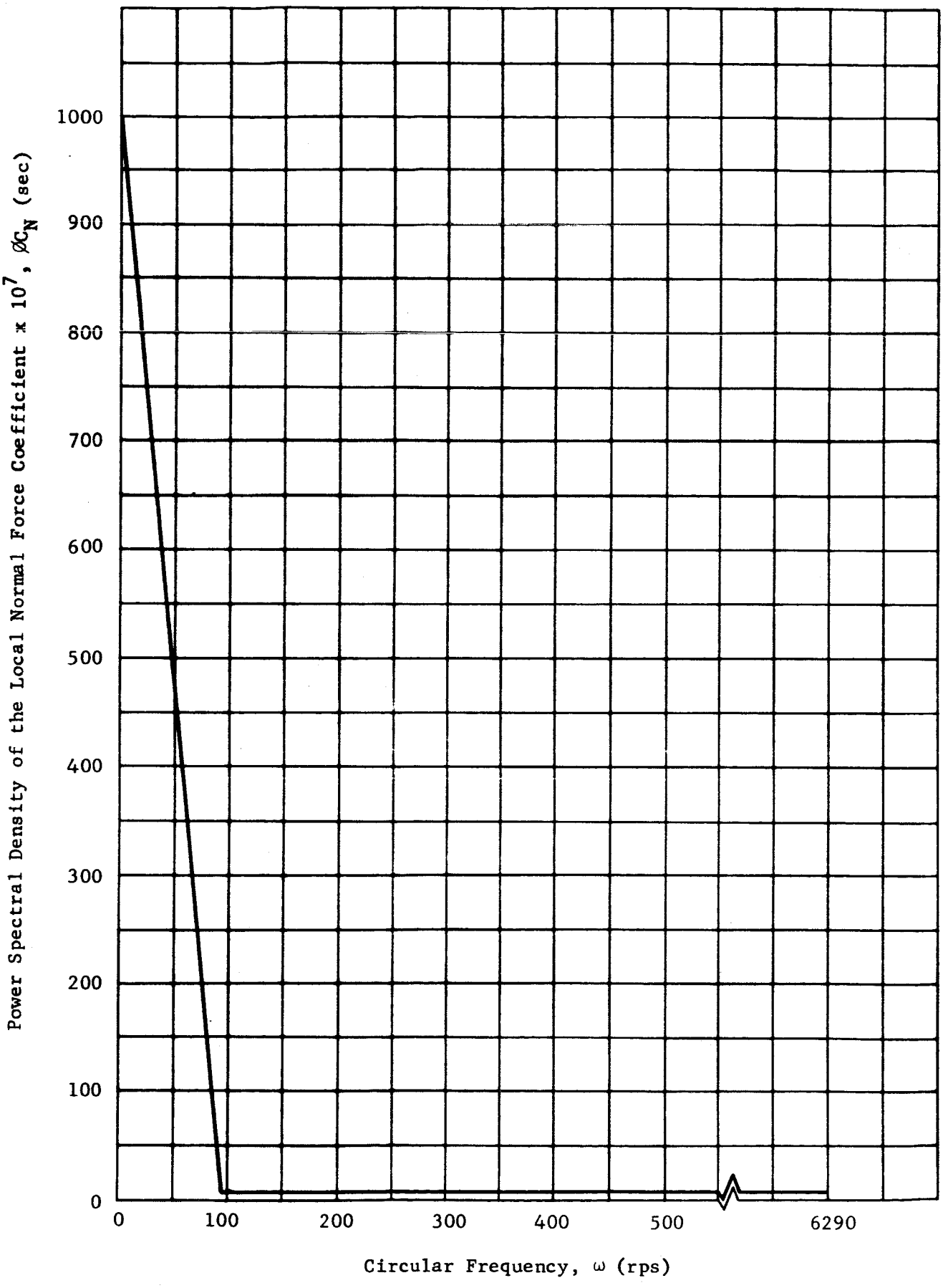

FIGURE 3. ESTIMATED SHAPE OF A TYPICAL LOCAL NORMAL FORCE COEFFICIENT POWER SPECTRAL DENSITY

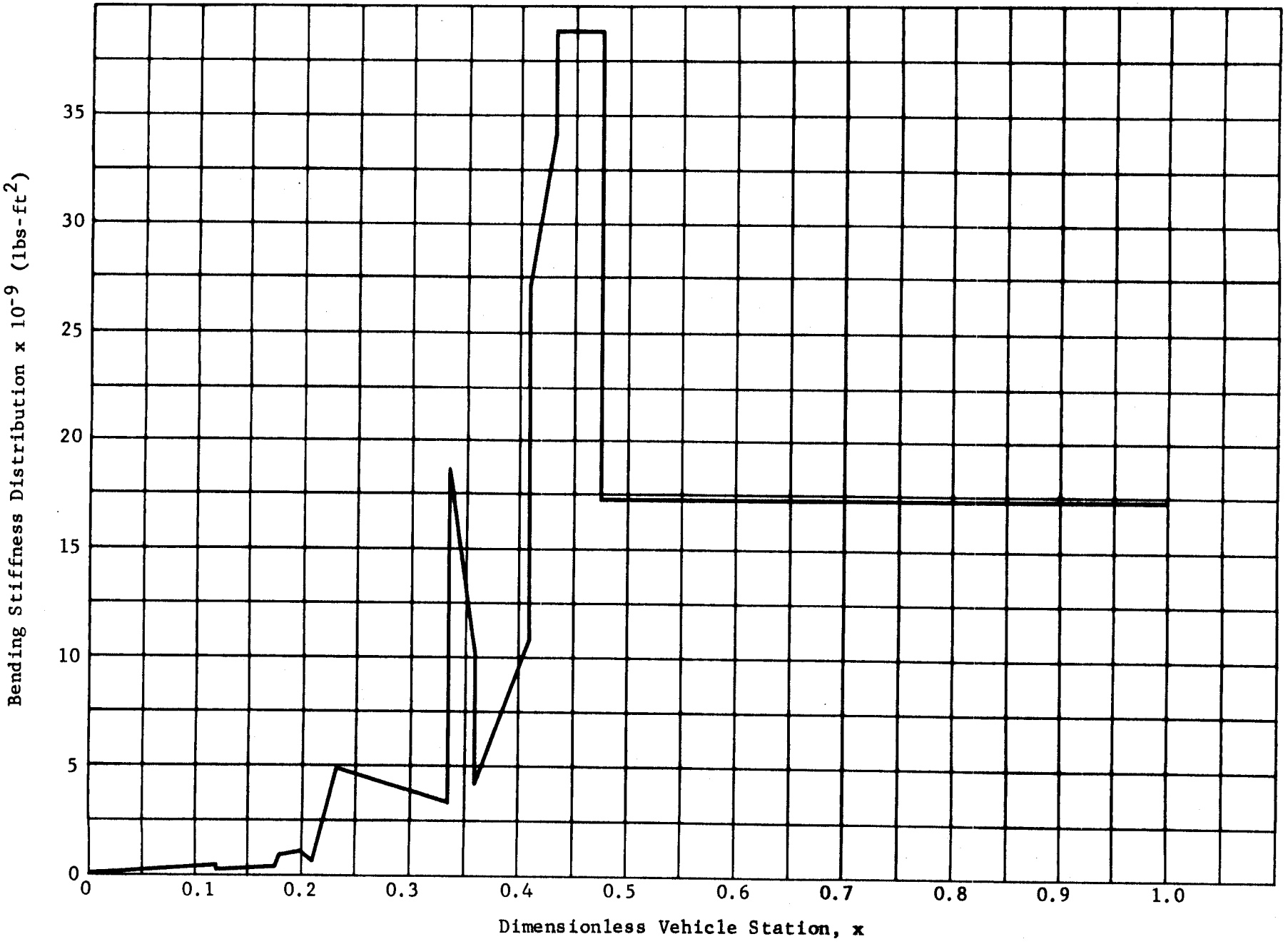

FIGURE 4. SATURN I FULL SCALE BENDING STIFFNESS DISTRIBUTION

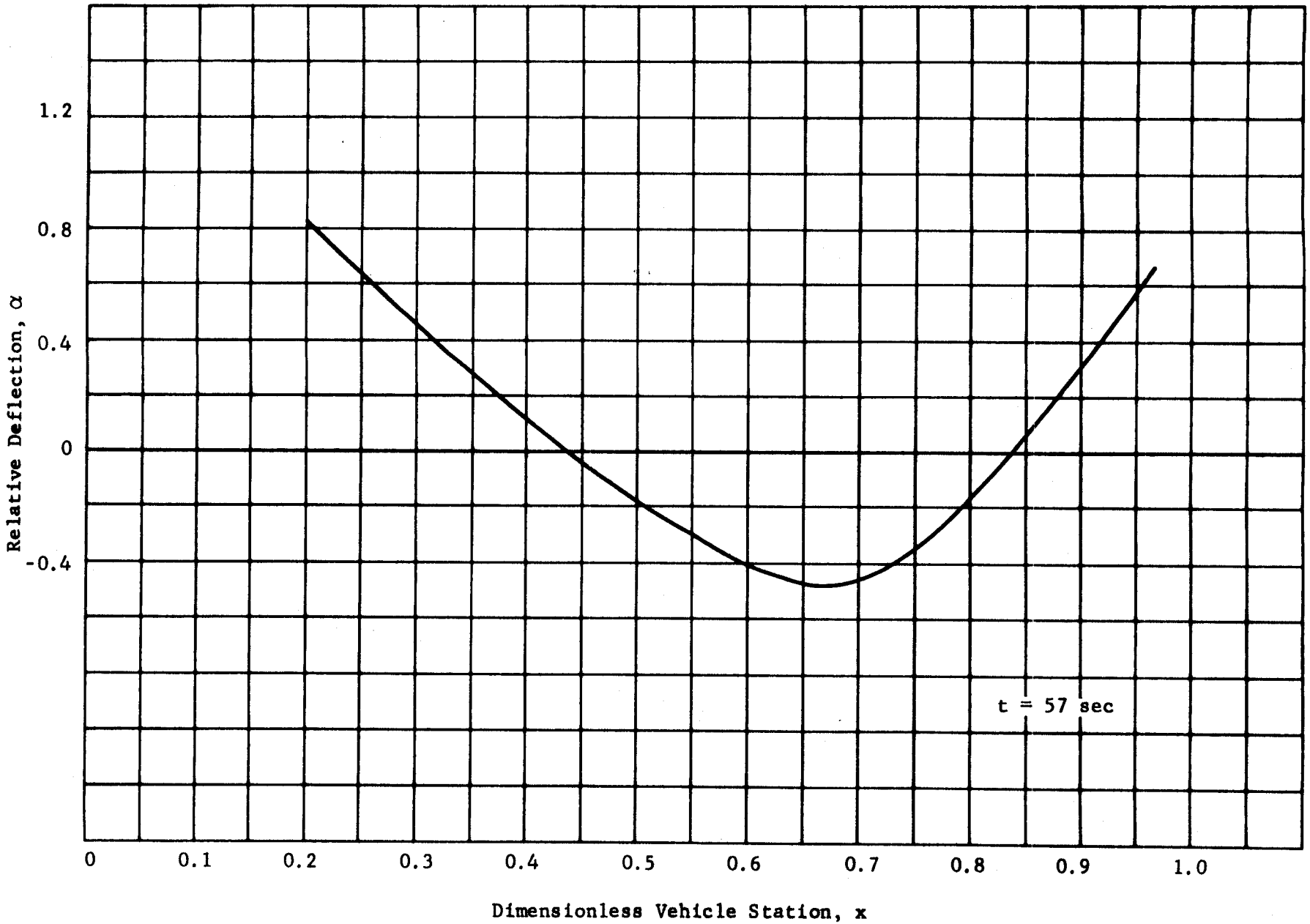

FIGURE 5. SATURN I FULL SCALE BENDING MODE 1

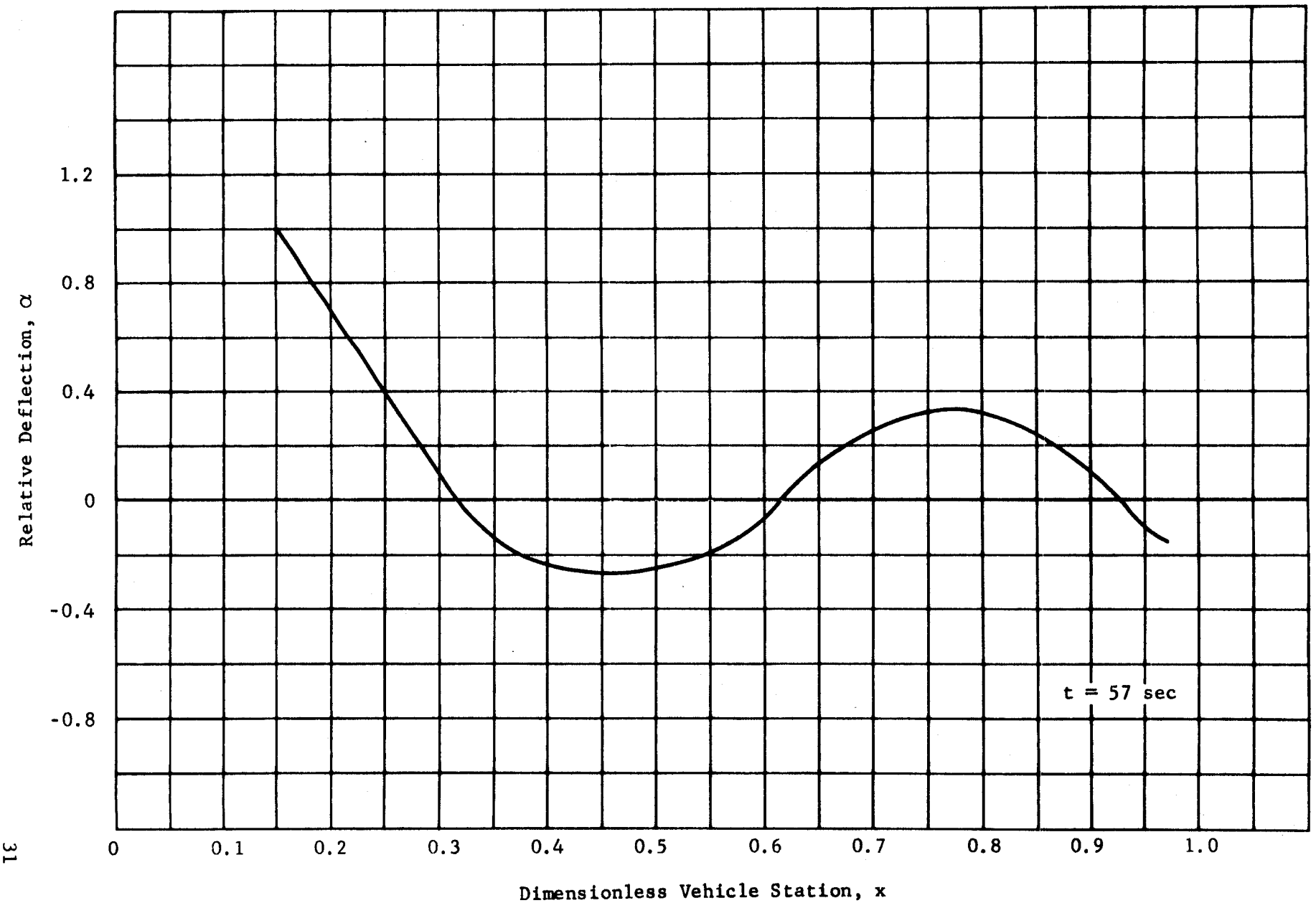

FIGURE 6. SATURN I FULL SCALE BENDING MODE 2

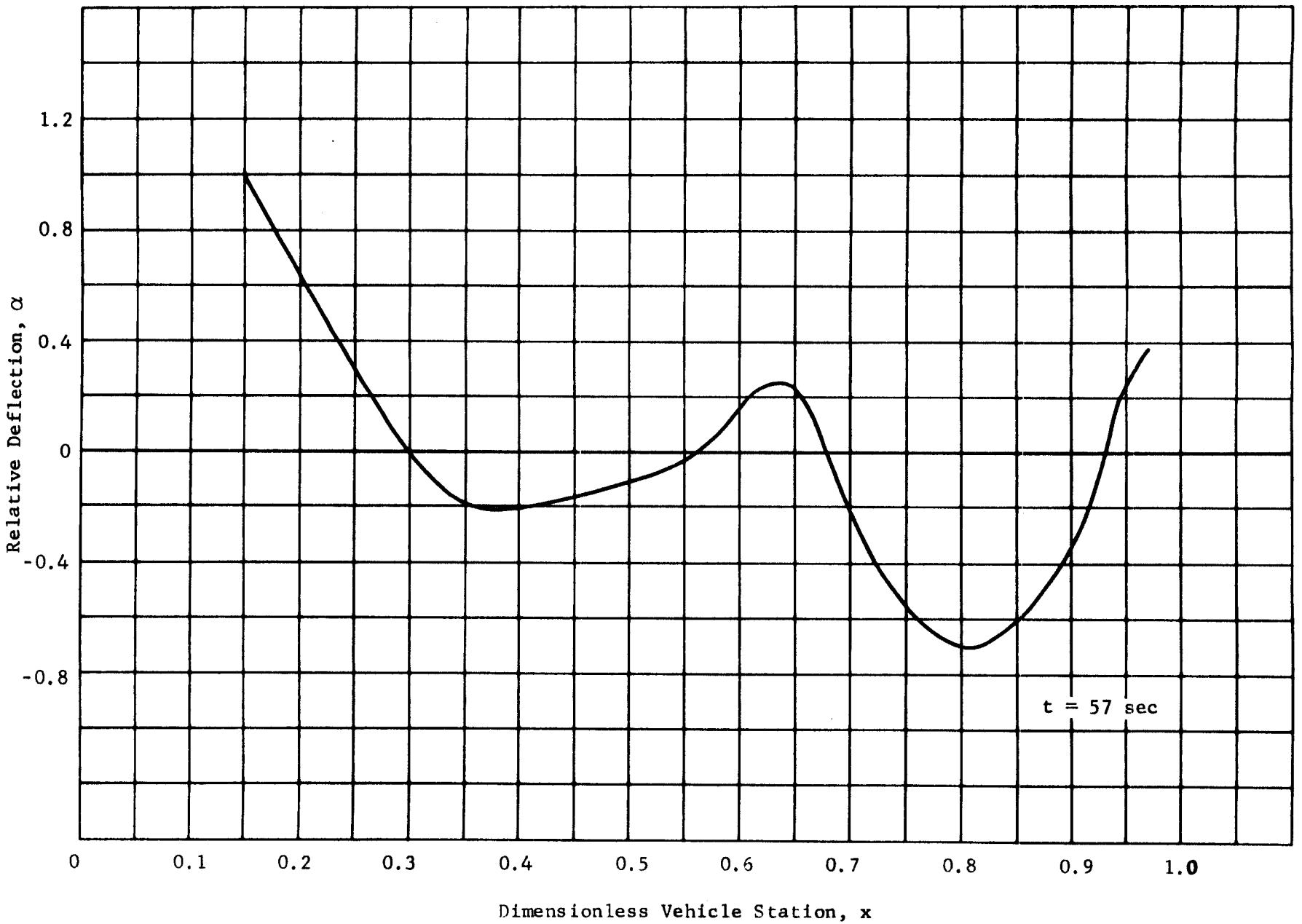

FIGURE 7. SATURN I FULL SCALE BENDING MODE 3

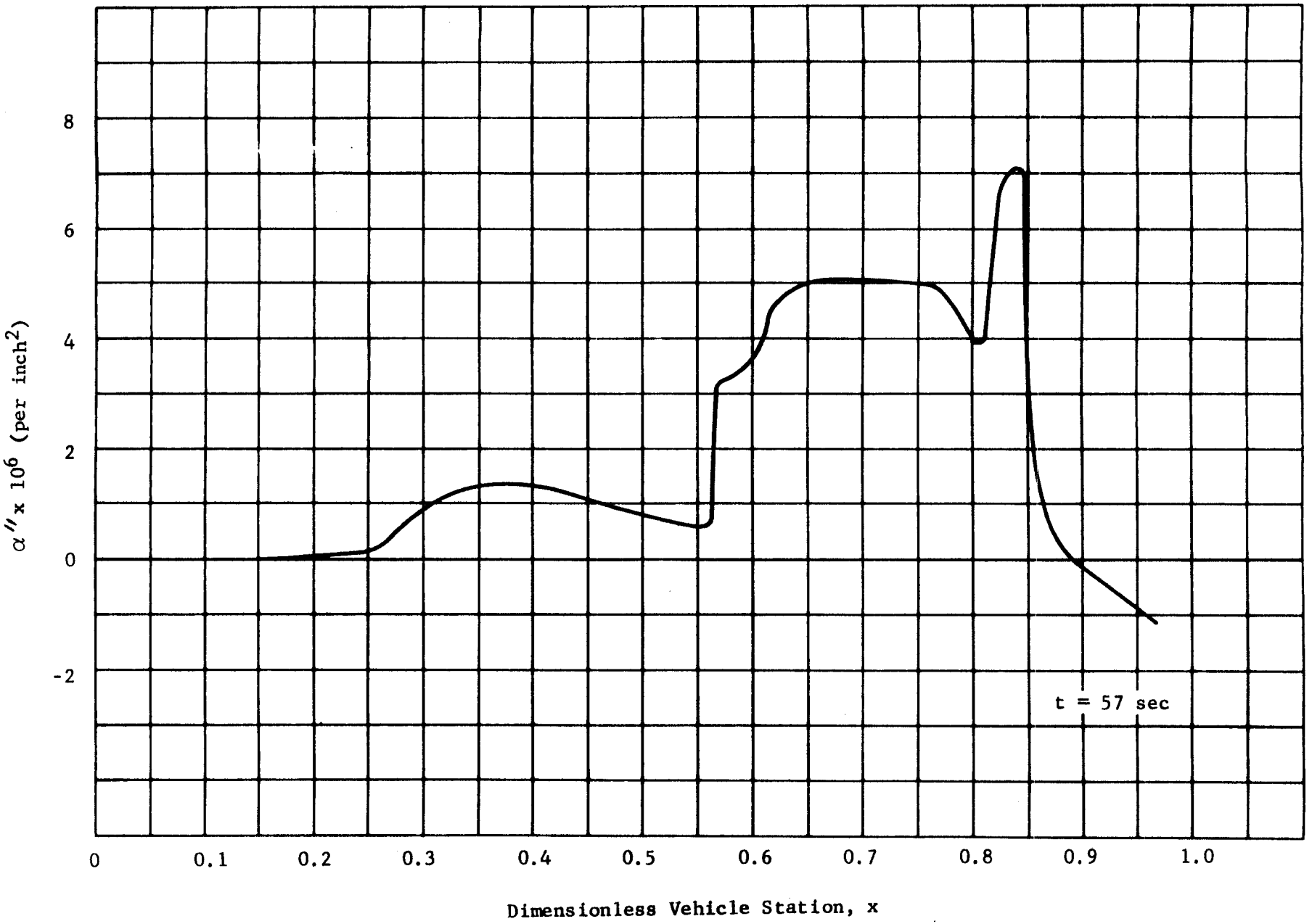

FIGURE 8. SECOND DERIVATIVE OF FULL SCALE BENDING MODE 1

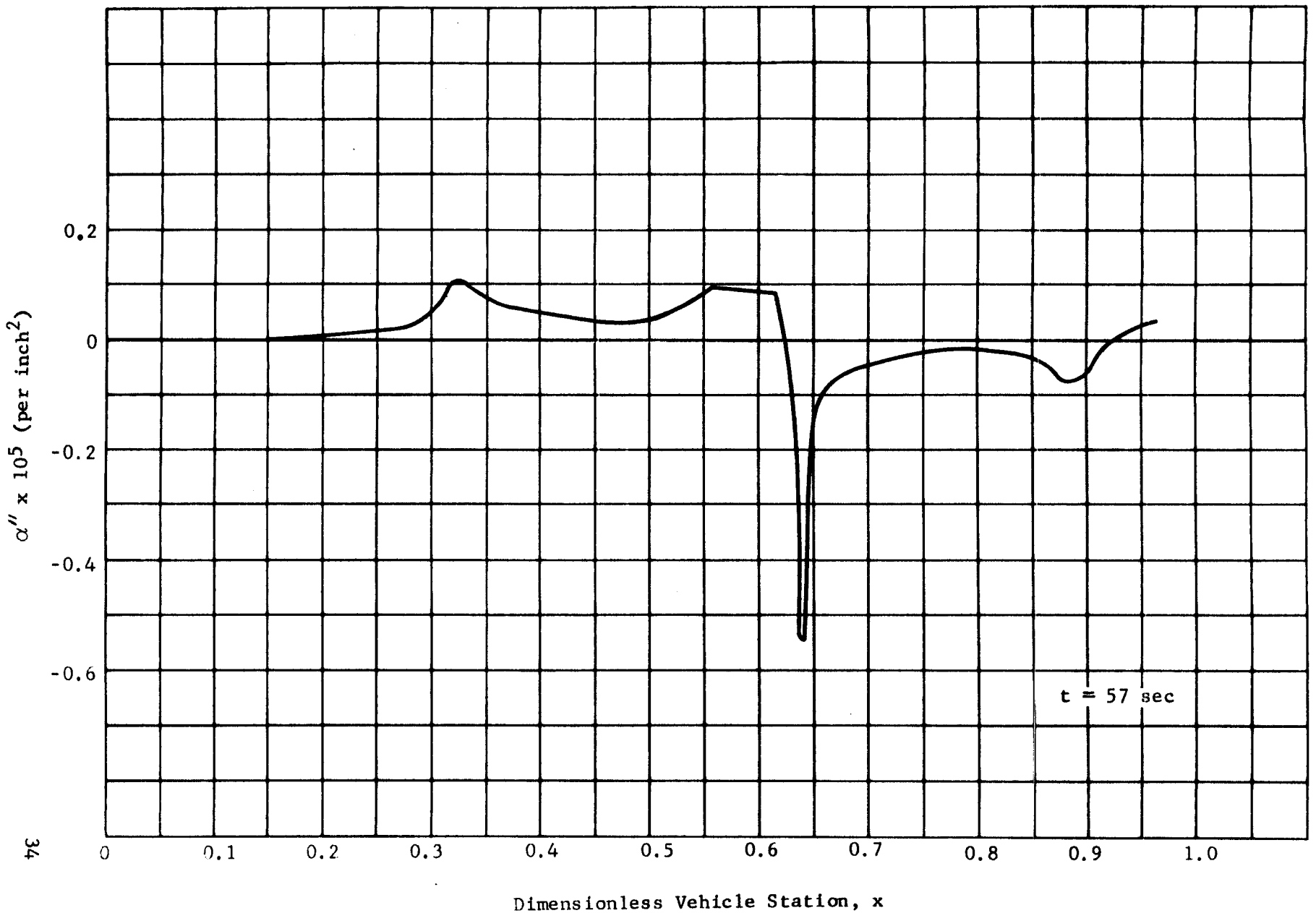

FIGURE 9. SECOND DERIVATIVE OF FULL SCALE BENDING MODE 2

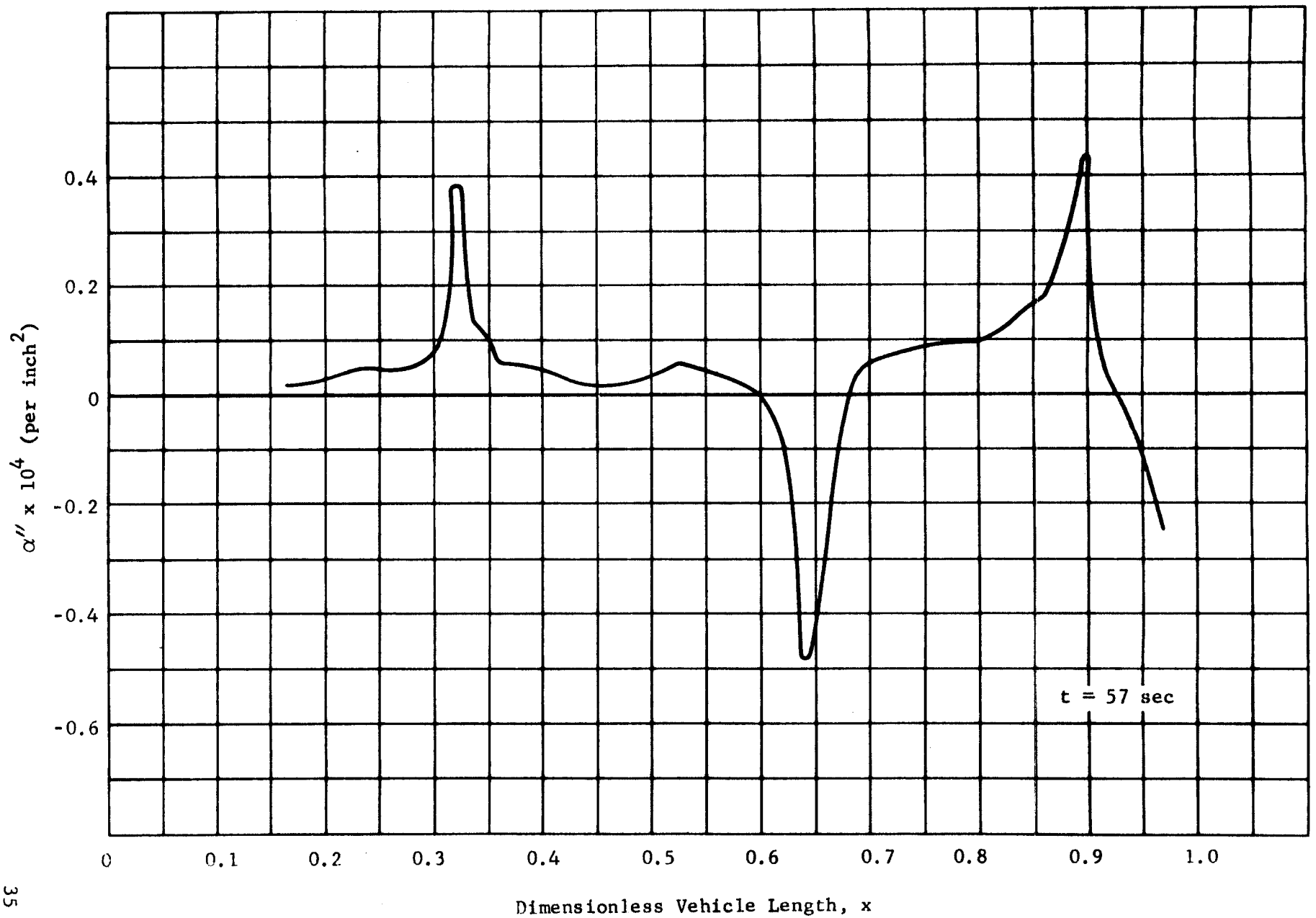

FIGURE 10. SECOND DERIVATIVE OF FULL SCALE BENDING MODE 3

as functions of vehicle circular frequency and vehicle length and the mean square bending moment and deflection caused by frequencies below the particular circular frequency.

The program that determines the RMS pitching moment coefficient (figure 13, Vol. II) is presented in Appendix H. It is necessary to determine the power spectral densities of the normal force coefficient, the vehicle coordinate at which the measurements are taken, the incremental length of each vehicle segment, and the local radii to operate this program. The principal output is the RMS pitching moment coefficient. Also output are the power spectral density of the pitching moment coefficient as a function of frequency (figures 14 and 15, Vol. II) and the mean square of the pitching moment coefficient caused by frequencies below the particular circular frequency.

Both programs are in a form which will accept only the power spectral densities of individual vehicle segments. In their present form they can compute the absolute value of the cross power spectral densities by Eq. (D-5). This choice of inputs is a consequence of the data form of the PSTL-1 tests. To modify these programs to accept cross power spectral density terms and calculate by the cross spectrum method, Section A of the programs, in Appendices F and H, must be removed and the second index on all PHCP (I, I)'s must be changed to J. Then J must be indexed in the read statement for reading the PHCP (I, J)'s. In the pitching moment coefficient program, statement number 21 must be changed to statement number 17; and in the bending moment and deflection program, statement number 19 must be changed to statement number 14. Modifications necessary to adapt these programs to the series method are to remove sections B and C in Appendices F and H. It will then be necessary to input the integrated power spectral density as a function of frequency. Also, the statement W = WD + WI in the pitching moment coefficient program must be given the statement number 13. These programs must be put on a larger computer than the GE 225 in order to have adequate storage to reduce data using either the cross spectrum method, with cross terms input to the program, or series methods of calculation.

The inputs and outputs of the programs described in Appendices E, F, and H are given below.

Table VI Buffeting Calculations

Appendix	Inputs	Outputs
E	$\Phi_N(x,x,\omega)$, EI(x), $\alpha_n(x)$, $\alpha_n''(x)$, r(x), x, Δx	RMS $M_n(x)$, RMS M(x), RMS $y_n(x)$ RMS y(x), $\Phi_M(x,x,\omega)$, $\Phi_y(x,x,\omega)$ frequency components of M_n and y_n
F	$\alpha_n(x)$, m(x)	normalized $\alpha_n(x)$
H	$\Phi_N(x,x,\omega)$, r(x), x, Δx	RMS C_μ, $\Phi_\mu(x,x,\omega)$ frequency component of C_μ

SECTION VI. SATURN I TEST DATA

Several rigid model buffeting tests have been conducted on various configurations (Ref. 3 through 9). The cross spectrum method was used to reduce the data in Ref. 5 and 9. The following general conclusions are drawn from these tests. Variations in angle of attack have only a small effect on the buffeting. In many cases variations in Reynolds number also have only a small effect on the buffeting. In these cases, however, the variation was not great enough to cause the boundary layer to change from turbulent to laminar flow where the measurements were taken. The decrease in buffeting was small as the Mach number increased above one. Removing the tower had only a small effect on the buffeting. The buffeting is not localized to the shock wave intersection with the body; in fact, it occurs over a considerable length. References 3 through 6 indicate that power spectral densities of the buffeting pressure have significant values in the low frequency range. Thus, buffeting occurs in the range where the control system can be affected.

To determine the effects of buffeting on the Saturn I, a series of wind tunnel tests was conducted by NASA/AMES. The objective of these tests was to establish the vehicle deflections and moments caused by buffeting. Rigid body tests were conducted with pressure transducers located in the model. These tests are identified as PSTL-1. Also, an aeroelastic wind tunnel test was conducted using a Saturn model. These two approaches to the problems of buffeting loads should yield identical results if the techniques upon which they are based are correct. Therefore, they should provide checks on one another. The PSTL-1 data are classified even though the results of the Saturn aeroelastic tests and the results of the actual Saturn flight tests are not.

The PSTL-1 tests were performed on a 0.055-scale model of the Saturn I Apollo vehicle at Ames Research Center in the 14-by-14 foot transonic wind tunnel (Ref. 6). The right-hand side of the model was instrumented at 22 stations with pressure transducers bridged to provide output signals proportional to the pressure loading, or local normal force, across the upper and lower halves of the model in the pitch plane. The output signals were also calibrated to be proportional to the moments for each model station and were electronically summed so that a single-trace time history was obtained representing the total fluctuating pitching moments about the first and second bending modal points, at model stations 46.0 and 59.3, respectively. The individual station and summed outputs were recorded on a 30-channel fm tape recorder. The root mean square values of the moment traces are shown in figure 13, Vol. II.

The local normal force traces were used to generate the power spectral densities of the local normal force coefficients (Ref. 6). The root mean square values of the local normal force coefficients were obtained from the power spectral densities (figure 16, Vol. II).

Unfortunately, neither the time traces nor the power spectral densities of the local normal force coefficients were available. The root mean square

values of local normal force coefficients and pitching moment coefficients had to be used as the basis of the data reduction. The direct terms in the power spectral density of the local normal force coefficients can be estimated from the RMS values of the coefficients and from observing power spectral densities obtained from other similar tests. The power spectral densities of the local normal force coefficients are then used to compute the bending dynamics of the vehicle by the cross spectrum method. The series method can not be used with the PSTL-1 data because time traces of the local normal force coefficients are required for the series calculations; thus, the cross spectrum method of analysis was applied to the data.

From an examination of the data presented in Ref. 4 through 9, the general shape of the local normal force coefficient power spectral densities was determined. This shape is composed of a line with a slope of $-0.4/q^2$ and of a line of zero slope (figure 3). An upper limiting value for the zero slope portion of the curve was determined from the above mentioned references as $4/q^2$. The zero slope portion of the curve is white noise, which can be caused by turbulence. Assuming that it is turbulence, the turbulent portion of the RMS local normal force coefficient is estimated by observing the normal force coefficients at portions of the body where shock waves and flow separations should not exist. The area under the zero slope lines of the power spectral density curve from $\omega = 0$ to $\omega = 6290$ radians/sec is equal to the mean square of the turbulent portions of the local normal force coefficient. This establishes the magnitude of the zero slope line. However, if the magnitude exceeds the upper limit of $4/q^2$, then this upper limit is used as the magnitude of the zero slope line. The area under the entire power spectral density curve from $\omega = 0$ to $\omega = 6290$ radians/sec is equal to the mean square of the local normal force coefficient. This establishes the $\omega = 0$ intercept of the $-0.4/q^2$ line. The absolute values of the cross terms were determined by the methods in Appendix D.

The procedure that permits the computation of the power spectral densities of the local normal force coefficients from the root mean square values of the local normal force coefficients is described in Appendix I. These power spectral densities are used to compute the root mean square buffeting pitching moment coefficient, the bending moments, and the bending deflections by the procedures presented in Appendices H and E, respectively.

The previous analysis required the use of certain vehicle parameters. The mass distribution, m, obtained from Ref. 10, is shown in figure 11. Bending stiffness distribution was also obtained and is shown in figure 4. The bending modes were taken from Ref. 11 and are shown in figures 5, 6, and 7. The second derivatives of the bending modes with respect to longitudinal distance were determined from figures 5, 6, and 7 and are presented in figures 8, 9, and 10. Both the bending modes and their second derivatives are normalized by the procedures presented in Appendix F. A damping ratio of 0.01, which is the damping ratio of the vehicle structure, was used in the reduction of the PSTL-1 data.

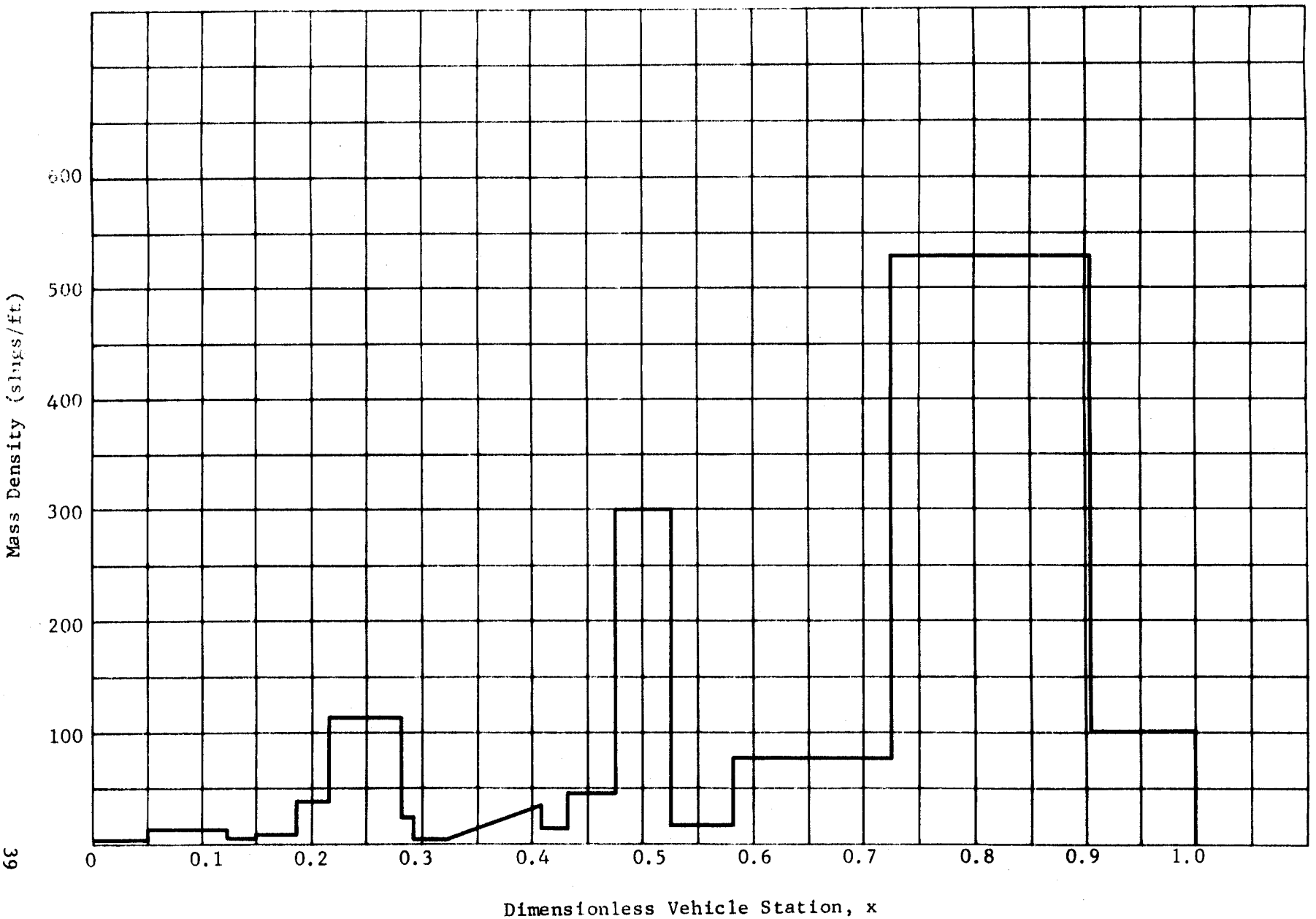

FIGURE 11. SATURN I FULL SCALE VEHICLE MASS DISTRIBUTION

The power spectral densities of the local normal force coefficients and the other parameters were inputs to the two programs. In one case, calculations are made based on no correlation between segments; i.e., $\phi_N(x_i,x_j,\omega) = 0$, for $i \neq j$. In the other, calculations were made assuming maximum correlation between segments (assuming the most adverse conditions). The results of these calculations are shown in figures 1 through 13, Vol. II.

A description of the bending modes that is more accurate than that used in the data reduction is given in Ref. 12 and 13. These mode data were obtained from dynamic tests of a full scale vehicle. However, these test data included the multitank data of the first stage. The analysis used in this report is based on the vehicle being represented by a single beam. Hence, the single beam modes of Ref. 11 were used in the data reduction.

SECTION VII. RESULTS AND CONCLUSIONS

Analyses have been made in the previous sections to determine suitable forms for wind tunnel buffeting data taken with rigid models. Data expressed in these forms will allow gross vehicle stresses and displacements to be calculated. Both the bending and the sloshing responses of the vehicle have been considered. Assumptions on which the analysis is based are listed in the introduction. Two methods of determining the integrated power spectral density of the local normal force coefficient are considered. One is the series method, the other is the cross spectrum method. The series method does not require that as many power spectral densities be calculated. Several approximations are made which greatly reduce the labor in calculating the bending dynamics of the vehicle.

The data reduction procedures previously described were applied to the PSTL-1 test results. The direct terms of power spectral densities were estimated from the RMS values of the local normal force coefficients by the methods of Appendix I. These were used to calculate the absolute values of the cross terms. The power spectral densities were used in turn to calculate the root mean square pitching moment coefficient about model stations 46 and 59.3, and are presented in figure 13, Vol. II. Two data reduction techniques were used. In one case it was assumed that there was no pressure correlation between segments, so the cross terms were set equal to zero. In the other case, the maximum possible correlation between segments was used. The power spectral densities of the pitching moments are shown in figures 14 and 15, Vol. II. The RMS moment calculations are compared with the measured value of the moment coefficient. The computed values bracket the experimental values. The results with the assumption of no correlation between segments compare more favorably with the experimental results than those based on maximum correlation. These results indicate that the method used to estimate the power spectral densities of the local normal force coefficients gives reasonable results. The bending deflections and moments based on these power spectral densities were determined and are shown in figures 1 through 12, Vol. II. The control system and aerodynamic damping was not considered. A damping ratio of 0.01 was used in the calculations.

Aeroelastic wind tunnel tests using a flexible model of the Saturn I, whose dynamic characteristics match those of the flight vehicle, were conducted at NASA/Langley. These tests are described in Ref. 14 and 15. The aeroelastic tests were conducted at $M = 0.9$, whereas the PSTL-1 test data were at $M = 0.8$. A strain gage was used to measure the model bending moment at a station. From this information, the model bending moments along the entire vehicle were determined. The vehicle bending moments were scaled from the model moments. The scaling rule (Ref. 14) includes the vehicle damping ratio. In reducing the aeroelastic data, a value for the vehicle damping ratio was obtained (Ref. 15) by summing the structural damping ratio, the aerodynamic damping ratio, and a control damping term. The values used in determining the total vehicle

damping of the 1st mode were 0.011, 0.006, and 0.0467, respectively, for a total of 0.0637. The RMS values of the bending moments obtained from these tests are shown in figure 12. In order to provide a basis of comparison between the aeroelastic tests and the PSTL-1 tests, the PSTL-1 data were reduced using a damping ratio of 0.064. The results of these calculations are shown in figures 17 and 18, Vol. II. The general magnitudes of the bending moments compare favorably in spite of the Mach number differences. However, the shape of the RMS bending moment curve is much more erratic than that obtained from the aeroelastic tests. The methods used to reduce the aeroelastic test data and the method used to reduce the PSTL-1 data were examined to determine why the shapes of the bending moment curves differ. The RMS bending moment of the aeroelastic test is based on figures 13, 14, and 15. These curves, the bending moments for unit nose deflections in feet, were computed by

$$\frac{M(x)}{y_n(0)L} = \frac{\omega_n^2 L^2}{\alpha_n(0)} \int_0^x m(x)\ (x - \bar{x})\ \alpha_n(\bar{x})\ d\bar{x} \tag{113}$$

where $M(x)/y_n(0)L$ is the bending moment for a unit nose deflection, and the length of the vehicle L includes the height of the tower. $\alpha_n(x)$ is based on this length. This equation is derived in Appendix K. The method used to compute the bending moment per unit nose deflection in reducing the PSTL-1 data is given by

$$\frac{M(x)}{y_n(0)L} = \frac{EI\ \alpha_n''(x)}{L^2\ \alpha_n(0)} \tag{40}$$

Results of these two methods are given in figures 16 through 19. The two methods are equivalent, as shown in Appendix L. However, their equivalence is dependent on α_n, m, and EI satisfying Eq. (9).

$$\alpha_n(x) = \frac{1}{m\omega_n^2} \left(\frac{EI}{L^4}\ \alpha_n''(x) \right)'' \tag{9}$$

These three factors were obtained from three different sources. If they do not satisfy the equation, then errors are introduced into the data reduction. Equation (9) is written in integral form in Appendix M. The equation was programed on a GE 225 computer, and is described in Appendix M. The inputs to the program consist of the bending mode, mass distribution, bending stiffness, length, and the natural frequency of the mode. The outputs are the computed bending mode and the input bending mode. These will be identical if Eq. (9) is satisfied.

The equation was solved on the computer using the vehicle parameters used in reducing the PSTL-1 data. The results are shown in figure 20. These results may explain the difference between the shapes of the two bending moment curves. They may also make the reduction of the PSTL-1 data suspect. However, the general agreement of the magnitudes of the root mean square values of the bending moments indicates that only small overall errors are caused by the inaccuracies in the vehicle parameters used.

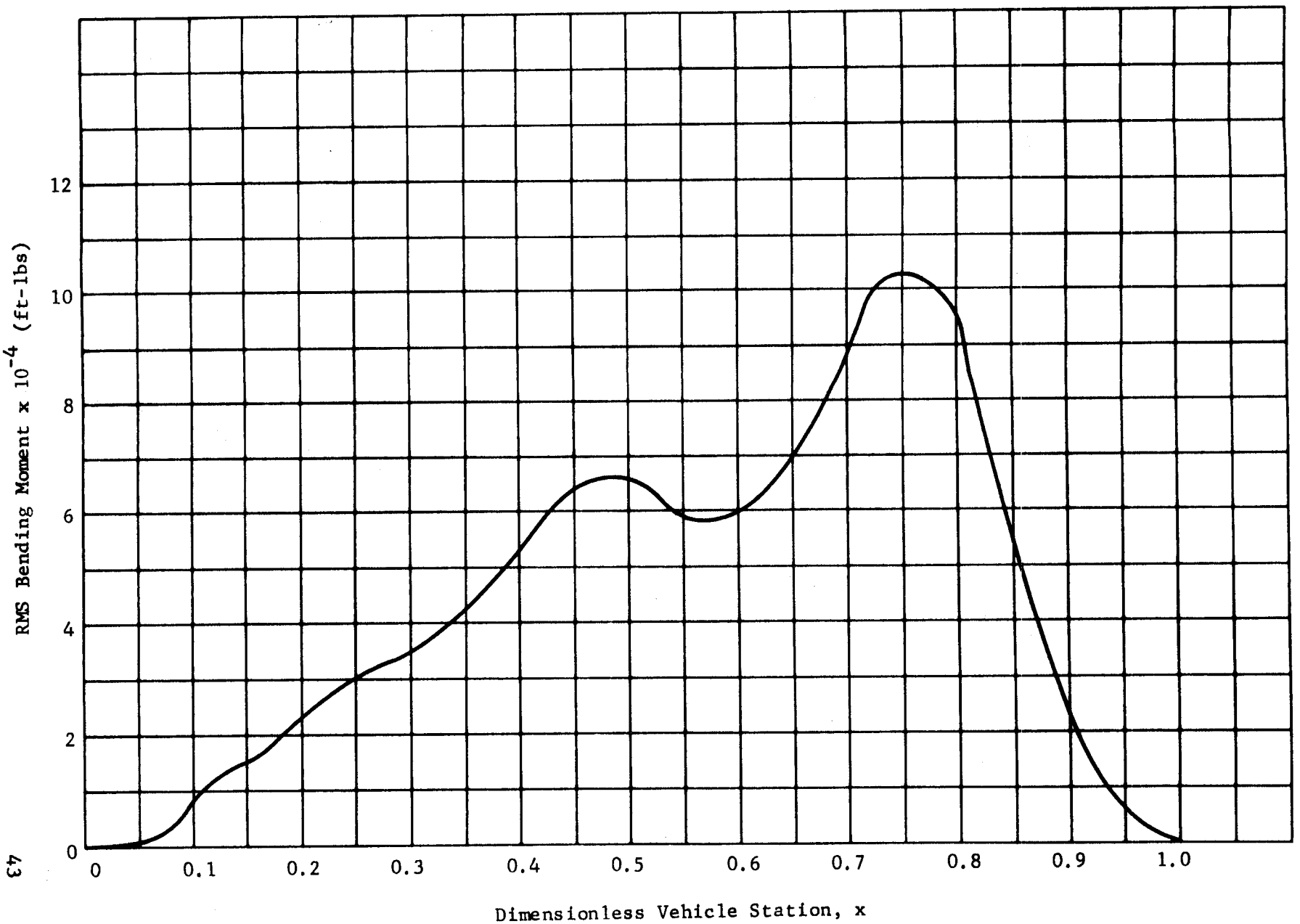

FIGURE 12. SATURN I FULL SCALE RMS BENDING MOMENT OBTAINED FROM AEROELASTIC TEST

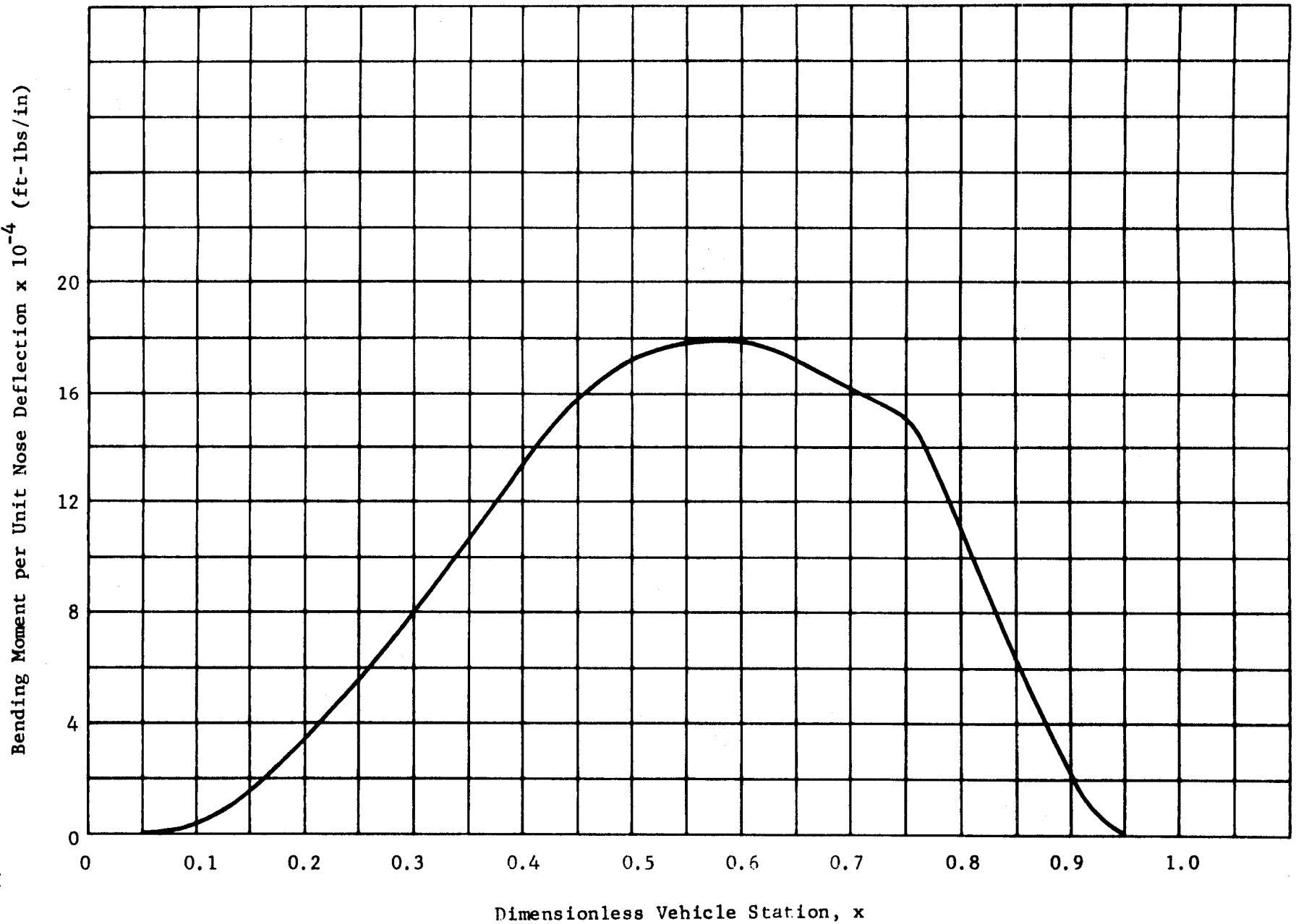

FIGURE 13. SATURN I FULL SCALE BENDING MOMENT PER UNIT NOSE DEFLECTION FOR MODE 1 FROM AEROELASTIC TEST

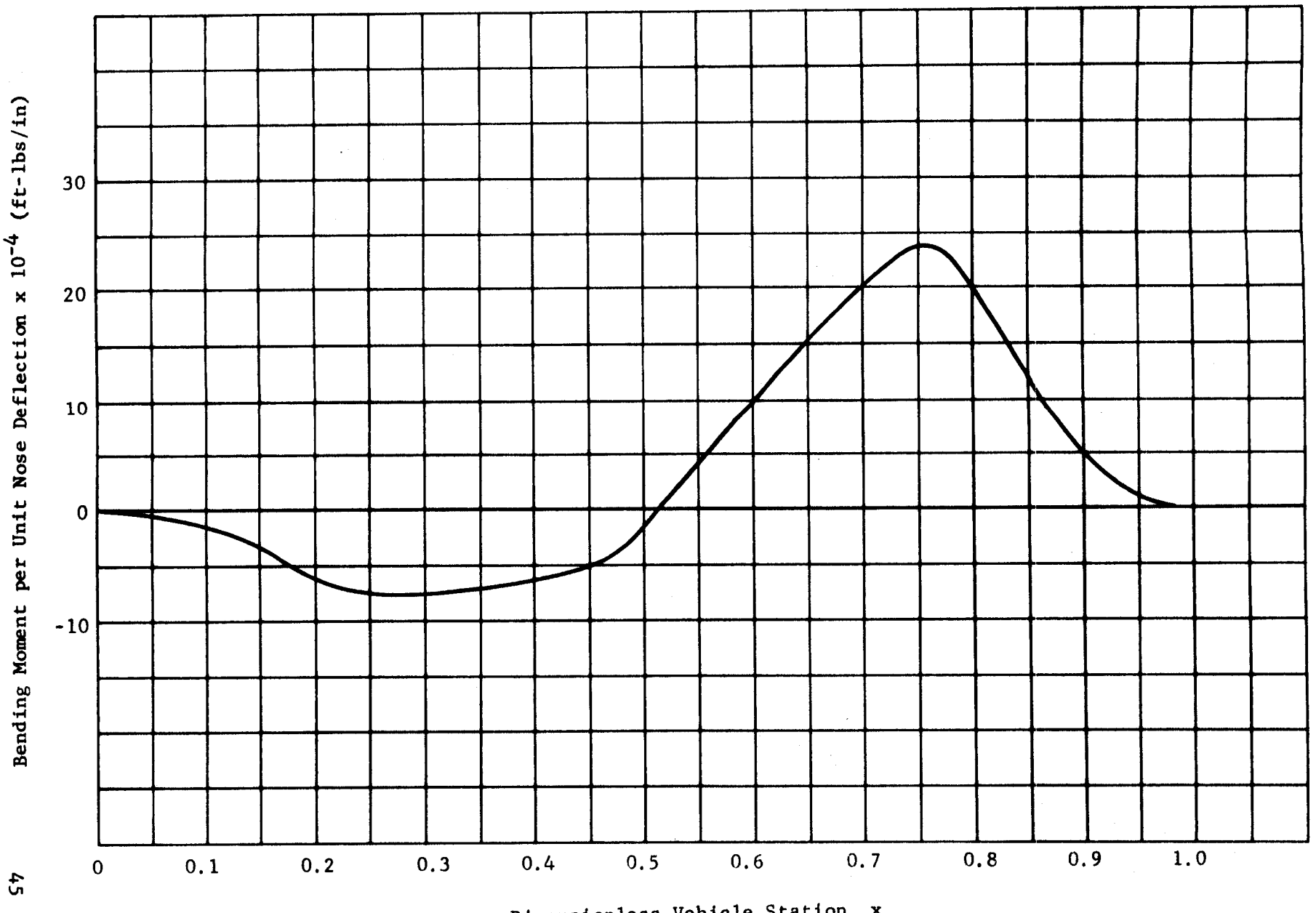

FIGURE 14. SATURN I FULL SCALE BENDING MOMENT PER UNIT NOSE DEFLECTION FOR MODE 2 FROM AEROELASTIC TEST

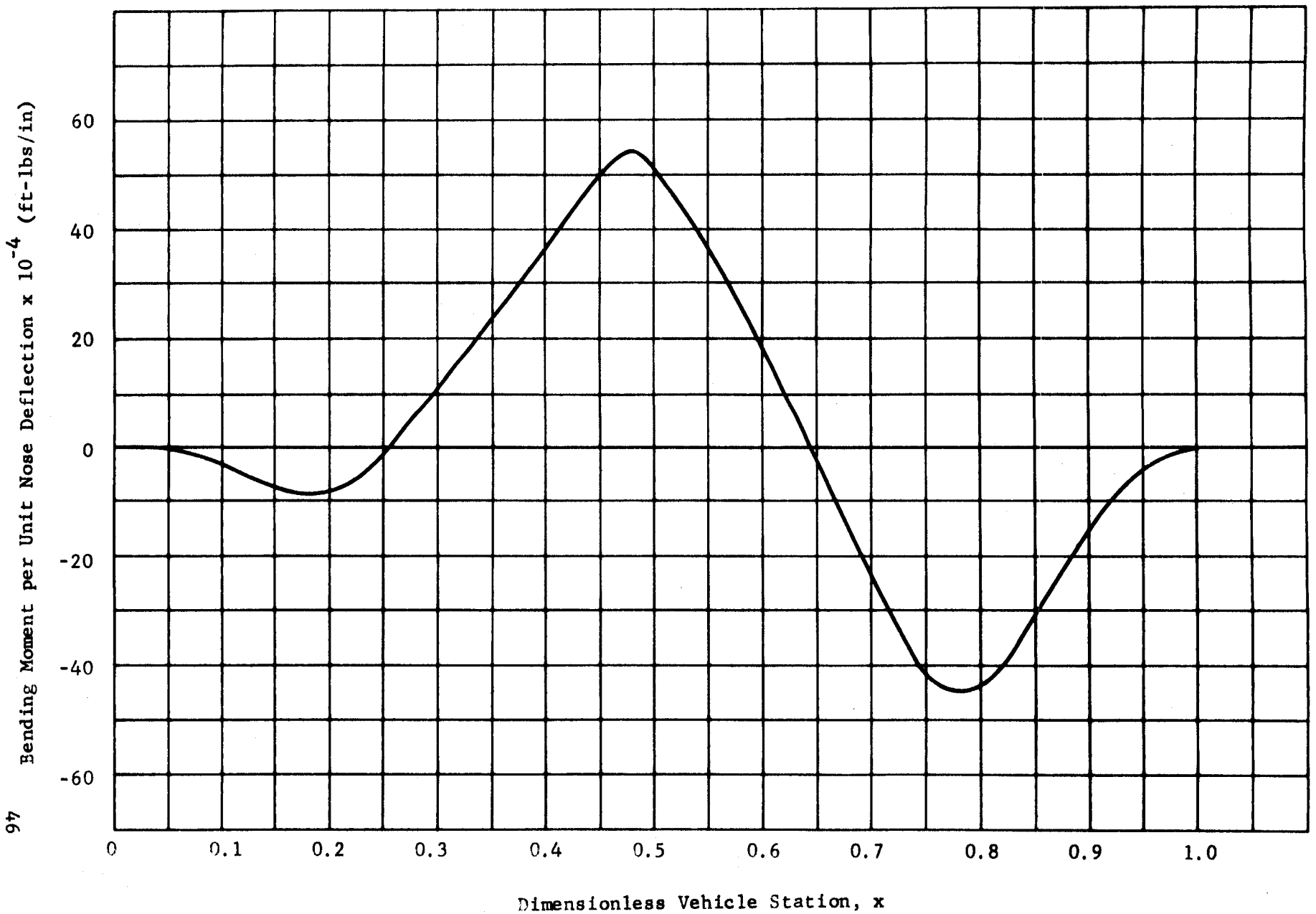

FIGURE 15. SATURN I FULL SCALE BENDING MOMENT PER UNIT NOSE DEFLECTION FOR MODE 3 FROM AEROELASTIC TEST

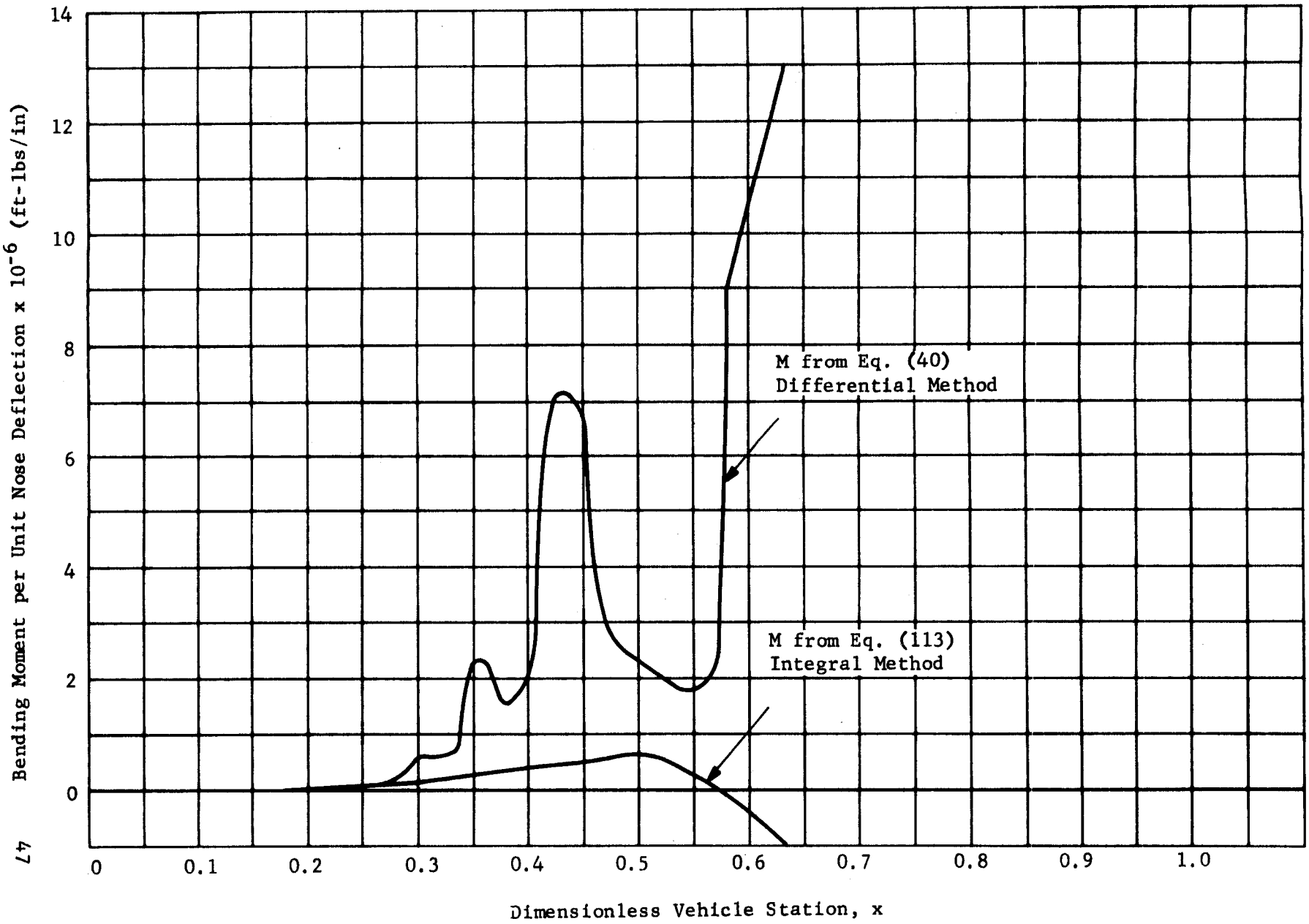

FIGURE 16. SATURN I FULL SCALE BENDING MOMENT PER UNIT NOSE DEFLECTION FOR MODE 1

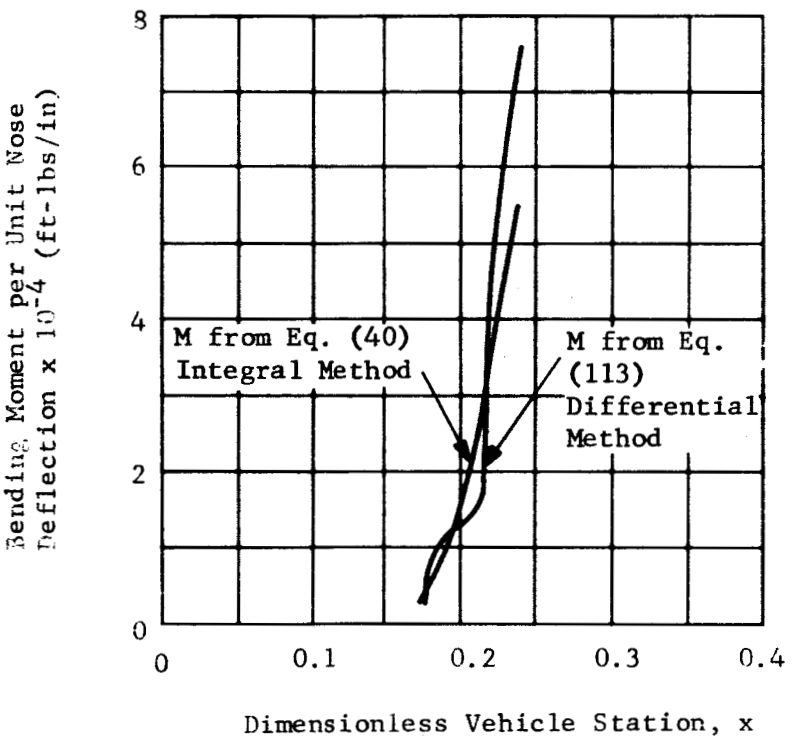

FIGURE 17. SATURN I FULL SCALE BENDING MOMENT PER UNIT NOSE DEFLECTION FOR MODE 1 ON AN EXPANDED SCALE

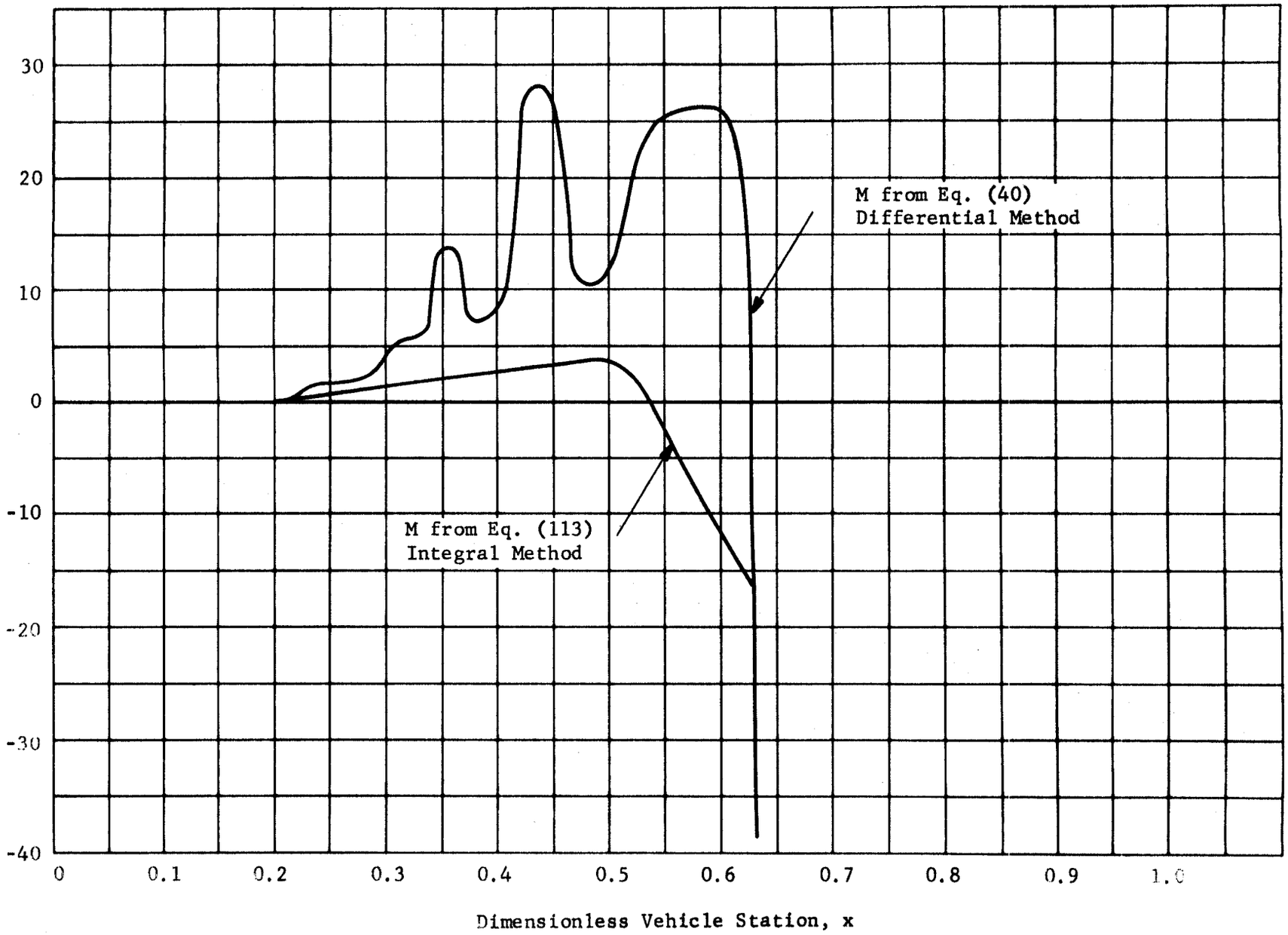

FIGURE 18. SATURN I FULL SCALE BENDING MOMENT PER UNIT NOSE DEFLECTION FOR MODE 2

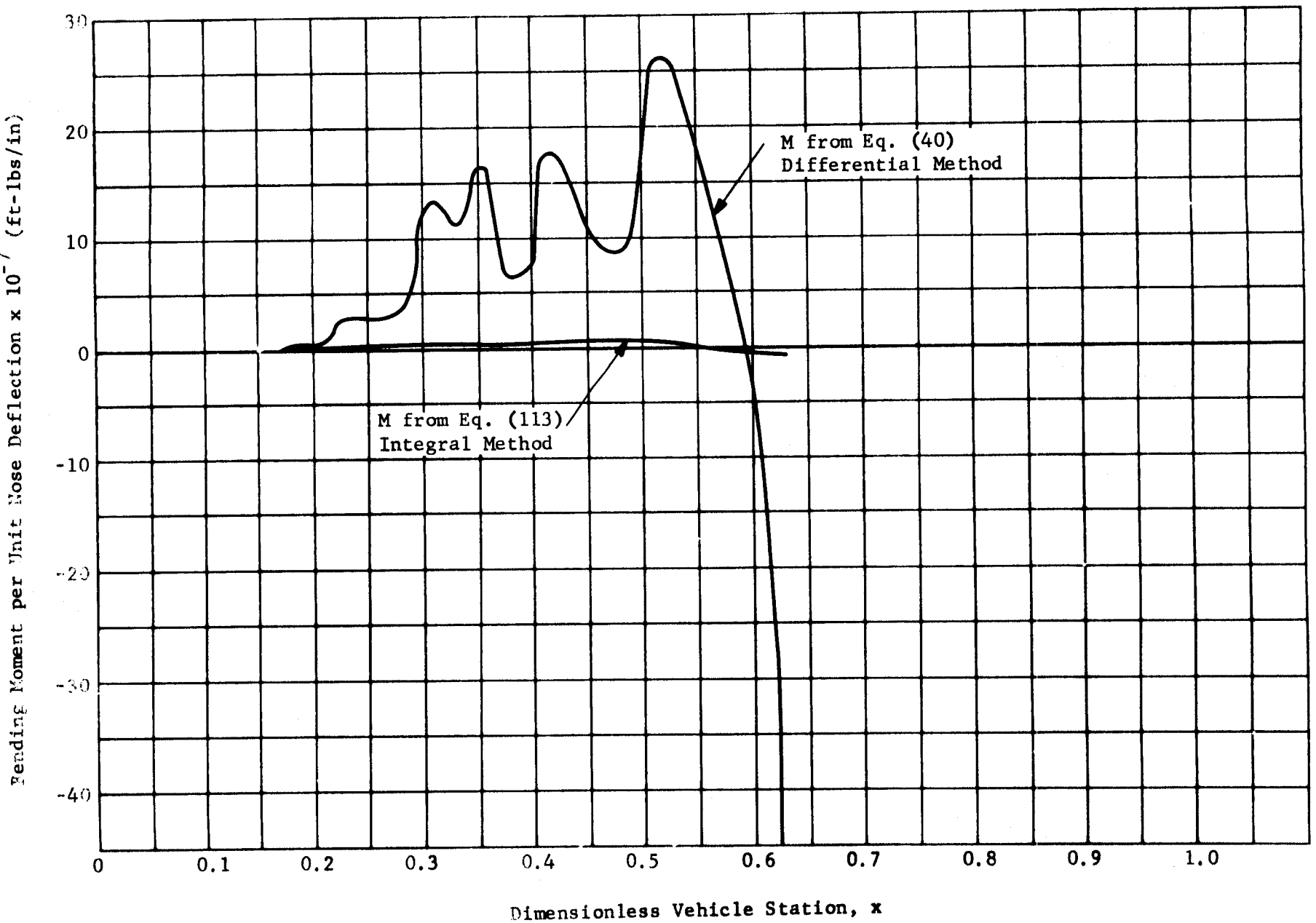

FIGURE 19. SATURN I FULL SCALE BENDING MOMENT PER UNIT NOSE DEFLECTION FOR MODE 3

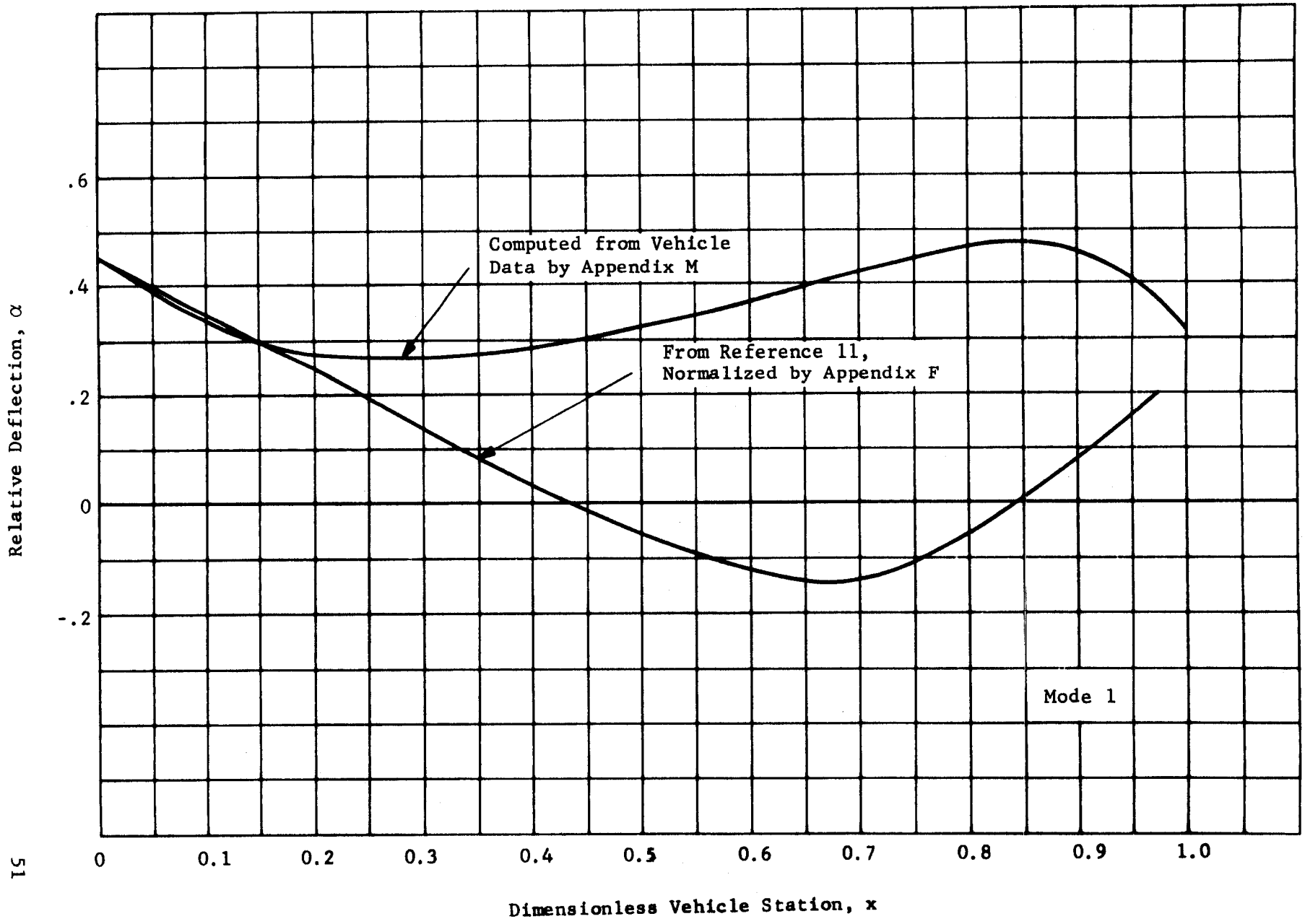

FIGURE 20. COMPARISON OF BENDING MODES

The flight test of SA-7 was examined for buffeting loads (Ref. 16). A graph showing the angular deflection in yaw at the instrumentation unit (vehicle station 0.342) with respect to the stabilized platform is shown in figure 19, Vol. II. This deflection includes the effects of winds, misalignments, flight path correction, and control errors, as well as the buffeting deflections. It is assumed that the signal is not filtered between 0.25 and 3.0 cps. The buffeting deflections occur at a frequency of 2.2 cps and higher. The principal fluctuations occur at a much lower frequency. RMS buffeting deflections of the first bending mode determined from the PSTL-1 test data yield deflections of 0.0117 degrees for the maximum case and 0.00344 degrees for the minimum case. These values are consistent with the higher frequency oscillations of the flight test data. The agreement between the results of the PSTL-1 tests and the flight tests appears satisfactory.

The following conclusions are drawn from the analyses and results of this report. Two methods can be employed in reducing the data of a rigid model buffeting test: the series method, and the cross spectrum method. The series method does not require that as many power spectral densities be computed as does the cross spectrum method. If local normal forces are measured with inertia-compensated balances, fewer measuring units are required than if pressures are measured at points along the body. Likewise, if local normal forces are measured with inertia-compensated balances, fewer measuring units will be required if the segments are divided such that variations in $r(x)\ \alpha_n(x)$ are small over each segment.

From a comparison of the reduced PSTL-1 test data with the results of the aeroelastic tests and the flight test, it can be concluded that the analyses and data reduction procedures derived in the report are accurate. Further, it can be concluded that, in general, the measurements taken during the test were accurate, and the method used in estimating the power spectral density of the local normal force coefficients is reasonably accurate. The results indicate that the gross effects of buffeting on a launch vehicle can be determined from rigid body tests. The PSTL-1 tests and the aeroelastic tests show that the gross vehicle effects of buffeting on the Saturn I are small.

Several general conclusions can be drawn from numerous tests that have been conducted in the field. The removal of the escape tower from the Saturn does not greatly reduce the buffeting. Small changes in angle of attack do not change the buffeting level. Changes in Reynolds number do not appear to change the buffeting level so long as transition of the boundary layer does not occur at the point in question. Buffeting occurs at Mach numbers considerably greater than one. The buffeting is not localized, but instead occurs over large portions of a body.

SECTION VIII. RECOMMENDATIONS

The following recommendations are made:

1. The buffeting data obtained in the PSTL-1 tests should be applied to the Saturn V. The upper portion of the Saturn V is similar to the upper portion of the Saturn I and most of the buffeting occurs in the upper region. By using the Saturn V mass, stiffness, and bending modes, the gross effects of buffeting on the Saturn V can be estimated.

2. The buffeting response of the Saturn I should be recomputed based on the PSTL-1 test data, but with better mass and stiffness characteristics and with better defined bending modes. These characteristics must satisfy Eq. (9). The information used in the computations of this report does not satisfy this equation. An accurate knowledge of vehicle characteristics should increase the accuracy of the buffeting calculations.

3. Wind tunnel tests should be run again with the same model used in the PSTL-1 tests. However, the tests should be run over a broader Mach number range and instrumentation should be placed on additional portions of the body. The raw data should be made available so that it can be reduced by the methods developed in this report. The estimates of the power spectral densities of the local normal force coefficients could be eliminated, thereby increasing the accuracy of the buffeting calculations.

4. An inertia-compensated balance system should be built that will yield the local normal force coefficients acting on each segment. The model should be physically constructed as independent segments. The segments should be divided such that either the variations in $r(x)\ \alpha_n(x)$ are small over each segment or the local normal force has unity spatial correlations over each segment. Each segment should be suspended from a central sting by an inertia-compensated balance system. An inertia-compensated balance consists of a strain gage bridge that will measure the normal force exerted on the segment by the sting and of an accelerometer, or accelerometers, mounted on the segment that will measure the normal accelerations of the segment. These readings will yield the aerodynamic normal forces exerted on each segment. This measuring system will require fewer measuring devices and will give more accurate results than a model with several pressure transducers at each segment.

5. The analysis should be extended to include the multitank dynamics of the vehicle. In the bending analysis presented in this report, the vehicle is considered to be a single nonuniform beam. However, the first stage of the Saturn I and Saturn IB consists of nine tanks, or beams, in parallel. Test data indicate that the single beam assumption needs improvement.

6. The dynamics of the control system should be included in the analysis of the vehicle dynamics. Angular deflections in the vehicle at the instrumentation unit cause the control system to actuate and generate side forces where the engines are located. These side forces cause bending deflections and sloshing, which, in turn, cause control deflections. This dynamic interaction between the vehicle structure and the control system was accounted for (Ref. 15) by increasing the damping term in the dynamic expression that represents the vehicle. This may account for the interaction of the structure and control system. However, the phenomena need further analysis.

7. The aerodynamic damping of the vehicle in bending should be computed and used as an input to the buffeting program. The aerodynamic damping may be negative on some vehicle configurations. Negative damping could have a significant influence on the design of the vehicle structure and the control system. The quasi-steady method of computing the aerodynamic damping of bodies with separate flow fields should be developed and programmed.

8. The analysis should be extended to include the effects of gusts on the vehicle. Gusts cause bending and sloshing and should be included with buffeting and aerodynamic damping as inputs to the gross vehicle dynamics. The gross vehicle dynamics consist of the bending (including the multitank case), sloshing, and control system dynamics.

SECTION IX. SUMMARY

The gross response of a vehicle to buffeting is determined. The bending dynamics of the vehicle is analyzed. The bending displacements and moments of the vehicle are expressed as a series in terms of its bending modes. The integrated power spectral densities of the local normal force coefficients are used to determine the power spectral densities of the displacements and moments which yield the mean square values of bending deflections and bending moments. The scaling rules for the power spectral densities are derived. Thus, wind tunnel data can be used to predict the gross loads induced in a vehicle by buffeting.

Approximations are introduced into the analysis. It is necessary to make some approximation for the longitudinal normal force distribution because it can not be measured as a continuous function of length. The cross modal terms in the integrated power spectral density of the local normal force coefficients are shown to be unimportant in comparison with the direct terms. It is further shown that the response of the vehicle can be estimated if the integrated power spectral density of the local normal force coefficients is evaluated only at the resonant frequency of the mode.

Two methods of determining the integrated power spectral density of the local normal force coefficients are considered, the series and cross spectrum methods. In the series method, the pressure distribution is expressed as a series of the bending modes. The coefficients in this series yield the integrated power spectral densities of the normal force coefficients. In the cross power spectrum method, the power spectral densities of the normal force coefficients are integrated to yield the integrated power spectral densities of the local normal force coefficients. If the series method is used, fewer power spectral densities will have to be determined.

Two techniques for measuring the local normal force are available. One consists of dividing the vehicle into segments over which the pressure has unity spatial correlation. The other technique consists of dividing the vehicle into segments such that variation in $r(x)\ \alpha_n(x)$ is small over each segment. The normal force coefficient for the segment can then be determined by measuring the pressure about the segment at several points with conventional pressure transducers. The coefficients can also be determined with inertia-compensated balances. Fewer measuring devices will be required if inertia-compensated balances are used.

The rigid and sloshing body dynamics are analyzed. The mean square displacement of the vehicle and sloshing liquids is determined as a function of the power spectral density of the buffeting moments about the vehicle center of gravity. Virtually any instrumentation that will yield the integrated power spectral densities of the local normal force coefficients will yield the power spectral density of the buffeting moment about the vehicle center of gravity.

Saturn I buffeting data, obtained with a rigid pressure model, was reduced by the methods developed in this report. The root mean square values of the vehicle bending moments and bending deflections were determined. These values compare favorably with the results of an aeroelastic model test and with the flight test results of Saturn I (SA-7). However, the bending modes, mass distribution, and bending stiffness do not represent a compatible set of data. This incompatibility causes some discrepancies in the data.

REFERENCES

1. Ashley, H., Bisplinghoff, and Halfman, R. L., "Aeroelasticity," Addison-Wesley Publishing Company, Inc., November 1957.

2. Crandall, S. H., "Random Vibration," Technology Press, 1958.

3. Jones, G. W., Jr., Foughner, J. T., Jr., "Investigation of Buffeting Pressures on Models of Large Manned Launch Vehicle Configurations," NASA TND 1633, 1963.

4. Goldberg, A. P., and Wood, J. D., "Dynamic Loads in the Atlas-Able 5 During Transonic Buffeting," STL/TM-60-0000-19075, August 1960.

5. Goldberg, A. P. and Adams, R. H., "Mercury-Atlas Buffeting Loads at Transonic and Low Supersonic Speeds," STL/TR-60-0000-AS431, November 1960.

6. "Aeroelastic and Acoustic Conference," Manned Spacecraft Center, March 1963. (Confidential)

7. Coe, C. F., "Steady and Fluctuating Pressures at Transonic Speeds on Two Space Vehicle Payload Shapes," NASA TM X 503.

8. Chevalier, H. L. and Robertson, J. E., "Pressure Fluctuations Resulting from an Alternating Flow Separation and Attachment at Transonic Speeds," AEDC-TDR-63-204, November 1963.

9. Peterson, H. C., "Dynamic Response of Launch Vehicles to Transonic Buffeting Forces," No. 63-209, AIAA Summer Meeting, June 1963.

10. Morgan, J. R., "Ground Wind Loads on the Saturn I Block II Vehicles for Steady Wind Conditions," NASA MSFC Memo R-AERO-AU-64-1, January 1964.

11. Kroll, G. A., "Preliminary Vibration Analysis of Saturn SA-3 Vehicle," NASA MSFC M-P&VE-SD-395-62, August 1962.

12. Kiefling, L., "Multiple Beam Vibration Analysis of Saturn I and IB Vehicles," NASA MSFC TM X-53072, June 1964.

13. McDonough, G. F., "Bending Vibrations, SA-8 and SA-9 Vehicles," NASA MSFC R-AERO-DD-2, March 1964.

14. Doggett, R. V., Jr., and Hanson, P. W., "An Aeroelastic Model Approach for the Prediction of Buffet Bending Loads on Launch Vehicles," NASA TN D-2022, October 1963.

REFERENCES (Cont.)

15. Hanson, P. W., and Doggett, R. V., Jr., "Aerodynamic Damping and Buffet Response of an Aeroelastic Model of the Saturn I Block II Launch Vehicle," (Review Copy) NASA L-4194, December 1964.

16. Saturn Flight Evaluation Working Group, "Results of the Seventh Saturn I Launch Vehicle Test Flight," NASA MSFC MPR-SAT-FE-64-17, November 1964. (Confidential)

APPENDIX A
ORTHOGONALITY OF THE BENDING MODES

Consider Eq. (9) when $\ell \neq n$.

$$\alpha_\ell(x) = \frac{1}{m\omega_\ell^2}\left(\frac{EI}{L^4}\,\alpha_\ell''(x)\right)'' \tag{A-1}$$

$$\alpha_n(x) = \frac{1}{m\omega_n^2}\left(\frac{EI}{L^4}\,\omega_n''(x)\right)'' \tag{A-2}$$

Multiplying Eq. (A-1) and (A-2) by $\alpha_n(x)$ and $\alpha_\ell(x)$, respectively, and integrating yields

$$\omega_\ell^2\, L^4 \int_0^1 m\,\alpha_\ell(x)\,\alpha_n(x)\,dx = \int_0^1 (EI\,\alpha_\ell''(x))''\,\alpha_n(x)\,dx \tag{A-3}$$

$$\omega_n^2\, L^4 \int_0^1 m\,\alpha_\ell(x)\,\alpha_n(x)\,dx = \int_0^1 (EI\,\alpha_n''(x))''\,\alpha_\ell(x)\,dx \tag{A-4}$$

Subtracting

$$(\omega_\ell^2 - \omega_n^2)\, L^4 \int_0^1 m\,\alpha_\ell(x)\,\alpha_n(x)\,dx$$

$$= \int_0^1 [(EI\,\alpha_\ell''(x))''\,\alpha_n(x) - (EI\,\alpha_n''(x))''\,\alpha_\ell(x)]\,dx \tag{A-5}$$

Integrating the right-hand side by parts

$$(\omega_\ell^2 - \omega_n^2)\, L^4 \int_0^1 m\,\alpha_\ell(x)\,\alpha_n(x)\,dx = [\alpha_n(x)\,(EI\,\alpha_\ell''(x))' - \alpha_\ell(x)\,(EI\,\alpha_n''(x))' - EI(\alpha_n'(x)\,\alpha_\ell''(x) - \alpha_\ell'(x)\,\alpha_n''(x))]_0^1 \tag{A-6}$$

From the boundary conditions $\alpha_n''(x)$ and $\alpha_n'''(x)$ are zero at $x = 0$ and $x = 1$. Thus

$$\int_0^1 m\,\alpha_\ell(x)\,\alpha_n(x)\,dx = 0 \qquad \text{when } \ell \neq n \tag{15}$$

APPENDIX B
COMPLEX CONJUGATES OF CROSS POWER SPECTRAL DENSITIES

Consider the Fourier transform of f(t)

$$\overline{f(\omega)} = \lim_{T \to \infty} \frac{1}{2\pi} \int_{-T/2}^{T/2} f(t)\, e^{-i\omega t}\, dt \tag{B-1}$$

$$\overline{f(\omega)} = \lim_{T \to \infty} \frac{1}{2\pi} \int_{-T/2}^{T/2} f(t) \cos \omega t\, dt - \lim_{T \to \infty} \frac{i}{2\pi} \int_{-T/2}^{T/2} f(t) \sin \omega t\, dt \tag{B-2}$$

Substituting for the two components

$$\overline{f(\omega)} = A(\omega) - iB(\omega) \tag{B-3}$$

From Eq. (B-1), $\overline{f(-\omega)}$ can be written

$$\overline{f(-\omega)} = \lim_{T \to \infty} \frac{1}{2\pi} \int_{-T/2}^{T/2} f(t)\, e^{i\omega t}\, dt \tag{B-4}$$

$$\overline{f(-\omega)} = \lim_{T \to \infty} \frac{1}{2\pi} \int_{-T/2}^{T/2} f(t) \cos \omega t\, dt + \lim_{T \to \infty} \frac{i}{2\pi} \int_{-T/2}^{T/2} f(t) \sin \omega t\, dt \tag{B-5}$$

Substituting for the two components

$$\overline{f(-\omega)} = A(\omega) + iB(\omega) \tag{B-6}$$

Comparing Eq. (B-3) and (B-6) reveals that $\overline{f(\omega)}$ and $\overline{f(-\omega)}$ are complex conjugates. Now consider the cross power spectral density function

$$\phi(x_\ell, x_n, \omega) = \lim_{T \to \infty} \frac{4\pi}{T} \overline{f(x_\ell, \omega)}\ \overline{f(x_n, -\omega)} \tag{B-7}$$

This can be written

$$\phi(x_\ell, x_n, \omega) = \lim_{T \to \infty} \frac{4\pi}{T} (A_\ell(\omega) - iB_\ell(\omega))\ (A_n(\omega) + iB_n(\omega)) \tag{B-8}$$

$$\phi(x_\ell, x_n, \omega) = \lim_{T \to \infty} \frac{4\pi}{T} (A_\ell(\omega)\, A_n(\omega) + B_\ell(\omega)\, B_n(\omega)) + i\,(A_\ell(\omega)\, B_n(\omega) - A_n(\omega)\, B_\ell(\omega)) \tag{B-9}$$

Consider

$$\phi(x_n,x_\ell,\omega) = \lim_{T \to \infty} \frac{4\pi}{T} \overline{f(x_n,\omega)}\ \overline{f(x_\ell,-\omega)} \tag{B-10}$$

$$\phi(x_n,x_\ell,\omega) = \lim_{T \to \infty} \frac{4\pi}{T} (A_n(\omega) - iB_n(\omega))\ (A_\ell(\omega) + iB_\ell(\omega)) \tag{B-11}$$

$$\phi(x_n,x_\ell,\omega) = \lim_{T \to \infty} \frac{4\pi}{T} (A_\ell(\omega)\ A_n(\omega) + B_\ell(\omega)\ B_n(\omega))$$

$$-i\ (A_\ell(\omega)\ B_n(\omega) - A_n(\omega)\ B_\ell(\omega)) \tag{B-12}$$

Comparing Eq. (B-9) and (B-12) shows that $\phi(x_\ell,x_n,\omega)$ and $\phi(x_n,x_\ell,\omega)$ are complex conjugates. When $\ell = n$, $\phi(x_\ell,x_\ell,\omega)$ is real from Eq. (B-9). Usually when the cross power spectral densities are required, they are added in pairs; i.e., $\phi(x_\ell,x_n,\omega) + \phi(x_n,x_\ell,\omega)$, where $\ell \neq n$. The imaginary components, when added, are equal to zero; so, only the real components of the cross power spectral densities are used. Thus, for many applications, only the real parts of the power spectral densities need be determined.

APPENDIX C
DETERMINATION OF THE MEAN SQUARE VALUES FROM THE POWER SPECTRAL DENSITIES

The mean square of a function is defined as

$$\langle y^2 \rangle = \lim_{T \to \infty} \frac{1}{T} \int_{-T/2}^{T/2} y(t)\, y(t)\, dt \tag{C-1}$$

Substituting the Fourier integral (Eq. (20)) for one of the functions

$$\langle y^2 \rangle = \lim_{T \to \infty} \frac{1}{T} \int_{-T/2}^{T/2} y(t) \left[\int_{-\infty}^{\infty} \overline{y(\omega)}\, e^{i\omega' t}\, d\omega' \right] dt \tag{C-2}$$

Letting $\omega' = -\omega$

$$\langle y^2 \rangle = \lim_{T \to \infty} \frac{1}{T} \int_{-T/2}^{T/2} y(t) \left[\int_{-\infty}^{\infty} \overline{y(-\omega)}\, e^{-i\omega t}\, d\omega \right] dt \tag{C-3}$$

Reversing the order of integration

$$\langle y^2 \rangle = \lim_{T \to \infty} \frac{1}{T} \int_{-\infty}^{\infty} \overline{y(-\omega)} \left[\int_{-T/2}^{T/2} y(t)\, e^{-i\omega t} dt \right] d\omega \tag{C-4}$$

From Eq. (19) this can be written

$$\langle y^2 \rangle = \lim_{T \to \infty} \frac{2\pi}{T} \int_{-\infty}^{\infty} \overline{y(-\omega)}\ \overline{y(\omega)}\, d\omega \tag{C-5}$$

From Appendix B, $\overline{y(-\omega)}$ and $\overline{y(\omega)}$ are complex conjugates. The product of two functions that are complex conjugates is equal to the square of the absolute magnitude of one of the functions. The integrand is an even function of ω. Thus, Eq. (C-5) can be written

$$\langle y^2 \rangle = \int_0^{\infty} \lim_{T \to \infty} \frac{4\pi}{T}\ \overline{y(-\omega)}\ \overline{y(\omega)}\, d\omega \tag{C-6}$$

From Eq. (24) the power spectral density function is defined as

$$\phi_y(\omega) = \lim_{T \to \infty} \frac{4\pi}{T}\ \overline{y(\omega)}\ \overline{y(-\omega)} \tag{C-7}$$

Thus Eq. (C-6) can be written

$$\langle y^2 \rangle = \int_0^{\infty} \phi_y(\omega)\, d\omega \tag{C-8}$$

APPENDIX D
RELATION BETWEEN $\phi_N(x_i,x_j,\omega)$, $\phi_N(x_i,x_i,\omega)$, and $\phi_N(x_j,x_j,\omega)$

The power spectral densities are given by

$$\phi_N(x_i,x_i,\omega) = \lim_{T \to \infty} \frac{4\pi}{T} \overline{C_N(x_i,\omega)}\ \overline{C_N(x_i,-\omega)} \tag{D-1}$$

$$\phi_N(x_j,x_j,\omega) = \lim_{T \to \infty} \frac{4\pi}{T} \overline{C_N(x_j,\omega)}\ \overline{C_N(x_j,-\omega)} \tag{D-2}$$

$$\phi_N(x_i,x_i,\omega)\ \phi_N(x_j,x_j,\omega) = \lim_{T \to \infty} \left[\frac{4\pi}{T} \overline{C_N(x_i,\omega)}\ \overline{C_N(x_j,-\omega)}\right] \cdot \left[\frac{4\pi}{T} \overline{C_N(x_j,\omega)}\ \overline{C_N(x_i,-\omega)}\right] \tag{D-3}$$

Thus

$$\phi_N(x_i,x_i,\omega)\ \phi_N(x_j,x_j,\omega) = \phi_N(x_i,x_j,\omega)\ \phi_N(x_j,x_i,\omega) \tag{D-4}$$

The two power spectral densities on the right-hand side of Eq. (D-4) are complex conjugates of one another, by Appendix B. The product of a function and its complex conjugate is equal to the square of the absolute value of the function. Thus, Eq. (D-4) can be written

$$|\phi_N(x_i,x_j,\omega)| = +\sqrt{\phi_N(x_i,x_i,\omega)\ \phi_N(x_j,x_j,\omega)} \tag{D-5}$$

The square root of the product of two power spectral densities is the absolute value of the cross power spectral density between the two power spectral densities.

APPENDIX E
BENDING MOMENT AND DEFLECTION PROGRAM

This program computes the bending moments and the bending deflections of an elastic vehicle from rigid body wind tunnel test data. The necessary inputs for the program are given in the description of the definitions in this appendix. The inputs ALP(I), ALP1(I), and PHCP(I,I), KK are the punched card outputs of the normalization program, described in Appendix F, and the local normal force power spectral density program, described in Appendix I. The outputs of the program are the RMS bending moments and deflections. If sense switch one is in the down position, the power spectral densities of the bending moments and deflections will be output as functions of frequency. The mean square values of the power spectral densities of the bending moments and deflections generated by fluctuations below a given frequency will also be output as functions of frequency.

This program must be modified if it is to be used to reduce data by the cross spectrum method using cross terms of the power spectral densities of the local normal force coefficients as inputs. Section A, which is indicated in the program listing, must be removed. The second index on all PHCP(I,I) must be changed to J. The read statement for PHCP(I,J) must include a J index. The statement number 19 must be changed to statement number 14.

If this program is to be used in reducing data by the series method, sections A, B, and C must be removed. Statements that provide for the input of the integrated power spectral densities of the local normal force coefficients to the computer program will have to be added.

Definitions

A. Inputs (must be in this order)

1. Single inputs

*IM	Month
*ID	Day
*IY	Year
*IF	Number of vehicle segments
*JL	Number of vehicle segments or number of cross terms
*M	Key to maximum or minimum case
*NF	Number of significant bending modes

**WF	Final value of the model circular frequency
**WI	Increment of the model circular frequency
**Q	Tunnel dynamic pressure
**TLM	Length of the model in inches
**VM	Velocity as seen by the model in ft/sec
**TL	Length of the vehicle in inches
**V	Velocity of the vehicle at the proper Mach no. ft/sec

2. Multiple inputs

**R(I)	Dimensionless radius of the vehicle at each segment
**DX(I)	Dimensionless length of each segment
**EI(I)	Bending stiffness at each station of the vehicle

3. Multiple inputs that must be input with each mode

**ALP(I)	Normalized bending mode of the vehicle
**ALP1(I)	Second derivative of the normalized bending mode
**RO	Damping ratio of the vehicle (first value on a card with RO and WN)
**WN	Natural frequency of the vehicle (second value on a card with RO and WN)
**PHCP(I,I)	Power spectral densities of the local normal force coefficients
***KK	Key that indicates that all of the power spectral densities have reached the zero slope portion of the curves

B. Internal Definitions

PM(I,J)	Multiplier of the power spectral density of the local normal force to yield the integrated power spectral density
PHY(I)	Power spectral density of the bending deflection
PHM(I)	Power spectral density of the bending moment

QUY(I)	Previous value of the power spectral density of the bending deflection
QUM(I)	Previous value of the power spectral density of the bending moment
QU(I)	Parameter that is set equal to the power spectral density of the bending moment or the bending deflection
QUP(I)	Parameter that is set equal to the previous value of the power spectral density of the bending moment or the bending deflection
SY(I)	Mean square of the bending deflection
SM(I)	Mean square of the bending moment
YN(I)	Root mean square of the bending deflection of an individual mode
PMN(I)	Root mean square of the bending moment of an individual mode
YT(I)	Root mean square of the bending deflection of the total of all modes
PMT(I)	Root mean square of the bending moment of the total of all modes
I	Index of the vehicle segments
J	Index of the vehicle segments
K	Index of the integration with circular frequency
WW	Initial value of the circular frequency
WP	Previous value of the circular frequency
KF	Key for the termination of the integration process
ZN	Integrated power spectral density
WX	Vehicle circular frequency
DI	Impedance
L	Key that determines whether the program is computing moments or deflections

D	Incremental value of the power spectral densities of either the moments or the deflections.
ZNP	Previous value of the integrated power spectral density
W	Value of the circular frequency at any particular calculation

*Single card input with last digit in column No. 5

**Single or multiple card input with a 12-column width (i.e., Format (6E12.4))

***Single card input with last digit in column No. 10

```
      DIMENSION R(22),DX(22),EI(22),ALP(22),ALP1(22),PHCP(22,22),PM(22,2
     12),PHY(22),PHM(22),QUY(22),QUM(22),QU(22),QUP(22),SY(22),SM(22),YN
     2(22),PMN(22),YT(22),PMT(22)
      READ 100,IM
      READ 100,ID
      READ 100,IY
      READ 100,IF
      READ 100,JL
      READ 100,M
      READ 100,NF
      READ 102,WF
      READ 102,WI
      READ 102,Q
      READ 102,TLM
      READ 102,VM
      READ 102,TL
      READ 102,V
      READ 102,(R(I),I=1,IF)
      READ102,(DX(I),I=1,IF)
      READ102,(EI(I),I=1,IF)
      PRINT104,IM,ID,IY,(R(I),DX(I),EI(I),I=1,IF)
      PRINT 114,IF,JL,NF,M,WF,WI,Q
      I = 1
    1 YT(I)=0.
      PMT(I)=0.
      IF(I-IF)8,2,2
    8 I= I+1
      GO TO 1
    2 WW=WI
      N=1
    3 WP=-WW
      KK = 0
      ZN=0.
      J=1
      KF=0
      L=0
      I=1
      ZNP=0.
      K=1
      READ102,(ALP(I),I=1,IF)
      READ102,(ALP1(I),I=1,IF)
      READ 102,RO,WN
      PRINT 113,N
      PRINT105,(ALP(I),ALP1(I),I=1,IF)
      PRINT 115,RO,WN
      WI=WW
    4 IF(KK) 5,5,6
    5 READ 102,(PHCP(I,I),I=1,IF)
      READ 106,KK
    6 I=1
      W=WP+WI
      IF(W-WF)12,11,10
   10 WI=WF-WP
      W=WP+WI
   11 KF=1
   12 IF(K-1)13,13,14
   13 PM(I,J)=R(I)*R(J)*DX(I)*DX(J)*ALP(I)*ALP(J)
```

B

(NEXT PAGE)

```
                                                        (FROM PREVIOUS PAGE)
   14 IF(M)15,16,16                                          |
   15 PM(I,J)=ABSF(PM(I,J))                                  |
      GO TO 18                                               |
   16 IF(I-J)17,18,17                          A              C
   17 PHCP(I,J)=0.                                           |
      GO TO 19                                               |
   18 PHCP(I,J)=SQRTF(PHCP(I,I)*PHCP(J,J))                   |
 * 19 ZN=ZN+PHCP(I,J)*PM(I,J)                                |
      IF(J-JL)20,21,21                                       |
   20 J=J+1                                                  |
      GO TO 12                                               |
   21 J=1                                                    |
      IF(I-IF)22,23,23                                       |
   22 I=I+1                                                  |
      GO TO 12                                               |
   23 I=1                                                    |
      I=1                                                    |
      ZN=ZN*(VM/TLM)*(TL/V)                                  |
      WX=W*(TLM/VM)*(V/TL)                                   |
      DI=(WN**2+WX**2)**2+(2.*RO*WX*WN)**2                   |
   24 PHY(I)=(ALP(I)**2*Q**2*ZN)/DI                          |
      PHM(I)=(ALP1(I)**2*EI(I)**2*Q**2*ZN)/(DI*(TL/12.)**2)  |
      IF(I-IF)25,26,26                                       |
   25 I=I+1                                                  |
      GO TO 24                                               |
   26 I=1                                                    |
   27 IF(K-2)39,28,28                                        |
   28 IF(L)29,29,30                                          |
   29 QU=PHY(I)                                              |
      QUP=QUY(I)                                             |
      GO TO 31                                               |
   30 QU= PHM(I)                                             |
      QUP=QUM(I)                                             |
   31 D=((QU-QUP)*WI/2.+QUP*WI)*(TLM/VM)*(V/TL)              |
      IF(L)32,32,33                                          |
   32 SY(I)=D+SY(I)                                          |
      GO TO 34                                               |
   33 SM(I)=D+SM(I)                                          |
   34 IF(I-IF)35,36,36                                       |
   35 I=I+1                                                  |
      GO TO 28                                               |
   36 I=1                                                    |
      IF(L)38,37,38                                          |
   37 L=1                                                    |
      GO TO 28                                               |
   38 L=0                                                    |
   39 IF(K-1)40,40,41                                        |
   40 SY(I)=0.                                               |
      SM(I)=0.                                               |
   41 QUY(I)=PHY(I)                                          |
      QUM(I)=PHM(I)                                          |
      IF(I-IF)42,43,43                                       |
   42 I=I+1                                                  |
      GO TO 39                                               |
   43 I=1                                                    |
      IF(SENSE SWITCH 1)120,121                              |
  120 PRINT 113,N
```

```
      PRINT 108
      PRINT 109,N,K,WX,WN,ZN,(PHY(I),SY(I),PHM(I),SM(I),I=1,IF)
  121 IF(KF)44,44,7
   44 K=K+1
      WP=W
      IF(ZNP-ZN)46,45,46
   45 W=1000.
   46 ZNP=ZN
      ZN=0.
      GO TO 4
    7 PRINT 110
      I=1
   47 YN(I)=SQRTF(SY(I))
      PMN(I)= SQRTF(SM(I))
      PRINT 111,I,YN(I),PMN(I)
      YT(I)=YN(I)+YT(I)
      PMT(I)=PMN(I)+PMT(I)
      IF(I-IF)48,49,49
   48 I=I+1
      GO TO 47
   49 I=1
      IF(N-NF)50,51,51
   50 N=N+1
      GO TO 3
   51 PRINT 112,(I,YT(I),PMT(I),I=1,IF)
      STOP
  100 FORMAT(I5)
  102 FORMAT(6E12.4)
  104 FORMAT(1H ,6HDATE  ,I2,1H-,I2,1H-,I2//1X54HTHE FOLLOWING ARE INPUT
     1S WHICH DO NOT CHANGE WITH MODE//7X4HR(I),9X5HDX(I),9X5HEI(I)//(3E1
     24.4))
  114 FORMAT(1H0,2X2HIF,3X2HJL,3X2HNF,4X1HM,5X2HWF,6X2HWI,9X1HW/415,3F10
     1.2)
  105 FORMAT(1H0,6X6HALP(I),8X7HALP1(I)/(2E14.6))
  115 FORMAT(1H0,5X2HR0,12X2HWN//2E14.6)
  106 FORMAT (I10)
  108 FORMAT(1H0,1X1HN,2X1HK,4X2HWX,9X2HWN,6X2HZN,12X6HPHY(I),6X4HY(I)/4
     13X6HPHM(I),8X4HM(I))
  109 FORMAT(213,2F10.3,3E14.6/40X2E14.6/(40X2E14.6/40X2E14.6))
  110 FORMAT(1H1,1X1HI,6X5HYN(I),8X5HMN(I))
  111 FORMAT(I3,2E14.6)
  112 FORMAT(1H1,1X1HI,6X5HYT(I),6X5HMT(I)//(I3,2E14.6))
  113 FORMAT(1H1,30HTHE FOLLOWING ARE FOR MODE NO.,I5)
      END
```

*STATEMENT NUMBER MUST BE CHANGED TO 14
**CHANGE TO: 5 READ 102, ((PHCP(I,J), J = 1, JF), I = 1, IF)

NOTE DIMENSION STATEMENT MUST ALSO BE MODIFIED

APPENDIX F
BENDING MODE NORMALIZATION

In the methods developed in this report it is necessary that the bending modes be normalized such that Eq. (7) is valid.

$$\int_0^1 m\,\alpha_n^2(x)\,dx = 1 \tag{7}$$

This program computes the normalized bending modes. A normalization constant C is computed by

$$C = \frac{1}{\sqrt{\int_0^1 m\,A_n(x)\,dx}} \tag{F-1}$$

where $A_n(x)$ is a bending mode which has not been normalized. The normalized bending mode is obtained by multiplying the unnormalized bending mode by the constant C. The second derivative of the normalized bending mode is obtained by multiplying the unnormalized second bending mode by the normalization constant and the square of the length of the vehicle in inches. The program outputs are the normalized bending modes and the second derivatives of these modes. The outputs are punched on cards and printed. The form of the punched outputs is such that the cards can be used as inputs to the programs described in Appendix I.

This program must be used in conjunction with the interpolation subroutine of Appendix G.

Definitions

A. Inputs (must be in this order)

1. Single inputs

*IM	Month
*ID	Day
*IY	Year
*JF	Number of vehicle segments
*KF	Length of the tables that are to be input
*NF	Number of significant bending modes

*DX	Integration interval
**XXI	Initial vehicle station
**TL	Length of the vehicle in inches

2. Multiple inputs

**P(K), X(K)	The mass at a particular station and the corresponding dimensionless vehicle station
**XM(J)	Dimensionless vehicle station where the local normal force is concentrated.

3. Multiple inputs that must be input with each mode

**AL(CK), X(K)	The unnormalized bending mode and the corresponding dimensionless vehicle station
**AL1(K), X(K)	The unnormalized second derivative of the bending mode with respect to vehicle length in inches and the corresponding dimensionless vehicle station

B. Internal Definitions

KB1	Beginning of the mass table
KF1	End of the mass table
KB2	Beginning of the unnormalized bending mode table
KF2	End of the unnormalized bending mode table
KB3	Beginning of the second derivative of the unnormalized bending mode table
KF3	End of the second derivative of the unnormalized bending mode table
N	Mode number
J	Vehicle segment number
ALP(I)	Normalized bending mode
ALP1(I)	Normalized second derivative of the bending mode
A	The area under the curve generated by multiplying the unnormalized bending mode and the mass

AA	Unnormalized bending mode at a particular vehicle station
BB	Unnormalized second derivative of the bending mode at a particular vehicle station
C	Normalization constant
DA	Incremental area under the curve
P1	Mass at a particular vehicle station
XS	Vehicle station for a particular loop
Y1	Previous value of Y2
Y2	Product of mass and the square of the unnormalized bending mode
K	Index of the tabular values

*Single card inputs with last digit in column 5

**Single or multiple card inputs on a 12-column width (i.e., Format (6E12.4))

```
      DIMENSION,P(40),X(120),XM(22),AL(80),AL1(120),ALP(22),ALP1(22)
      READ 100,IM
      READ 100,ID
      READ 100,IY
      READ 100,JF
      READ 100,KF
      READ 100,NF
      READ 102,DX
      READ 102,XXI
      READ 102,TL
      READ102,(P(K),X(K),K=1,KF)
      PRINT 103,IM,ID,IY,DX,XXI,JF,NF,KF,TL
      PRINT 104,(P(K),X(K),K,K=1,KF)
      KB1=1
      KF1=KF
      KB2=KF1+1
      KF2=2*KF
      KB3=KF2+1
      KF3=3*KF
      READ 102,(XM(J),J=1,JF)
      PRINT 111,(XM(J),J,J=1,JF)
      N=1
    1 J=1
      A=0.
      READ 102,(AL(K),X(K),K=KB2,KF2)
      READ 102,(AL1(K),X(K),K=KB3,KF3)
      PRINT 105,N
      PRINT108,(AL(K),X(K),K,K=KB2,KF2)
      PRINT 105,N
      PRINT109,(AL1(K),X(K),K,K=KB3,KF3)
      XS=XXI
    2 CALL INT(KB1,KF1,XS,X,P,P1)
      CALL INT(KB2,KF2,XS,X,AL,AA)
      Y2=P1*(AA**2)
      IF(XS-XXI)4,4,3
    3 DA=(Y2-Y1)*DX/2.+Y1*DX
      A=A+DA
    4 Y1=Y2
      XS=XS+.0001
      IF(XS-1.0)5,8,8
    5 XS=XS-.0001
      XS=XS+DX
      IF(XS-1.0)7,7,6
    6 DX=ABSF(1.0-XS)
      XS=1.0
    7 GO TO 2
    8 C=1.0/SQRTF(A)
    9 XS=XM(J)
      CALL INT(KB2,KF2,XS,X,AL,AA)
      ALP(J)=C*AA
      CALL INT(KB3,KF3,XS,X,AL1,BB)
      ALP1(J)=C*(TL**2)*BB
      IF(J-JF)10,11,11
   10 J=J+1
      GO TO 9
   11 PRINT 106,(ALP(J),J=1,JF)
      PUNCH 106,(ALP(J),J=1,JF)
```

```
      PRINT 107,(ALP1(J),J=1,JF)
      PUNCH 107,(ALP1(J),J=1,JF)
      IF(N-NF)12,13,13
   12 N=N+1
      GO TO 1
   13 STOP
  100 FORMAT(I5)
  102 FORMAT(6E12.4)
  103 FORMAT(1HO,6HDATE  ,I2,1H-,I2,1H-,I2//1X2HDX,2X3HXXI,2X2HJF,2X2HNF
     1,2X2HKF/F4.2,F5.2,1X12,2I4//1X3HTL=F10.2//)
  104 FORMAT(5X4HMASS,10X4HX(K),23X1HK/(2E14.5,I20))
  106 FORMAT(1H1,14X6HALP(J)/(6E12.4))
  107 FORMAT(1HO,14X7HALP1(J)/(6E12.4))
  105 FORMAT(1H1,30HTHE FOLLOWING ARE FOR MODE NO.,I5)
  108 FORMAT(1HO,4X5HAL(K),10X4HX(K),23X1HK/(2E14.5,I20))
  109 FORMAT(1HO,3X6HAL1(K),10X4HX(K),23X1HK/(2E14.5,I20))
  111 FORMAT(1H1,4X5HXM(J),10X1HJ/(E14.5,I9))
  112 FORMAT(1XE11.4,E12.4,1XE11.4,E12.4,1XE11.4,E12.4)
      END
```

APPENDIX G
INTERPOLATION SUBROUTINE

This program performs the interpolation in a two dimensional system. The program checks to see first if the value of the independent variable is outside the table that has been input. If the value is outside the program limits, the program outputs the table length, the independent variable value, and the first and last values in the table. If the independent variable is within the limits of the program, a linear interpolation is conducted. The program always starts at the beginning of the table and runs until it reaches the proper value.

The linkage or connection between the main program and this subroutine supplies the data specified in the definition section and in the order specified. The length of storage space specified in the dimension statement for the dependent and independent variables must be the same as in the main program.

Definitions

A. Linkage Connection (must be in this order)

1. Input to the subroutine from the main program

KK	The beginning index number of each table
KKL	The ending index number of each table
XS	The present value of the independent variable
X	Independent variable
Y	Dependent variable

2. Transferred from the subroutine to the main program

PAR	Interpolated value of the dependent variable

B. Internal Definitions

L	Index of the second value of the table
LL	Index of the last value of the table

```
      SUBROUTINE INT(KK,KKL,XS,X,Y,PAR)
      DIMENSION,X(120),Y(120)
      IF((XS-X(KK))*(XS-X(KKL)))1,1,50
    1 L=KK+1
      LL=KKL
      DO 2 I=L,LL
      IF((XS-X(I))*(X(I-1)-XS))2,3,6
    2 CONTINUE
    3 IF(XS-X(I))4,5,51
    4 I=I-1
      PAR=Y(I)
      GO TO 7
    5 PAR=Y(I)
      GO TO 7
    6 PAR=Y(I)-((X(I)-XS)*(Y(I)-Y(I-1)))/(X(I)-X(I-1))
      GO TO 7
   50 PRINT110,KK,KKL,XS,X(KK),X(KKL),Y(KK)
      STOP 1
   51 PRINT110,KK,KKL,XS,X(KK),X(KKL),Y(KK)
      STOP 2
    7 RETURN
  110 FORMAT(1H ,2I5,4E14.5)
      END
```

APPENDIX H
BUFFETING PITCHING MOMENT PROGRAM

The root mean square of the pitching moment coefficient due to buffeting is computed by this program. The required inputs are shown in the definition section of this appendix. It should be noted that the PHCP(I,I) and KK portions of the input are the punched output of the local normal force coefficient power spectral density program described in Appendix I. It must be in the same order as it is output by the procedure of Appendix I. The power spectral densities of the pitching moment and pitching moment coefficient, as well as the values of the mean square pitching moment coefficients generated below various frequencies, are output as a function of model frequency. All outputs are for the model and must be scaled to the full vehicle.

This program must be modified if it is to be used to reduce data by the cross spectrum method using cross terms of the power spectral densities of the local normal force coefficients as inputs. Section A, which is indicated in the program listing, must be removed. The second index on all PHCP(I,I) must be changed to J. The read statement for PHCP(I,J) must include a J index. Statement number 21 must be changed to statement number 17.

If this program is to be used in reducing data by the series method, sections A, B, and C must be removed. Statement W = WP + WI should be numbered 13. Statements that input the integrated power spectral densities of the local normal force coefficients to the computer program will have to be added.

Definitions

A. Inputs (must be in this order)

1. Single inputs

*IM	Month
*ID	Day
*IY	Year
*IF	Number of vehicle segments
*JL	Number of vehicle segments or the number of cross terms
*M	Index to maximum or minimum case
**WF	Final value of the model circular frequency

**WI	Increment on the model circular frequency
**XI	Dimensionless vehicle station about which the pitching moment is computed
**RR	Dimensionless reference radius = 0.0489
**PHI	3.1416

2. Multiple inputs

**R(I)	Dimensionless radius of the vehicle at each segment
**DX(I)	Dimensionless length of each vehicle segment
**X(I)	Dimensionless station at which the local normal force on the vehicle segment is concentrated
**PHCP(I,I)	Power spectral density of the local normal force coefficients
***KK	Key that indicates that all of the power spectral densities have reached the zero slope portion of the curves

B. Internal Definitions

WP	Previous value of the circular frequency
W	Value of the circular frequency at any particular calculation
PM(I,J)	Multiplier of the power spectral density of the local normal force that yields the integrated power spectral density
ZN	Integrated power spectral density
ZM	Power spectral density of the pitching moment
PHM	Power spectral density of the pitching moment coefficient
QUM	Previous value of the power spectral density of the pitching moment coefficient
D	Incremental value of the mean square pitching moment coefficient
TM	Mean square pitching moment coefficient generated up to a given frequency

DCM	Root mean square pitching moment coefficient
KF	Key to the end of the integration process
I	Index of the vehicle segments
J	Index of the vehicle segments or the cross power spectral densities
K	Index on the integration process

*Single card input with the last digit in column 5

**Single or multiple card inputs with a 12-column width (i.e., Format (6E12.4))

***Single card inputs with the last digit in column 10

```
      DIMENSION PHCP(22,22),PM(22,22),R(22),DX(22),X(22)
      KK=0
      KF=0
      K=1
      J=1
      I=1
      TM=0.
      ZN=0.
      QUM=0.
      READ 100, IM
      READ 100, ID
      READ 100, IY
      READ 100, IF
      READ 100, JL
      READ 100, M
      READ 102, WF
      READ 102, WI
      READ 102, X1
      READ 102, RR
      READ 102, PHI
      READ 102, (R(I),I=1,IF)
      READ 102, (DX(I),I=1,IF)
      READ 102,(X(I),I=1,IF)
      PRINT 106, IM, ID, IY, X1
      PRINT 107, (R(I),DX(I),X(I),I,I=1,IF)
      PRINT 108,IF,JL,M,WF,WI,RR
      PRINT 109
      PRINT 110
      I=1
      WP=-WI
   13 IF(KK)1,1,2
    1 READ 102,(PHCP(I,I),I=1,IF)
      READ 103,KK
    2 I=1
    * W=WP+WI
      IF(W-WF)7,9,35
   35 WI=WF-WP
      W=WP+WI
    9 KF=1
    7 IF(K-1) 16,16,17
   16 PM(I,J)=R(I)*R(J)*(X(I)-X1)*(X(J)-X1)*DX(I)*DX(J)
   17 IF(M)99,19,18
   99 PM(I,J)=ABSF(PM(I,J))
      GO TO 19
   18 IF(I-J)20,19,20
   19 PHCP(I,J)=SQRTF(PHCP(I,I)*PHCP(J,J))
      GO TO 21
   20 PHCP(I,J)=0.
** 21 ZN=ZN+PHCP(I,J)*PM(I,J)
      IF(J-JL)22,23,23
   22 J=J+1
      GO TO 7
   23 J=1
      IF(I-IF)25,26,26
   25 I=I+1
      GO TO 7
   26 I=1
```

B

A

C

```
      ZM=.485*(10.**12)*ZN
      PHM=(1./(4.*(PHI**2)*(RR**6)))*ZN
      IF(K-2)27,28,28
   28 D=(PHM-QUM)*WI/ 2. +QUM*WI
      TM=TM+D
   27 IF(QUM-PHM)32,31,32
   31 WI=100.
   32 QUM=PHM
      PRINT101,K,W,ZM,PHM,TM
      IF(KF)30,30,29
   30 K=K+1
      WP=W
      ZN=0.
      GO TO 13
   29 DCM=SQRTF(TM)
      PRINT112,DCM
      STOP
  100 FORMAT(I5)
  101 FORMAT(1H ,10X,I2,4E14.5)
  102 FORMAT(6E12.4)
  103 FORMAT(I10)
  106 FORMAT(1H ,15X,6HDATE  ,I2,1H-,I2,1H-,I2//10X,12HDCM ABOUT X=F6.4/
     1/14X,28HTHE FOLLOWING ARE INPUT DATA)
  107 FORMAT(1H0,6X6HRADIUS,6X7HDELTA X,6X9HX STATION,6X1HI/(3E14.5,I8))
  108 FORMAT(1H0,7X2HIF,3X2HJL,4X1HM,8X2HWF,8X2HWI,8X2HRR/5X,3I5,2F10.1,
     1F10.4)
  109 FORMAT(1H1,34H           THE FOLLOWING ARE OUTPUT)
  110 FORMAT(1H ,11X1HK,3X9HFREQUENCY,7X5HPHI M,9X6HPHI CM,11X2HTM)
  112 FORMAT(1H0,10X4HDCM=E12.4)
      END
```

*IF B AND C ARE REMOVED THIS STATEMENT MUST BE NUMBERED 13

**IF A IS REMOVED THIS STATEMENT MUST BE RENUMBERED 17

APPENDIX I
LOCAL NORMAL FORCE COEFFICIENT POWER SPECTRAL DENSITIES

This program computes the power spectral densities of the local normal force coefficients from root mean square values of the local normal force coefficients. This procedure is necessary for reducing the PSTL-1 data since only the RMS values of the normal force coefficients are available. The power spectral densities of the local normal force coefficients are necessary to compute the RMS pitching moment coefficients and the RMS bending moments and deflections caused by buffeting. The required inputs for the program are indicated under the listing of the definitions. Included in the inputs are the turbulent components and total root mean square values of the local normal force coefficients. The outputs are printed and punched. The punched outputs are in the proper form to be used in both the pitching moment coefficient program described in Appendix H and the bending moment and deflection program described in Appendix E.

Definitions

A. Inputs (must be in this order)

1. Single input

*IM	Month
*ID	Day
*IY	Year
*IF	Number of vehicle segments
**WF	Final value of the model circular frequency
**WI	Increment on the model circular frequency
**SLP	A value which when divided by Q will yield the slope, usually -0.4
**Q	Tunnel dynamic pressure

2. Multiple inputs

**TCP(I)	Root mean square local normal force coefficient
**CPT(I)	Turbulent portion of the root mean square local normal force coefficient

B. Internal Definitions

A(I)	The height of the portion of the curve with slope of $-0.4/Q^2$
I	Index for the vehicle segments
K	Index for the frequency increment
KK	Key that indicates that all of the power spectral densities of the local normal force coefficients have reached the zero slope portion of the curves
KF	Key for the termination of the integration process
M	Counter that indicates that the zero slope portion of all the local normal force power spectral densities has been reached
PHT(I)	Power spectral density of the turbulent portion of the local normal force coefficient
PHCP(I)	Power spectral densities of the local normal force coefficient
T(I)	Difference between the squares of the turbulent and total root mean square local normal force coefficients
WS(I)	The model frequency at which the portion of the local normal force power spectral density with a slope of $-0.4/Q^2$ terminates

*Single card input with last digit in column 5

**Single or multiple card input in a 12-column width (i.e., Format (6E12.4))

```
      DIMENSION CPT(22),TCP(22)
      DIMENSION PHT(22),T(22),WS(22),A(22),PHCP(22,22)
      KK=0
      KF=0
      K=1
      I=1
      READ 100,IM
      READ 100,ID
      READ 100,IY
      READ 100,IF
      READ 102,WF
      READ 102,WI
      READ 102,SLP
      READ 102,Q
      READ102,(TCP(I),I=1,IF)
      READ102,(CPT(I),I=1,IF)
      PRINT 104,IM,ID,IY
      PRINT 105,(TCP(I),CPT(I),I=1,IF)
      PRINT 106,SLP,WF,WI,Q,IF
      PRINT 107
      WP=-WI
      I=1
      SLP=SLP/Q**2
   13 IF(K-1)1,1,2
    1 PHT(I)=CPT(I)**2/WF
      IF(PHT(I)-4./(Q**2))3,3,4
    4 PHT(I)=4./(Q**2)
    3 T(I)=(TCP(I)**2-CPT(I)**2 )
      IF(T(I))6,5,5
    6 PRINT 110, T(I),PHT(I),WF,Q,I
      GO TO 19
    5 WS(I) = SQRTF(2.*T(I)/ABSF(SLP))
      A(I)=ABSF(SLP)*WS(I)
    2 IF(I-1)8,8,7
    8 W=WP+WI
      IF(W-WF)7,9,35
   35 WI=WF-WP
      W=WP+WI
    9 KF=1
    7 IF(WS(I)-W)11,10,10
   10 WC=W
      M= 0
      GO TO 12
   11 WC=WS(I)
      M=M+1
   12 PHCP(I,I)=PHT(I)+A(I)+SLP*WC
      IF(I-IF)14,15,15
   14 I=I+1
      GO TO 13
   15 I=1
      IF(M-22)17,16,16
   16 KK=1
      KF=1
   17 PRINT 108,(PHCP(I,I),I=1,IF),KK
      PUNCH 108,(PHCP(I,I),I=1,IF),KK
      I=1
      WP=W
```

```
      IF(KF)18,18,19
   18 K=K+1
      GO TO 13
   19 STOP
  100 FORMAT(I5)
  102 FORMAT(6E12.4)
  104 FORMAT(1H ,15X6HDATE  ,I2,1H-,I2,1H-,I2//16X37HTHE FOLLOWING ARE R
     1MS PRESSURE INPUTS)
  105 FORMAT(1HO,15X6HTCP(I),8X6HCPT(I)//(10X2E14.4))
  106 FORMAT(1HO,10X5HSLOPE,5X2HWF,7X2HWI,8X1HQ,7X2HIF//10XF5.2,3XF7.1,2
     1XF6.1,3XF6.1,5XI2)
  107 FORMAT(1H1,46HTHE FOLLOWING ARE THE POWER SPECTRAL DENSITIES/1X32H
     1OF THE RMS PRESSURE COEFFICIENTS)
  108 FORMAT(6E12.4/6E12.4/6E12.4/4E12.4/I10)
  110 FORMAT (1HO,10X,5HT(I)=,E12.4,2X,7HPHT(I)=,E12.4,2X,3HWF=,E12.4,
     12X,2HQ=E12.4,2X,2HI=I5)
      END
```

APPENDIX J
BENDING MOMENT COMPUTED BY SECOND DERIVATIVE METHOD

This program computes the vehicle bending moment for a unit nose deflection by means of equation 40. This will allow a comparison to be made with the integral method of Appendix K that was used in the aeroelastic tests. The inputs for the program are shown in the definitions given in this Appendix. The outputs consist of the bending moments at arbitarily selected vehicle stations caused by a nose deflection of one foot. These calculations are made by the second derivative method.

Definitions

A. Inputs (must be in this order)

1. Single input

*IM	Month
*ID	Day
*IY	Year
*IF	Number of vehicle segments
*JL	Number of vehicle segments or number of cross terms
*M	Key to the maximum or minimum case
*NF	Number of significant modes
**WF	First value of the mode circular frequency
**WI	Increment of the circular frequency
**Q	Dynamic pressure
**TLM	Model length in inches
**VM	Model velocity in ft/sec
**TL	Length of the vehicle in inches
**V	Vehicle velocity in ft/sec

2. Multiple inputs

**R(I)	Dimensionless radius at each vehicle segment
**DX(I)	Dimensionless length of each vehicle segment
**EI(I)	Bending stiffness of each vehicle segment

3. Multiple inputs which must be reinput for each mode

**ALP(I)	Normalized bending modes at each vehicle segment
**ALP1(I)	Normalized second derivative of the bending modes at each vehicle segment
**PHCP(I,I)	Local normal force power spectral densities
***KK	Key that indicates that all of the power spectral densities of the local normal forces have reached the zero slope portion of the curves

B. Internal Definitions

PM(I,J)	Multiplier of the local normal force coefficients power spectral density to yield the integrated power spectral density
PHY(I)	= 0
PHM(I)	Power spectral density of the bending moment determined by the cross spectrum method
QUY(I)	= 0
QUM(I)	Previous value of the power spectral density of the bending moment determined by the cross spectrum method
QU(I)	Parameters set equal to PHM(I)
QUP(I)	Parameters set equal to QUM(I)
SY(I)	= 0
SM(I)	Mean square of the bending moment computed by the cross spectrum method
YN(I)	The bending moment obtained by equation 40
PMN(I)	Root mean square bending moment for a particular mode

YT(I)	The total bending moment determined by equation 40
PMT(I)	Root mean square bending moment determined by the cross spectrum methods for the total of all modes
I	Index of vehicle segment
J	Index of vehicle segment or number of cross term
K	Index of the integration with respect to circular frequency
WW	Storage for the initial value of the circular frequency increment
WP	Previous value of the circular frequency
KF	Key to the termination of the integration
ZN	Integrated power spectral density I_{nn}
ZNP	Previous value of the integrated power spectral density
WX	Vehicle circular frequency
DI	Impedance
L	= 0
D	Incremental value of the power spectral density of the bending moment computed by the cross spectrum method

*Single card input with the last digit in column 5

**Single or multiple card input with a 12-column width (i.e., Format (6E12.4))

***Single card input with the last digit in column 10

```
      DIMENSION R(22),DX(22),EI(22),ALP(22),ALP1(22),PHCP(22,22),PM(22,2
     12),PHY(22),PHM(22),QUY(22),QUM(22),QU(22),QUP(22),SY(22),SM(22),YN
     2(22),PMN(22),YT(22),PMT(22)
      READ 100,IM
      READ 100,ID
      READ 100,IY
      READ 100,IF
      READ 100,JL
      READ 100,M
      READ 100,NF
      READ 102,WF
      READ 102,WI
      READ 102,Q
      READ 102,TLM
      READ 102,VM
      READ 102,TL
      READ 102,V
      READ 102,(R(I),I=1,IF)
      READ102,(DX(I),I=1,IF)
      READ102,(EI(I),I=1,IF)
      PRINT104,IM,ID,IY,(R(I),DX(I),EI(I),I=1,IF)
      PRINT 114,IF,JL,NF,M,WF,WI,Q
      I = 1
    1 YT(I)=0.
      PMT(I)=0.
      IF(I-IF)8,2,2
    8 I= I+1
      GO TO 1
    2 WW=WI
      N=1
    3 WP=-WW
      KK = 0
      ZN=0.
      J=1
      KF=0
      L=1
      I=1
      ZNP=0.
      K=1
      READ102,(ALP(I),I=1,IF)
      READ102,(ALP1(I),I=1,IF)
      READ 102,R0,WN
      PRINT 113,N
      PRINT105,(ALP(I),ALP1(I),I=1,IF)
      PRINT 115,R0,WN
      WI=WW
    4 IF(KK) 5,5,6
    5 READ 102,(PHCP(I,I),I=1,IF)
      READ 100,KK
    6 I=1
      W=WP+WI
      IF(W-WF)12,11,10
   10 WI=WF-WP
      W=WP+WI
   11 KF=1
   12 IF(K-1)13,13,14
   13 PM(I,J)=R(I)*R(J)*DX(I)*DX(J)*ALP(I)*ALP(J)
```

```
14 IF(M)15,18,16
15 PM(I,J)=ABSF(PM(I,J))
   GO TO 18
16 IF(I-J)17,18,17
17 PHCP(I,J)=0.
   GO TO 19
18 PHCP(I,J)=SQRTF(PHCP(I,I)*PHCP(J,J))
19 ZN=ZN+PHCP(I,J)*PM(I,J)
   IF(J-JL)20,21,21
20 J=J+1
   GO TO 12
21 J=1
   IF(I-IF)22,23,23
22 I=I+1
   GO TO 12
23 I=1
   I=1
   ZN=ZN*(VM/TLM)*(TL/V)
   WX=W*(TLM/VM)*(V/TL)
   DI=(WN**2+WX**2)**2+(2.*R0*WX*WN)**2
24 PHY(I)=0.
   PHM(I)=(ALP1(I)**2*EI(I)**2*Q**2*ZN)/(DI*(TL/12.)**2)
   IF(I-IF)25,26,26
25 I=I+1
   GO TO 24
26 I=1
27 IF(K-2)39,28,28
28 IF(L)29,29,30
29 QU=PHY(I)
   QUP=QUY(I)
   GO TO 31
30 QU= PHM(I)
   QUP=QUM(I)
31 D=((QU-QUP)*WI/2.+QU*WI)*(TLM/VM)*(V/TL)
   IF(L)32,32,33
32 SY(I)=D+SY(I)
   GO TO 34
33 SM(I)=D+SM(I)
34 IF(I-IF)35,36,36
35 I=I+1
   GO TO 28
36 I=1
   IF(L)38,37,38
37 L=1
   GO TO 28
38 L=1
39 IF(K-1)40,40,41
40 SY(I)=0.
   SM(I)=0.
41 QUY(I)=PHY(I)
   QUM(I)=PHM(I)
   IF(I-IF)42,43,43
42 I=I+1
   GO TO 39
43 I=1
   IF(KF)44,44,7
44 K=K+1
```

```
      WP=W
      IF(ZNP-ZN)46,45,46
   45 WI=100.
   46 ZNP=ZN
      ZN=0.
      GO TO 4
    7 PRINT 110
      I=1
   47 YN(I)=(EI(I)*ALP1(I))/(ALP(1)*((TL/12.)**2))
      PMN(I)= SQRTF(SM(I))/ALP(1)
      PRINT 111,I,YN(I),PMN(I)
      YT(I)=YN(I)+YT(I)
      PMT(I)=PMN(I)+PMT(I)
      IF(I-IF)48,49,49
   48 I=I+1
      GO TO 47
   49 I=1
      IF(N-NF)50,51,51
   50 N=N+1
      GO TO 3
   51 PRINT 112,(I,YT(I),PMT(I),I=1,IF)
      STOP
  100 FORMAT(I5)
  102 FORMAT(6E12.4)
  104 FORMAT(1H ,6HDATE  ,I2,1H-,I2,1H-,I2//1X54HTHE FOLLOWING ARE INPUT
     1S WHICH DO NOT CHANGE WITH MODE///X4HR(I),9X5HDX(I),9X5HEI(I)/(3E1
     24.4))
  114 FORMAT(1H0,2X2HIF,3X2HJL,3X2HNF,4X1HM,5X2HWF,8X2HWI,9X1HU/415,3F10
     1.2)
  105 FORMAT(1H0,6X6HALP(I),8X7HALP1(I)/(2E14.6))
  115 FORMAT(1H0,5X2HRO,12X2HWN//2E14.6)
  106 FORMAT (I10)
  108 FORMAT(1H0,1X1HN,2X1HK,4X2HWX,9X2HWN,6X2HZN,12X6HPHY(I),8X4HY(I)/4
     13X6HPHM(I),8X4HM(I))
  109 FORMAT(2I3,2F10.3,3E14.6/40X2E14.6/(40X2E14.6/40X2E14.6))
  110 FORMAT(1H1,1X1HI,4X9HELASTIC M,7X5HPSD M)
  111 FORMAT(I3,2E14.6)
  112 FORMAT(1H1,1X1HI,3X10HELASTIC MT,7X6HPSD MT//(I3,2E14.6))
  113 FORMAT(1H1,30HTHE FOLLOWING ARE FOR MODE NO.,I5)
      END
```

Definitions

A. Inputs (must be in this order)

1. Single inputs

*IM	Month
*ID	Day
*IY	Year
*JF	Number of vehicle segments
*KF	Length of the tables that are to be read in
*NF	Number of significant modes
**DX	Integration interval
**XXI	Initial vehicle station
**TL	Length of the vehicle in inches

2. Multiple inputs

**P(K), X(K)	The mass at a particular station and the corresponding dimensionless vehicle station
**XX(I)	Dimensionless vehicle station where the local normal force can be considered to act

3. Multiple inputs that must be re-entered with each mode

**AL(K), X(K)	The unnormalized bending mode and the corresponding dimensionless vehicle station
**AL1(K), X(K)	The unnormalized second derivative of the bending mode with respect to vehicle length, in inches, and the corresponding dimensionless vehicle station

B. Internal Definition

KB1	Beginning of the mass table
KF1	End of the mass table
KB2	Beginning of the unnormalized bending mode table
KF2	End of the unnormalized bending mode table

KB3	Beginning of the second derivative of the unnormalized bending mode table
KF3	End of the second derivative of the unnormalized bending mode table
N	Index on the mode number
J	Index on the vehicle segments
DXI	Initial value of the integration interval
XS	Vehicle station at any particular increment
XO	Vehicle segment of interest
PI	Mass at a particular vehicle station
AA	Unnormalized bending mode at a particular vehicle station
Y2	The value of the quantity to be integrated at a particular vehicle station
DA	Incremental area of the moment integral
DX	Integration interval
A	Area up to the particular vehicle station under the curve
Y1	Previous value of the quantity to be integrated at a particular vehicle station
WN	Natural frequency of the mode

*Single card inputs with the last digit in column 5

**Single or multiple card inputs with a 12-column width (i.e., Format (6E12.4))

```
      DIMENSION,P(40),X(120),XM(22),AL(60),AL1(120),ALP(22),ALP1(22)
      READ 100,IM
      READ 100,ID
      READ 100,IY
      READ 100,JF
      READ 100,KF
      READ 100,NF
      READ 102,DX
      READ 102,XXI
      READ 102,TL
      READ102,(P(K),X(K),K=1,KF)
      PRINT 103,IM,ID,IY,DX,XXI,JF,NF,KF,TL
      PRINT 104,(P(K),X(K),K,K=1,KF)
      KB1=1
      KF1=KF
      KB2=KF1+1
      KF2=2*KF
      KB3=KF2+1
      KF3=3*KF
      READ 102,(XM(J),J=1,JF)
      PRINT 111,(XM(J),J,J=1,JF)
      N=1
    1 J=1
      DXI=DX
      A=0.
      READ 102,(AL(K),X(K),K=KB2,KF2)
      READ 102,(AL1(K),X(K),K=KB3,KF3)
      READ 102,WN
      PRINT 105,N
      PRINT108,(AL(K),X(K),K,K=KB2,KF2)
      PRINT 105,N
      PRINT109,(AL1(K),X(K),K,K=KB3,KF3)
      PRINT 122,WN
      PRINT 121
   10 XO=XM(J)
    2 CALL INT(KB1,KF1,XS,X,P,P1)
      CALL INT(KB2,KF2,XS,X,AL,AA)
      Y2=P1*(AA)*(XO-XS)/1.0
      IF(XS-XXI)4,4,3
    3 DA=(Y2-Y1)*DX/2.+Y1*DX
      A=A+DA
    4 Y1=Y2
      XS=XS+.0001
      IF(XS-XO)5,8,8
    5 XS=XS-.0001
      XS=XS+DX
      IF(XS-XO)7,7,6
    6 DX=ABSF(XO-XS)
      XS=XO
    7 GO TO 2
    8 A=(WN**2)*((TL/12.)**2)*A
      PRINT 120,A
      A=0.
      XS=XXI
      DX=DXI
      IF(J-JF)11,12,12
```

```
   11 J=J+1
      GO TO 10
   12 IF(N-NF)13,14,14
   13 N=N+1
      GO TO 1
   14 STOP
  100 FORMAT(I5)
  102 FORMAT(6E12.4)
  103 FORMAT(1H0,6HDATE  ,I2,1H-,I2,1H-,I2//1X2HUX,2X3HXXI,2X2HJF,2X2HNF
     1,2X2HKF/F4.2,F5.2,1X12,2I4//1X3HTL=F10.2//)
  104 FORMAT(5X4HMASS,10X4HX(K),23X1HK/(2E14.5,I20))
  105 FORMAT(1H1,30HTHE FOLLOWING ARE FOR MODE NO.,I5)
  108 FORMAT(1H0,4X5HAL(K),10X4HX(K),23X1HK/(2E14.5,I20))
  109 FORMAT(1H0,3X6HAL1(K),10X4HX(K),23X1HK/(2E14.5,I20))
  111 FORMAT(1H1,4X5HXM(J),10X1HJ/(E14.5,I9))
  121 FORMAT(1H1,9X13HINTERGRATED M)
  120 FORMAT(10XE14.6)
  122 FORMAT(1H0,4X3HWN=,F10.5)
      END
```

APPENDIX L
EQUIVALENCE OF THE TWO METHODS OF COMPUTING BENDING MOMENT PER UNIT NOSE DEFLECTION

Consider Eq. (113)

$$\frac{M_n(x)}{y_n(0)L} = \frac{\omega_n^2 L^2}{\alpha_n(0)} \int_0^x m(z)\,(x-z)\,\alpha_n(z)\,dz \tag{113}$$

and Eq. (9)

$$\alpha_n(z) = \frac{1}{m(z)\,\omega_n^2}\left(\frac{EI}{L^4}\,\alpha_n''(z)\right)'' \tag{9}$$

Substituting Eq. (9) into Eq. (113) gives

$$\frac{M_n(x)}{y_n(0)} = \frac{1}{\alpha_n(0)L} \int_0^x (EI\,\alpha_n''(z))''(x-z)\,dz \tag{L-1}$$

$$\frac{M_n(x)}{y_n(0)} = \frac{x}{\alpha_n(0)L} \int_0^x (EI\,\alpha_n''(z))''\,dz - \frac{1}{\alpha_n(0)L} \int_0^x (EI\,\alpha''(x))''\,z\,dz \tag{L-2}$$

Integrating the first term in Eq. (L-2)

$$\frac{x}{\alpha_n(0)L} \int_0^x [illegible]\,dz - \frac{x}{\alpha_n(0)L} [illegible]\Big]_0^x \tag{L-3}$$

Since the second and third derivatives of the bending modes of a beam at a free end are equal to zero, Eq. (L-3) can be written

$$\frac{x}{\alpha_n(0)L} \int_0^x (EI\,\alpha_n''(z))''\,dz = \frac{x}{\alpha_n(0)L}\,(EI\,\alpha_n''(x))' \tag{L-4}$$

Integrating the second term in Eq. (L-2) by parts

$$\frac{1}{\alpha_n(0)L} \int_0^x (EI\,\alpha_n''(z))''\,z\,dz = \frac{1}{\alpha_n(0)L}\left\{z(EI\,\alpha_n''(z))'\Big]_0^x - \int_0^x (EI\,\alpha_n''(z))'\,dz\right\} \tag{L-5}$$

Since the second and third derivatives of a bending mode are zero at $x = 0$

$$\frac{1}{\alpha_n(0)L} \int_0^x (EI\,\alpha_n''(z))''\,z\,dz = \frac{1}{\alpha_n(0)L}\left\{x(EI\,\alpha_n''(x))' - (EI\,\alpha_n''(x))\right\} \tag{L-6}$$

Substituting Eq. (L-4) and (L-6) into Eq. (L-2) yields

$$\frac{M_n(x)}{y_n(0)} = \frac{EI}{L\alpha_n(0)\ \gamma_n(t)}\ \alpha_n''(x)\ \gamma_n(t) \qquad \text{(L-7)}$$

which is the same as Eq. (40) by Eq. (11) and its second derivative.

$$\frac{M_n(x)}{y_n(0)} = \frac{EI\ y_n''(x_n,t)}{Ly_n(0,t)} \qquad (40)$$

APPENDIX M
COMPATABILITY OF INPUT DATA

The mass distribution, bending stiffness, and bending modes, which were obtained from several sources, must represent a consistent set of data and satisfy Eq. (9). The procedure presented in this appendix applies data to the equation to verify this fact. However, Eq. (9) contains fourth derivatives of the bending modes, and since the accuracy of obtaining the fourth derivative of the bending mode from experimental data is questionable, the equation must be integrated.

Consider

$$\alpha_n(z) = \frac{1}{m(z)} \left(\frac{EI(z)}{W_n^2 L^4} \alpha_n''(z) \right)'' \tag{9}$$

Integration yields

$$IA_n(W) = \int_0^W m(z)\, \alpha_n(z)\, dz = \left(\frac{EI(W)}{W_n^2 L^4} \alpha_n''(W) \right)' - 0 \tag{M-1}$$

$$IB_n(s) = \int_0^s IA_n(W)\, dW = \frac{EI(s)}{\omega_n^2 L^4} \alpha_n''(s) - 0 \tag{M-2}$$

$$IC_n(p) = \omega_n^2 L^4 \int_0^p \frac{m(s)}{EI(s)}\, ds = \alpha_n'(p) - \alpha_n'(0) \tag{M-3}$$

$$ID_n(x) = \int_0^x IC_n(p)\, dp = \alpha_n(x) - \alpha_n(0) - x\, \alpha_n'(0) \tag{M-4}$$

or

$$\alpha_n(x) = \alpha_n(0) + x\, \alpha_n'(0) + ID_n(x) \tag{M-5}$$

which is the integrated form of Eq. (9) for a free-free beam.

To check the compatibility of the mass distribution, the bending stiffness distribution, and the bending mode, the above equations have been programmed. The data must be input in the order prescribed in the definition section of this appendix. The program will compute for one mode only. Additional computer runs must be made for each mode after the new bending mode and first derivative of the bending mode at x = 0 replace the previous values in the input data. The output is the computed bending mode, the input bending mode, IA_n, IB_M, IC_n, and ID_n. The results of this comparison are shown in figure 20.

APPENDIX K
BENDING MOMENT COMPUTED BY INTEGRAL METHOD

The modal bending moment, for unity nose displacement in feet, about point x generated by the force per unit dimensionless length, F(x), acting over the dimensionless length (Δz_i) is given by

$$\frac{M_n(x,t)}{y(0,t)L} = \frac{-L}{y(0,t)L} \sum_i F(z_i,t)\ (x-z_i)\ \Delta z_i \qquad \text{(K-1)}$$

The force per unit dimensionless length $F(x_i)$ for mode n is given by

$$F_n(z_i,t) = m(z_i)\ L^2\ \ddot{y}_n(z_i,t) \qquad \text{(K-2)}$$

From Eq. (11)

$$y_n(z_i,t) = \alpha_n(z_i)\ \gamma_n(t) \qquad (11)$$

Since $\gamma_n(t)$ is sinusoidal, the second time derivative of $y(x_i,t)$ can be written

$$\ddot{y}_n(z_i,t) = -\omega_n^2\ \alpha_n(z_i)\ \gamma_n(t) \qquad \text{(K-3)}$$

Substituting Eq. (K-3) into (K-2) and Eq. (K-2) into (K-1) yields

$$\frac{M_n(x,t)}{y_n(0,t)L} = \frac{\omega_n^2 L^3}{y_n(0,t)L} \sum_i m(z_i)\ (x-z_i)\ \alpha_n(z_i)\ \gamma_n(t)\ \Delta z_i \qquad \text{(K-4)}$$

From Eq. (11), this can be written

$$\frac{M_n(x)}{y_n(0)L} = \frac{\omega_n^2 L^3}{\alpha_n(0)L} \int_0^x m(z)\ (x-z)\ \alpha_n(z)\ dz \qquad (113)$$

for all values of t.

Evaluation of Eq. (113) by the computer program presented in this appendix will yield the modal bending moments for unity nose deflection in feet, at each vehicle segment. The inputs required are defined and listed in their proper input order in the definition section of this appendix. The input bending modes, AL(K), are not those normalized by the methods presented in Appendix F. They must have unity displacement at the nose. The output is given for each vehicle segment and each mode.

This program must be used in conjunction with the interpolation subroutine described in Appendix G.

Definitions

A. Inputs (must be in this order)

1. Single input

*IM	Month
*ID	Day
*IY	Year
*KM	Length of mass table
*KE	Length of bending stiffness table
*KA	Length of bending mode table
**TL	Length of the vehicle in inches
**DX	Integration interval
**WN	Natural frequency
**XI	Initial vehicle station
**XF	Final vehicle station
**ALP1	Normalized derivative at initial vehicle station of the bending mode

2. Multiple inputs

**PM(K)	Mass as a function of vehicle station
**PX(K)	Vehicle stations corresponding to the above mass
**EI(K)	Bending stiffness as a function of vehicle station
**EX(K)	Vehicle station corresponding to the above bending stiffness
**ALP(K)	Normalized bending mode as a function of vehicle station
**AX(K)	Vehicle station corresponding to the above normalized bending mode

B. Internal Definitions

KB1	Beginning of the mass table

KF1	End of the mass table
KB2	Beginning of the bending stiffness table
KF2	End of the bending stiffness table
KB3	Beginning of the normalized mode table
KF3	End of the normalized mode table
PA	Previous value of the integral A
PB	Previous value of the integral B
PC	Previous value of the integral C
PD	Previous value of the integral D
PMP	Previous value of the mass
AAP	Previous value of the bending mode
PEI	Previous value of the bending stiffness
X	Vehicle station for each increment
PMM	Mass at a particular vehicle station
EEI	Bending stiffness at a particular vehicle station
AALP	Bending mode value at a particular vehicle station
A	Integral A
B	Integral B
C	Integral C
D	Integral D
ALPA	Calculated bending mode

*Single card inputs with the last digit in column 5

**Multiple inputs and or multiple card inputs with a 12-column width (i.e., Format (6E12.4))

```
      DIMENSION PM(100),PX(100),EI(100),EX(100),ALP(100),AX(100)
      READ 100,IM
      READ 100,ID
      READ 100,IY
      READ 100,KM
      READ 100,KE
      READ 100,KA
      READ 102,TL
      READ 102,DX
      READ 102,WN
      READ 102,XI
      READ 102,XF
      READ 102,ALP1
      KB1=1
      KF1=KM
      KB2=KM+1
      KF2=KF1+KE
      KB3=KF2+1
      KF3=KF2+KA
      READ 102,(PM(K),K=KB1,KF1)
      READ 102,(PX(K),K=KB1,KF1)
      READ 102,(EI(K),K=KB2,KF2)
      READ 102,(EX(K),K=KB2,KF2)
      READ 102,(ALP(K),K=KB3,KF3)
      READ 102,(AX(K),K=KB3,KF3)
      PRINT 104,IM,ID,IY
      PRINT 107
      PRINT 103,(PM(K),PX(K),K,K=KB1,KF1)
      PRINT108
      PRINT 103,(EI(K),EX(K),K,K=KB2,KF2)
      PRINT109
      PRINT 103,(ALP(K),AX(K),K,K=KB3,KF3)
      PRINT 105,KM,KE,KA
      PRINT 106,DX,TL,WN,XI,XF
      PA=0.
      PB=0.
      PC=0.
      PD=0.
      PMP=0.
      AAP=0.
      PEI=1.
      X=XI
      PRINT111
    1 CALL INT (KB1,KF1,X,PX,PM,PMM)
      CALL INT(KB2,KF2,X,EX,EI,EEI)
      CALL INT(KB3,KF3,X,AX,ALP,AALP)
      A=(PMM+AALP+PMP+AAP)*DX/2.+PA
      B=(A+PA)*DX/2.+PB
      C=(B/EEI+PB/PEI)*(WN**2)*((TL/12.)**4)*DX/2.+PC
      D=(C+PC)*DX/2.+PD
      ALPA=ALP(KB3)+X*ALP1+D
      PRINT112,X,A,B,ALPA,C,D,AALP
      PMP=PMM
      AAP=AALP
      PEI=EEI
      PA=A
      PB=B
```

```
      PC=C
      PD=D
      X=X+.0001
      IF(X-XF)2,5,5
    2 X=X-.0001
      X=X+DX
      X=X+.0001
      IF(X-XF)3,3,4
    3 X=X-.0001
      GO TO 1
    4 X=X-.0001
      X=X-DX
      DX=XF-X
      X=XF
      GO TO 1
    5 STOP
  100 FORMAT(I5)
  102 FORMAT(6E12.4)
  103 FORMAT(2E14.5,I9)
  104 FORMAT(1H0,6HDATE  ,I2,1H-,I2,1H-,I2)
  105 FORMAT(1H0,7X2HKM,8X2HKE,8X2HKA//3I10)
  106 FORMAT(1H0,7X2HDX,8X2HTL,8X2HWN,8X2HXI,8X2HXF//5X,5F10.5)
  107 FORMAT(6X4HMASS,7X9HX STATION,10X1HK)
  108 FORMAT(1H1,4X9HSTIFFNESS,3X9HX STATION,10X1HK)
  109 FORMAT(1H1,4X4HALPA,8X9HX STATION,10X1HK)
  111 FORMAT(1H1,8X1HX,12X1HA,13X1HB,9X4HALPA/22X1HC,13X1HD,9X3HALP//)
  112 FORMAT(4E14.5/14X,3E14.5//)
      END
```

Technical Report HSM-R114

METHODS OF DETERMINING THE SATURN I BUFFETING RESPONSE FROM RIGID MODEL WIND TUNNEL TESTS

VOLUME I

June 1965

BY: George F. McCanless
George F. McCanless

James R. Boone
James R. Boone

APPROVED: L. G. Alexakos, Jr.
L. G. Alexakos, Jr.
Manager, Aerodynamics
Section

APPROVED: M. L. Bell
M. L. Bell
Manager, Aero-Space
Mechanics Branch